INFORMATION TO USERS

This manuscript has been reproduced from the microfilm master. UMI films the text directly from the original or copy submitted. Thus, some thesis and dissertation copies are in typewriter face, while others may be from any type of computer printer.

The quality of this reproduction is dependent upon the quality of the copy submitted. Broken or indistinct print, colored or poor quality illustrations and photographs, print bleedthrough, substandard margins, and improper alignment can adversely affect reproduction.

In the unlikely event that the author did not send UMI a complete manuscript and there are missing pages, these will be noted. Also, if unauthorized copyright material had to be removed, a note will indicate the deletion.

Oversize materials (e.g., maps, drawings, charts) are reproduced by sectioning the original, beginning at the upper left-hand corner and continuing from left to right in equal sections with small overlaps.

Photographs included in the original manuscript have been reproduced xerographically in this copy. Higher quality 6" x 9" black and white photographic prints are available for any photographs or illustrations appearing in this copy for an additional charge. Contact UMI directly to order.

Bell & Howell Information and Learning
300 North Zeeb Road, Ann Arbor, MI 48106-1346 USA
800-521-0600

UMI®

THE EFFECT OF OXYGENATED ADDITIVES ON SOOT PRECURSOR FORMATION

by

Lauretta Rubino

A thesis submitted in conformity with the requirements for the degree of Master of Applied Science

Department of Mechanical & Industrial Engineering

University of Toronto

ABSTRACT

A counter-flow propane/air diffusion flame (ϕ=1.79) is used for a fundamental analysis of the effects of oxygenated additives on soot precursor formation.

Experiments are conducted at atmospheric pressure using a quartz micro-probe for sampling and Gas Chromatography for gas sample analysis. C1-C6 species have been identified and measured.

The oxygenated additives dimethyl carbonate (DMC) and ethanol are added to the fuel stream keeping the total volumetric flow rate constant. Results show 10 vol% DMC significantly reduces acetylene, benzene and other flame pyrolysis products. Ethanol addition (10 vol%) shows instead more modest reductions. Peak acetylene and benzene levels decrease as the additive dosage increases for both ethanol and DMC.

The additive's effect on adiabatic flame temperature and fuel stream carbon content does not correlate significantly with acetylene levels. However, there does appear to be a linear relationship between oxygen content and acetylene concentrations as well as C-C content and acetylene concentrations.

ACKNOWLEDGMENTS

I would like to express my sincere gratitude to my supervisor, Professor M. J. Thomson for his guidance, encouragement and support throughout this project.

I would like to thank also everybody working in the Machine Shop for their help during the experimental setup of my study. My special thanks are given to Mr. D. Esdaile and Mr. P. Loite and Mr. D. Kalra for their availability and patience. I want also to acknowledge all my colleagues in the Mechanical & Industrial Engineering Department for their advise, support, and most of all, their friendships.

Table of contents

Abstract ii

Acknowledgment iii

Table of contents iv

List of Figures vii

List of Tables x

List of Appendices xi

CHAPTER 1 INTRODUCTION

1.1 Motivation 1-2

1.2 Objective 1-3

CHAPTER 2 LITERATURE REVIEW

2.1 Overview of soot formation mechanisms 2-1

2.2 Soot precursors 2-4

2.3 Formation of the first aromatic ring 2-5

2.4 Growth of aromatics (PAH) beyond the first ring 2-7

2.5 From PAH to soot particle formation 2-8

2.6 The role of Acetylene in soot formation 2-9

2.6.1 Models linking acetylene to soot particle formation 2-12

2.7 Pyrolysis of Alkanes 2-15

2.8 Soot formation and flames 2-18

2.9 Premixed flame 2-18

2.10 Diffusion flames 2-19

2.11 Influence of physical and chemical parameters on soot formation 2-21

2.12 Influence of additives on soot formation 2-22

2.13 Fuel dilution effect 2-24

2.14 Chemical effect 2-25

2.15 Additives in Diesel engines 2-27

2.16 Laboratory diffusion flames 2-31

2.16.1 Counter-flow diffusion flames 2-33

2.16.2 Sooting structure in counter-flow diffusion flames 2-34

CHAPTER 3 APPARATUS AND PROCEDURES

3.1 Counter-flow Burner 3-3

3.2 Additive addition setup 3-7

3.3 Gas sampling system 3-9

3.4 Measurement procedures 3-12

3.5 GC Method 3-14

3.6 GC equipment 3-17

3.6.1 Flame Ionization Detector 3-17

3.6.2 Carrier Gas supply 3-18

3.6.3 Injector system 3-19

3.6.4 Rotary sample valve 3-19

3.6.5 Capillary columns 3-20

3.7 Quantitative analysis 3-22

3.7.1 Calibration and standards 3-22

CHAPTER 4 RESULTS AND DISCUSSION

4.1 Flame and intermediates species 4-1

4.2 DMC addition 4-11

4.3 Ethanol addition 4-16

4.4 Comparison of the additive effects 4-20

4.5 Potential mechanisms of acetylene reduction 4-23

4.5.1 The influence of the flame temperature on acetylene levels 4-23

4.5.2 The influence of fuel stream carbon content on acetylene levels 4-26

4.5.3 The influence of fuel oxygen content on acetylene levels 4-27

CHAPTER 5 CONCLUSIONS AND RECOMMENDATION

5.1 Conclusions 5-1

5.2 Recommendations 5-4

List of References R-1

List of Appendices xi

List of Figures

CHAPTER 2

Figure 2-1	A rough picture for soot formation in premixed flames	2-3
Figure 2-2	The two reaction steps pathways for the formation of the first aromatic ring	2-5
Figure 2-3	HACA mechanism	2-8
Figure 2-4	Schematic of the role of acetylene in soot formation	2-10
Figure 2-5	Soot particle growth rate as function of acetylene concentration for both laminar premixed and diffusion flames	2-11
Figure 2-6	General scheme of alkane oxidation	2-16
Figure 2-7	Sooting tendency of hydrocarbon fuels	2-20
Figure 2-8	Soot volume fraction as function of time for the flame front	2-25
Figure 2-9	Effect of DMC addition for various injection timings	2-29
Figure 2-10	The average (engine load speed) effects of various brand of fuel additives on smoke opacity	2-30
Figure 2-11	Normal co-flow diffusion flame burner	2-32
Figure 2-12	Local soot loading in an n-hexane/air diffusion flame	2-33
Figure 2-13	Counter-flow diffusion flame located on the fuel and oxidizer side	2-35
Figure 2-14	Schematic of the counter-flow diffusion flame structure for methane fuel	2-37

CHAPTER 3

Figure 3-1	Schematic of the experimental setup; not to scale	3-2
Figure 3-2	Burner setup	3-5
Figure 3-3	Additive addition setup	3-8
Figure 3-4	Dependence of CO measurements on probe pressure for two flames conditions for two types of probes (water cooled stainless steel/quartz) and laser adsorption spectroscopy	3-10
Figure 3-5	Schematic of quartz micro-probe; not to scale	3-11
Figure 3-6	Column oven temperature program	3-16
Figure 3-7	Schematic of Flame Ionization Detector	3-17

CHAPTER 4

Figure 4-1	Sooting structure of counter-flow diffusion flames with flame located on the fuel (a) and oxidizer side (b)	4-3
Figure 4-2	Pictures of the flame used as baseline for additive Investigation (a), (b)	4-5
Figure 4-3	Flame shape and color increasing N_2 in the fuel stream	4-6
Figure 4-4	Flame shape and color increasing O_2 in the oxidizer stream	4-6
Figure 4-5	Propane profile across the flame	4-8
Figure 4-6	Major species profile across the flame	4-8
Figure 4-7	Minor species profile across the flame	4-9
Figure 4-8	Ethylene scatter at flame plane	4-10
Figure 4-9	Acetylene scatter at flame plane	4-10
Figure 4-10	DMC addition 10% by volume	4-13

Figure 4-11	DMC addition 15% by volume	4-13
Figure 4-12	Reduction in acetylene levels with DMC 10% and 15%	4-14
Figure 4-13	Reduction in benzene levels with DMC 10% and 15%	4-14
Figure 4-14	Ethanol addition 10% by volume	4-17
Figure 4-15	Ethanol addition 15% by volume	4-17
Figure 4-16	Reduction in acetylene levels with Ethanol 10% and 15%	4-18
Figure 4-17	Reduction in acetylene levels with Ethanol 10% and 15%	4-18
Figure 4-18	Ethanol and DMC effects in 10% and 15% on acetylene levels	4-21
Figure 4-19	Ethanol and DMC effects in 10% and 15% on benzene levels	4-21
Figure 4-20	Comparison of ethanol and DMC effects in different percentage on acetylene (counter-flow) and smoke (diesel engines)	4-22
Figure 4-21	Acetylene concentration versus adiabatic flame temperatures with and without additive addition	4-25
Figure 4-22	Acetylene concentration versus oxygen/carbon ratio	4-28
Figure 4-23	Acetylene concentration versus C-C content	4-28

APPENDICES

Figure C-1	Diagram showing the separation of a mixture of components A and B by column elution chromatography	C-3
Figure C-2	General chromatogram shape	C-4
Figure C-3	Different capillary columns	C-8
Figure C-4	Comparison between isothermal and temperature Programmed chromatograms	C-10

List of Tables

Table 2-1:	Oxygenated fuel additives chemical characteristics	2-28
Table 3-1:	Flame characteristics	3-6
Table 3-2:	DMC and Ethanol chemical characteristics	3-8
Table 3-3:	Rotary sample valve	3-16
Table 3-4:	Gas supply specifications	3-19
Table C-1:	Classification of column chromatographic methods	C-1
Table C-2:	Capillary columns versus packed columns	C-9
Table 3-5:	C1-C6 species detected	3-24
Table 3-6:	Supelco Gas Mix (Cat. No. 501832)	3-24
Table 3-10:	Supelco Gas Mix (Cat. No. 2-3470 U)	3-25
Table 4-1:	Flame characteristics with and without additive addition	4-1
Table 4-2:	DMC and ethanol chemical characteristics	4-2

List of Appendices

APPENDIX A Experimental setup: A-1

1. View of counter-flow burner, microprobe and micrometer during sampling A-2
2. Original draft (hand drawing) of counter-flow burner A-3
3. Vacuum pump characteristics A-7

APPENDIX B Flame characteristics with and without additives: B-1

1. Report on fuel and oxidizer composition, flow rates and gas flow-meter readings:
   - a) Additive 0% (Pure Fuel) (C_3 H_8) B-2
   - b) Ethanol 10% B-3
   - c) Ethanol 15% B-4
   - d) DMC 10% B-5
   - e) DMC 15% B-6
2. Raw data (in area count) of the flame species detected by Gas Chromatography:
   - a) Flame species profile without additives B-7
   - b) DMC addition data B-8
   - c) Ethanol addition data B-10

APPENDIC C Gas Chromatography C-1

C.1 Overview C-1

C.2 Chromatograms C-4

C.3 Chromatographic Detectors C-5

C.4 Chromatographic column configuration C-6

C.5 Temperature programming (PTGC) C-9

C.6 The Van Deemter equation C-11

APPENDIX D Gas Chromatography D-1

1. PLOT Column Characteristics D-2

2. PLOT Column Temperature Programming D-3

3. Chromatograms of gas sample at the flame plane position D-5

   a) Additive 0% D-5

   b) DMC 10% (by volume) D-6

   c) DMC 15% (by volume) D-7

   d) Ethanol 10% (by volume) D-8

   e) Ethanol 15% (by volume) D-9

4. Calibration Gas Standards D-10

   a) SCOTTY IV-CAT NO. 2-3470-U D-10

   b) SCOTTY IV-CAT NO. 501832 D-11

5. Calibration curves D-12

Chapter 1: INTRODUCTION

1.1 Motivation

Increases in ambient particle concentrations are associated with serious adverse health outcomes. These outcomes range from the least adverse, such as increases in symptoms of respiratory irritation and decreases in level of lung function, to the most adverse, mortality [1]. Several 4- and 5-aromatic ring compounds (PAHs) have been proved to be mutagenic while others (i.e. benzo-(a)-pyrene and benzene) to be carcinogenic. Recently the U.S. Environmental Protection Agency (EPA) has made a strong case for focusing regulatory efforts on the fine enhalable particle fraction $PM_{2.5}$ according to the fact that many experimental studies proved them to be harmful because they penetrate deep into lung tissue [1]. The observed particle health effects have persisted despite the use of many approaches to control, regulate, and reduce these pollutants.

Combustion is one of the main sources of particulate emissions (i.e. soot) and in particular diesel engine emissions are of special concern. Particulate emissions from heavy-duty diesel engines are now regulated by the U.S EPA to below 0.1 gm/bhphr, which is a factor of 6 below the unregulated levels existing prior to 1991 [10]. Although many efforts have been done to reduce particulate emissions, a better understanding of the mechanism of soot formation is needed.

Many investigators have focused on soot and soot precursor formation in laboratory flames [2, 3, 4, 5, 9]. Most of these studies have utilized premixed flames.

However, non-premixed flames represent a better model of the real combustion situation (i.e. diesel engines) [7, 8, 20, 63].

Fuel additives represent an attractive alternative for reducing soot. Fuel additives can produce immediate emission reductions across the entire vehicle fleet. A variety of fuel additives have been proposed for soot reductions, from metal additives [53, 69] to oxygenated additives [15, 18, 19]. While metal additives have the drawback of metal emissions, oxygenated additives are "clean" and have been found to be effective on particulate as well as on NOx emissions in diesel engines. In particular, additives with higher oxygen content such as dimethyl carbonate (DMC) examined at 5% and 10% by volume in conventional diesel fuels showed significant reductions on soot formation [15, 19].

In diesel engines, complexities due to many simultaneous parameters such as fluid flow, vaporization and chemical processes limit our ability to determine how these additives operate. One- and two-dimensional laminar flames are more suitable devices to obtain this fundamental information. Due to the very short time scales associated with soot formation and oxidation, only simple, but well-controlled laboratory flames can provide the detailed information required [20].

Phenomenological theories have been suggested to explain the influence of additives on the formation of soot particles. For example, modest reductions in soot loading in diffusion flames by addition of inert species, such as Ar and N_2, have been attributed to lower flame temperatures and decreased fuel concentrations [72, 74, 75].

Such effects are believed to significantly decrease the reaction rates of processes leading to soot formation. However, reductions in soot formation by a variety of additives

have been explained by chemical mechanisms. Soot suppression by alcohol addition has been observed both in shock tubes and in laboratory flames [6]. Investigations have been carried out on the effects of methanol and ethanol on soot formation [6, 75]. Many questions regarding additive effects on soot still remain and a better understanding of their fundamental mechanisms can provide the desired answers.

1.2 Objective

Motivated by the previous observations, the main objective of the present study is to investigate the chemical and physical mechanisms by which oxygenated additives affect soot formation in diffusion flames. The focus is on soot precursor formation such as acetylene, benzene and PAHs as they are key species in soot particle formation mechanisms. The investigation of oxygenated fuel additives on soot precursors is carried out in counter-flow propane-air diffusion flames. Dimethyl carbonate (DMC) and Ethanol are chosen among other additives because they reduce soot emissions in diesel engines [16, 19]. The counter-flow diffusion flame configuration is adopted because it provides a well-defined one-dimensional system convenient for both experiments and theoretical modeling. Propane is used as fuel as it eliminates fuel vaporization effects. Gas chromatography is applied as it can detect and quantify low molecular weight compounds as well as higher molecular weight compounds (C1-C10) across the flame.

Chapter 2: LITERATURE REVIEW

2.1 Overview of soot formation mechanisms

Soot formation occurs in both premixed and non-premixed combustion in applications ranging from house fires to internal combustion engines and gas turbine combustion chambers. The conditions under which soot is formed vary widely and depend on several factors, such as pressure, temperature, fuel, oxidant and geometry. Although progress has been achieved in understanding the essential chemistry and physics, many questions persist and some debate continues with regard to the details of soot formation, growth and oxidation. This chapter gives an overview of soot particulate formation mechanisms in combustion.

Soot is mostly carbon; other elements such as hydrogen and oxygen are usually present in small amounts. It is produced during the high temperature pyrolysis (or combustion) of hydrocarbons. The formation of soot particulate occurs by the conversion of a hydrocarbon fuel with molecules containing a few carbon atoms into carbonaceous agglomerate containing some millions of carbon atoms; this happens in a few milliseconds. According to the literature on soot formation mechanisms, soot particles are generated through four distinct steps [29, 3]:

Precursor formation→ Particle inception → Particle growth →Particle oxidation.

Precursor formation:

This process involves a complex sequence of fuel pyrolysis reactions, which eventually result in the formation of precursors needed to form the first soot particle. These precursor compounds typically include various unsaturated hydrocarbons, particularly acetylene C_2H_2, its higher analogues $C_{2n}H_2$ and polycyclic aromatic hydrocarbons (PAH). In fact, as shown in Figure 2-1, the hydrocarbon fuel in premixed flames is degraded during oxidation into small hydrocarbon radicals from which, under fuel-rich condition, small hydrocarbons, particularly acetylene are formed. Acetylene adds hydrocarbon radicals for growth and the growing unsaturated hydrocarbon forms aromatic rings if there is a sufficient large number of carbon atoms. The formation of larger aromatic rings (PAHs) occurs mainly through acetylene addition mechanism. All these processes occur within the molecular length scale [29].

Particle inception:

In this process, chemical and physical growth of precursors results in the formation of numerous very small primary particles with diameters less than 1.5 manometer (nm) in diameter. It is the condensation reactions of these gas phase species that lead to the appearance of the first "solid-phase" material. Thus, the transformation from a molecular system to a particulate system takes place (see Fig.2-1).

Particle growth:

The primary soot particles formed during inception grow by surface reactions as well as by coagulation. Surface growth involves the attachment of gas phase species to the surface of the particles and their incorporation into the particulate phase [69]. Surface growth reactions lead to an increase in the amount of soot (ϕ) but the number of soot particles (N) remains unchanged by

this process. The opposite is true for growth by coagulation, where particles collide and coalesce, thereby decreasing N, while ϕ remains constant. Particle growth, which is characterized by an increase in the size of the particles (diameter d), is the result of simultaneous surface growth and coagulation. These stages of combined particle generation and growth constitute the soot formation process. The final size of the soot particles results from coagulation of primary particles to larger aggregates (see Fig. 2-1).

Particle oxidation:

Experimental studies have shown that molecular oxygen (O_2) and OH radicals are the primary agents of soot particle oxidation [22]. There is substantial evidence that the fuel pyrolysis rate controls the tendency of a given fuel to soot. However, the eventual emission of soot from any combustion device is determined by the competition between soot formation and oxidation.

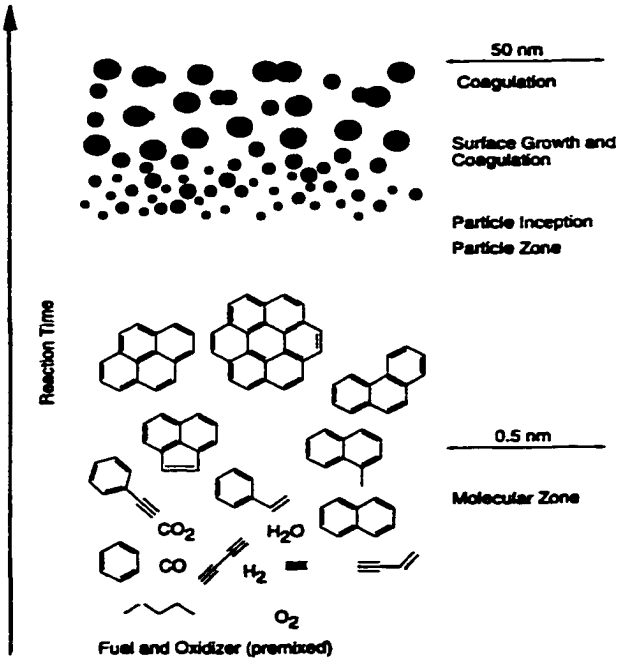

Figure 2-1: A rough picture for soot formation in premixed flames [29].

A key element in the soot formation process is the rapidity with which soot particles form in flames. The particles form in less than 1 millisecond and reach diameter of 500-1000 Angstroms in less than 10 milliseconds.

2.2 Soot Precursors

Many suggestions have been made as to the nature of possible soot precursors, e.g., acetylene, poly-acetylenes, allene, butadiene, polycyclic aromatic hydrocarbons (PAH), etc. [36, 53, 63]. There is growing experimental, thermodynamic and kinetic evidence that the formation of soot proceeds via PAH's. Some authors suggest that the molecular growth involves reactions between aromatics and acetylene species, others further supported this proposal, suggesting several possible chemical reactions [29]. Studies of soot formation in shock-tubes indicated that the overall kinetics is consistent with the critical role of aromatic-acetylenic interactions and this is valid also for the building steps that lead to PAHs formation [31, 30]. Results from modeling studies have been found to support this conceptual view [22].

In the following paragraphs it is outlined more in details the process that leads to soot particles from the formation of the first aromatic ring:

First aromatic ring formation → Growth of aromatics beyond the first ring (PAHs) → Soot particles.

2.3 Formation of the First Aromatic Ring

The formation of the first aromatic ring in flames of non-aromatic fuels begins usually with vinyl (C_2H_3) addition to acetylene. The two reaction pathways for the formation of the first aromatic ring respectively at high and low-temperature are shown in Figure 2-2.

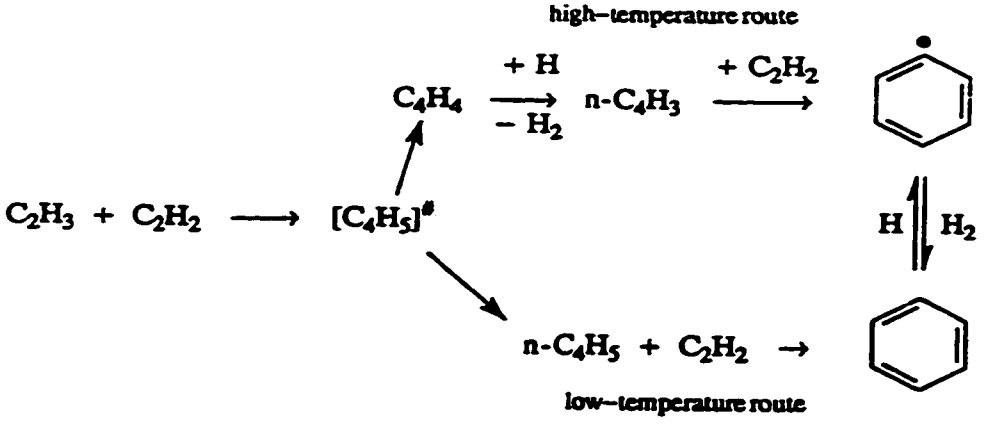

Figure 2-2: The two reaction pathways for the formation of the first aromatic ring [29].

At high temperature, we have the formation of vinyl-acetylene followed by acetylene addition to n-C_4H_3 radical, formed by the H-abstraction from the vinyl-acetylene (Fig. 2-2). At low temperature, the addition of acetylene to vinyl results in n-C_4H_5 formation, which upon addition of acetylene produces benzene. Benzene and phenyl are converted to one another by the H-abstraction reaction and its reverse [29].

Benzene is of crucial importance as the first single-ring aromatic formed from smaller non-aromatic hydrocarbons. In non-aromatic fuels, the formation of benzene can be expected to precede the formation of PAH's and soot. Several benzene formation paths via C2-C4

hydrocarbons have been suggested [24]. While the reaction path involving recombination reactions of linear C2 and C4 species have been favored in the past to account for the formation of benzene and other precursors [32], more recent work suggests that propargyl radical (C_3H_3) recombination may be also a major contributor to the formation of benzene in flames [30]. Other experiments suggests that linear C6 species are the initial products of propargyl recombination followed by ring closure. The chemistry of the C4 chain is also important since it contains potential benzene precursors [30].

The recombination reaction between propargyl (C_3H_3) and methyl (CH_3) radicals is the dominant path for butadiene (C_4H_6) formation in propane flame as well as in methane flame.

Aromatics have been suggested to form as a consequence of the reactions of species containing even number of carbon atoms, such as C_2H_x and C_4H_y [30]. However, Senkan, Vincitore and Castaldi [2], suggested the importance of reactions that involve species having an odd number of carbon atoms such as CH_i and C_3H_i in the production of aromatics and PAH. For example, they pointed out that the recombination of CH_3 radicals rapidly result in C_2H_6 production, which, in turn, can lead to C_2H_4 and C_2H_3 formation [2].

Benzene formation can then occur by the recombination of C_3H_3 radicals, as well as the recombination of CH_3 and C_5H_5 such as [30, 29]:

$$C_3H_3 + C_3H_3 = [C_6H_6]^* \rightarrow C_6H_6$$

$$CH_3 + C_5H_5 = [C_6H_8]^* \rightarrow C_6H_6 + H_2$$

2.4 Growth of aromatics (PAH) beyond the first ring

Frencklach and co-workers (1985, 1994) have suggested that PAH growth in hydrocarbon pyrolysis and oxidation begins after the formation of the first aromatic ring. This growth sequence occurs by way of a two step process involving hydrogen abstraction to activate the aromatic molecule followed by subsequent acetylene addition, which propagates molecular growth and cyclization of PAHs. This process known as the HACA mechanism continues leading to the sequential formation of multi-ring structures such as naphthalene (2-aromatic fused rings), phenanthrene (3-aromatic fused rings), pyrene (4-aromatic fused rings) and higher order aromatic rings.

Although in pyrolysis of hydrocarbon fuels, reactions of aromatic rings with species other than acetylene may be important initially, as the pyrolysis progresses, the aromatic growth becomes dominated by the HACA mechanism [29, 30]. Some of the acetylene addition reactions in the HACA sequence form particularly stable aromatic molecules, like pyrene, coronene, etc. These reactions become practically irreversible and this has the effect of "pulling" the reaction sequence forward, towards formation of larger PAH molecules. Figure 2-3 illustrates the HACA mechanism [29].

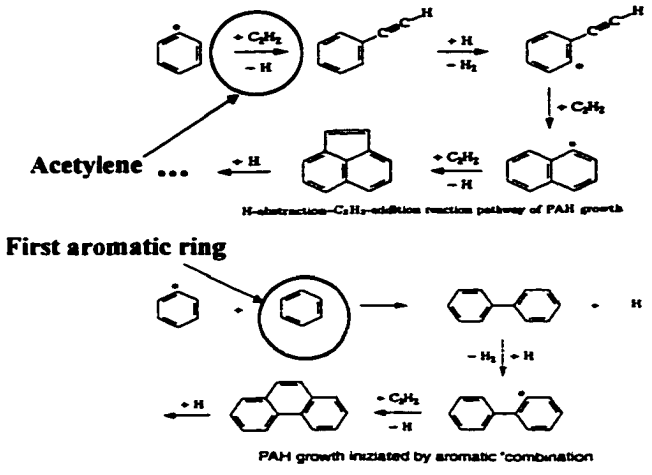

Figure 2-3: HACA mechanism [29].

2.5 From PAH to soot particles formation

While the formation of larger aromatic rings (PAH) occurs within molecular length scales, the growth in the third dimension is supposed to happen by coagulation of larger aromatic structures forming primary soot particles (see Fig. 2-1). The process in fact involves a transition from gaseous to solid phase where the solid phase does not exhibit any well defined chemical and physical structure. These primary particles (about 1.5 nm) quickly coagulate picking up at the same time molecule from the gas phase for surface growth, whose rate is one of the determining factors in final soot concentration [29, 69, 20]. Surface growth takes the major part to the final soot concentration in sooting flames while coagulation, switching the length scale to particle dimensions, determines the final size of soot particles. Due to coagulation, soot particles

present irregular structures. The possible mechanisms of soot nucleation and mass growth include:

- Sequential addition of acetylene
- Reactive coagulation of PAH

Sequential addition of acetylene to PAHs is an extension of the mechanism, which has been proposed for PAH growth into the regime of particle inception. Reactive coagulation refers to sticking collisions between PAHs, which are stabilized by the formation of a chemical bond. The processes mentioned above contribute to the bulk of soot [29, 69, 20].

2.6 The role of Acetylene in soot formation

The important role of acetylene as soot precursor is discussed with the purpose of highlighting the connection of acetylene to soot particle formation and growth.

Soot nucleation (or inception) and growth in flames occur in an environment rich in acetylene and polycyclic aromatic hydrocarbons (PAH) [5, 21]. Acetylene has long has been regarded as the dominant mass source for soot growth (Porter, 1953), primarily because it is the most abundant hydrocarbon species in the sooting region of a flame [36]. Acetylene reacts with C4 and C3 species to form the first aromatic ring. By acetylene addition aromatic species grow into polycyclic aromatic hydrocarbons (PAH) and larger aromatic rings. Coagulation of these larger aromatic ring compounds is proposed to account for the formation of primary soot particles. Figure 2-4 summarizes schematically the role of acetylene in the soot formation process as discussed before.

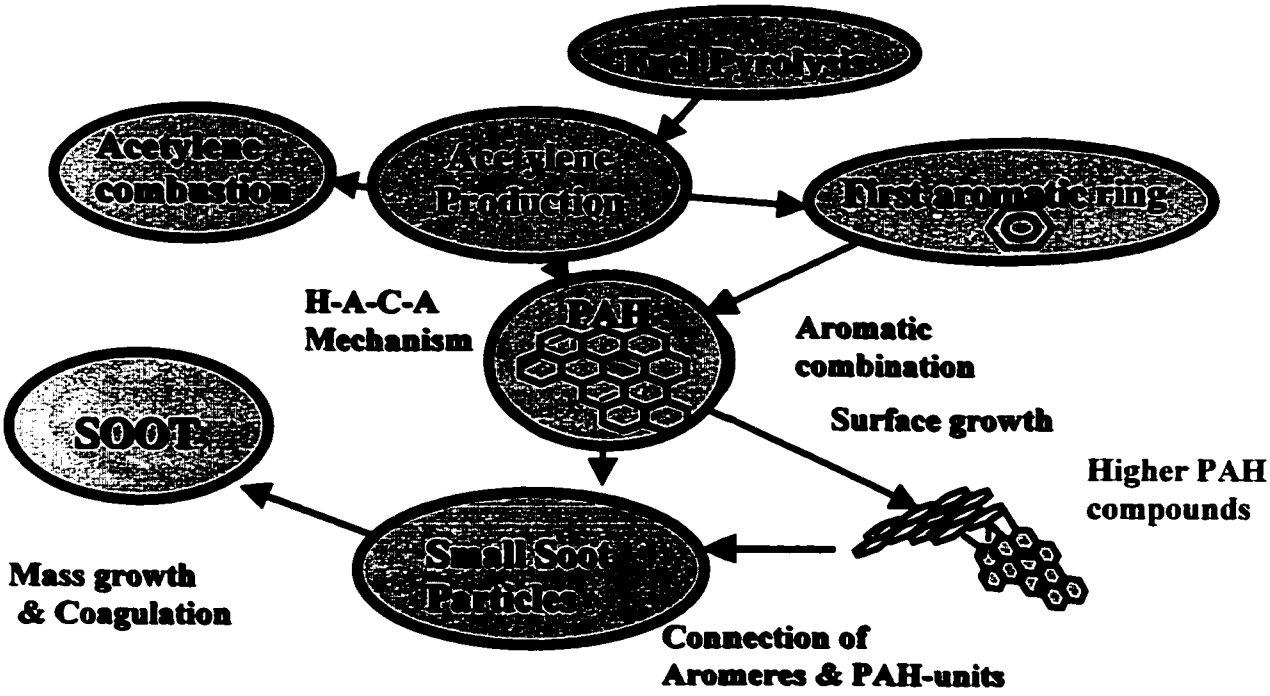

Fig 2-4: Schematic of the role of acetylene in soot formation.

The mass of the soot system can be described then, as coming from C_2H_2 through the growth of PAH that add to the soot and direct C_2H_2 addition to soot. The addition of C_2H_2 to PAH, however, is not itself sufficiently fast to account for the formation of the first soot particles also indicated as soot nuclei. The reactive coagulation of heavy PAHs, forming higher molecular compound (aromeres), can account for the rate of appearance of the small soot particles [5, 35]. Experimental studies with laminar premixed flames of ethylene concluded that the main surface growth species is acetylene and that surface growth exhibits first-order-kinetics with respect to the concentration of acetylene [5].

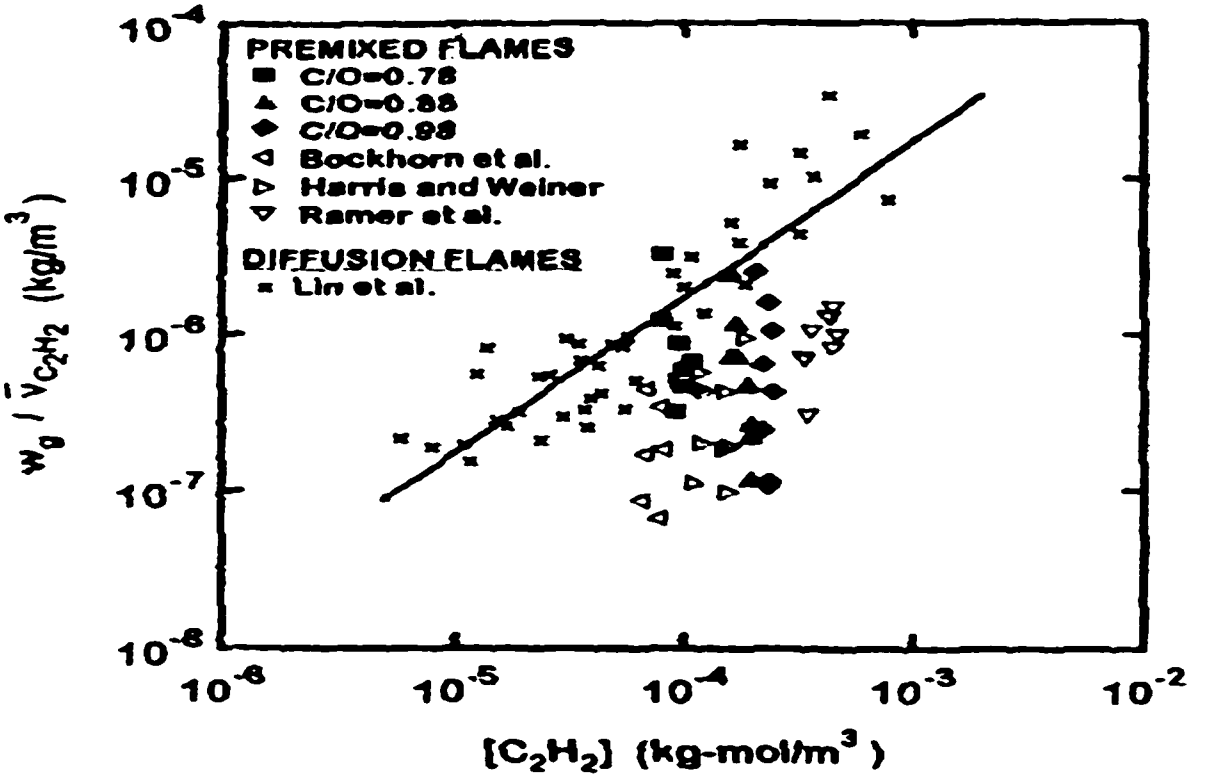

Figure 2-5: Soot particle surface growth rate as a function of acetylene concentrations for both laminar premixed and diffusion flames [33].

Figure 2-5 shows the soot particle surface growth rate as a function of acetylene concentrations for both laminar premixed and diffusion flames [33]. Premixed data and diffusion data are taken from different researchers as reported in Fig. 2-5. The line in the figure is the best-fit correlation for soot growth in the diffusion flames of Refs [33]; the axes anticipate simple collision efficiency for soot growth [33]. It is clear that acetylene is linearly linked to soot particle surface growth in diffusion flames. A detailed reaction mechanism for surface growth was suggested by Frenklach [23, 30]. At this point it is interesting to see how acetylene is a crucial species in soot formation modeling for non-premixed counter-flow diffusion flames.

2.6.1 Models linking acetylene to soot particle formation

There is fairly broad agreement from past experimental and theoretical work that the basic steps required to model the formation of soot particulate should include soot inception, surface growth, particle agglomeration and finally oxidation. Measurements indicate that soot formation is dependent upon the breakdown path of the fuel and the presence of pyrolysis products such as acetylene and polyunsaturated cyclical hydrocarbons such as benzene.

In view of the above a simplified approach for soot modeling has been adopted by Leung, Lindstedt and Jones in 1991 [17]. In this work, it is assumed that the presence of pyrolysis products is a crucial feature of the soot formation process and that the sooting propensity of a particular fuel-oxidant system is linked quantitatively to the regions of the flame where gas-phase pyrolysis occurs.

Here, acetylene is used as indicative species of the propensity of soot to form. The choice of acetylene is strongly supported by experimental evidence [17]. The proposed model would work also for other species commonly associated to soot formation such as C_6H_6, C_4H_2, and C_4H_6 because they show similar profiles but with varying magnitudes [17]. Good agreement with measured data for counter-flow propane and ethylene flames were obtained as well as for co-flowing methane flames [17, 29].

The nucleation steps used by Lindstedt, 1991 [17] can be written as,

$$C_2H_2 \rightarrow 2\ C(s) + H_2 \qquad (1)$$

The reaction rates are formulated as first order in the indicative species giving,

$R_1 = K(1)\left[C_2H_2\right]$ [kmol/m^3/s]

The notation C(s) is strictly speaking not correct as young soot particles contain significant amount of hydrogen, but it has been adopted as simplification note by the author [17, 29]. The second reaction responsible for soot mass formation is assumed to be surface growth due to the adsorption of acetylene on the surface of soot particles. It can be written as,

$$C_2H_2 + n\,C_S \rightarrow (n+2)\,Cs + H_2 \qquad (2)$$

With the reaction rate,

$R_2 = K\ f(As)\left[C_2H_2\right]$

Where f(As) is a function of the total surface area As ($m^2 / m^3 - mixure$). The notation s, indicates soot, the subscript n, the number of particles [17, 36, 29]. The oxidation step is assumed to be:

$$C_S + \tfrac{1}{2}\,O_2 \rightarrow CO \qquad (3)$$

The decrease in particle number density is simply assumed to occur accordingly to particle agglomeration [17]:

$$nC_S \rightarrow C_{n(S)} \qquad (4)$$

The reaction step, which is mainly responsible for the increase in soot mass, is then assumed to be surface growth due to the adsorption of acetylene on the surface of soot particles [29].

More recently, a comprehensive particle kinetics model has been applied to a non-premixed ethylene-air counter-flow diffusion flame at atmospheric pressure with the reactants at

room temperature [58]. Particularly interesting are the assumptions made; this model bases the inception step of soot formation on the local acetylene, benzene, phenyl, and molecular hydrogen concentrations. The rate of production of the poly-aromatic species in the soot formation process was estimated to be dependent on the acetylene and benzene concentrations as follows (1, 2).

$$\frac{d[C_{10}H_7]}{dt} = 10^{11.88} e^{(-4378/T)} \frac{[C_2H_2]^2}{[H_2]} [C_6H_5] \text{ cc/mole/sec,} \quad (5)$$

$$\frac{d[C_{14}H_{10}]}{dt} = 10^{12.50} e^{(-6390/T)} \frac{[C_2H_2]}{[H_2]} [C_6H_6][C_6H_5] \text{ cc/mole/sec,} \quad (6)$$

Where the gas-phase concentrations and temperatures are evaluated at local conditions; the inception rate, S_i (gr/cc-sec) was written as:

$$S_i = 127 \text{ x } \frac{d[C_{10}H_7]}{dt} + 178 \text{ x } \frac{d[C_{14}H_{10}]}{dt} \quad (7)$$

Where the constants above are provided to convert from molar to mass units. Thus, the expression above (7) links linearly soot formation to its most important precursors such as acetylene and benzene. Soot modeling in diesel engines has recognized the importance of acetylene as well. In particular the three reaction steps illustrated above (1,2,3,4) developed for the counter-flow configuration [17], were implemented and applied in the development of a soot particle model in diesel engines [25]. Therefore, acetylene is a crucial species in soot modeling for both counter-flow diffusion flames and diesel engines.

2.7 Pyrolysis of Alkanes

As we use propane as fuel, the understanding of the high-temperature oxidation of paraffin larger than methane is essential. This knowledge is somewhat complicated by the greater instability of the higher-order alkyl radicals and the great variety of minor species. Nevertheless, it is possible to identify the most important steps in this complex subject.

There are two essential thermal zones in flames [70, 54]: The primary zone in which the initial hydrocarbons are attacked and reduced to products (CO, H_2, H_2O) and radicals (H, O, OH) and the secondary zone in which CO and H_2 are oxidized. The intermediates are said to form in the primary zone. In oxygen-rich saturated hydrocarbon flames, they suggested that initially hydrocarbons of lower order than the initial fuel form according to Glassman, [70]:

$$OH + C_nH_{2n+2} \rightarrow H_2O + C_nH_{2n+1} \rightarrow C_{n-1}H_{2n-2} + CH_3$$

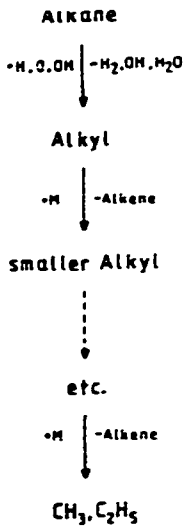

Figure 2-6: general scheme of alkane oxidation [59].

Because hydrocarbon radicals of higher order than ethyl are unstable, the initial alkyl radical C_nH_{2n+1} usually splits off an alkane, as shown in the schematic of Fig. 2-6.

As shown in Fig. 2-6, the pyrolysis process is initiated by rupture of the weakest bond (usually a C-C bond) to form radicals. At combustion temperatures, some CH bonds are broken and H atoms appear. The alkyl radicals decay into a smaller alkyl radical and an olefin (alkene). The initiation step provides H atoms that react with the oxygen in the system to begin the chain propagating sequence that nourishes the radical reservoir of OH, O and H. The chain of reaction is carried by H, CH_3 and possibly C_2H_5 and broken by various radical-radical terminations. Of importance is the decomposition by loss of H (or β-scission) of certain species of radical, until a radical is achieved that cannot decompose readily [54].

The problem of alkane oxidation can be reduced to the oxydation of methyl and ethyl radicals. In rich flames the oxidation of acetylene is a predominant part in the formation of

higher hydrocarbons independently of the nature of the fuels. Once the radical pool forms, the disappearance of the fuel is controlled by the reaction [70]:

$$RH + OH \rightarrow R + H_2O$$

$$RH + X \rightarrow R + XH$$

In the case of propane as a fuel, H, O and OH radicals provide the first attack as shown in the general scheme of alkanes oxidation (Fig. 2-6).

After this initial attack, thermal decomposition turns out to be the only relevant reaction of the higher alkyl radicals due to their thermal instability. Therefore, it is the task to determine the oxidation mechanism of the correspondent alkyl radical.

Propane leads to n-propyl and i-propyl radicals' (C_3H_7). These radicals decompose according to the β-scission rule. Thus, in the case of isopropyl radical, propene (C_3H_6) and an H atom form; in the case of n-propyl radical, ethene (C_2H_4) and a methyl radical (CH_3) form. More ethene (C_2H_4) than propene is usually found as an intermediary in the oxidation process of propane [70].

2.8 Soot formation and Flames

The tendency of fuels to soot has been measured in laminar premixed flames, laminar diffusion flames and turbulent diffusion flames. The amount of soot that will form from a particular combustion process is the result of sequential and overlapping steps more or less complicated by the nature of the flame itself. In laminar flame processes, the spatial distribution of the soot formation steps is sequential while in turbulent flames the processes are spatially mixed and complicated by the turbulent nature of the flow [68, 69].

In premixed flames, the chemistry is rate controlled while in non-premixed laminar flames, the chemistry is diffusion controlled. In this study, the focus is on laminar diffusion flames and in particular on counter-flow diffusion flames. However, a brief overview of how soot is related to the different type of flames is given as follows.

2.9 Premixed flames

From a thermodynamic point of view, in premixed flames, the formation of soot should only occur when in [68],

$$C_m H_n + 2yO_2 \rightarrow 2yCO + \frac{n}{2} H_2 + (m-2y)C_s$$

m becomes larger than 2 y, i.e. when the C/O ratio exceeds unity.

Experimentally, limits of soot formation are usually equated with the onset of luminosity, and this occurs not at C/O = 1 but usually in the vicinity of C/O= 0.5.

The tendency to soot can be correlated with the equivalence ratio at which luminosity just begins. The smaller the equivalence-ratio (ϕ), defined as the actual fuel-air ratio to the stoichiometric value, at the sooting point, the greater the tendency to soot [69].

2.10 Diffusion flames

In diffusion flames, fuel and oxidizer enter through separate inlet leads to a combustion process that is diffusion controlled, or, in more general terms, mixing controlled. Under such circumstances, the C/O ratio cannot everywhere stay below its critical limit. Thus, the formation and emission of soot from diffusion flames depends on the flow situation.

In gas jet diffusion flame tests, the tendency to soot is measured by the height of the fuel jet, or the mass flow of fuel, at which the luminous diffusion flame breaks opens near its apex and emits stream of particles. The smaller the flame height at the breakthrough (called the sooting height or smoke point) or the smaller the mass flow rate the greater the tendency to soot [72].

Fuel pyrolysis mechanisms have an important role in estimating the tendency of a particular fuel to soot. The sooting tendency of a fuel is strictly related to the flame temperature. Fig. 2-7 shows the critical sooting equivalence ratio at fixed temperature as function of the structure of 29 hydrocarbon fuels. There is a consistent increase in sooting

tendency as the adiabatic flame temperature increases. In fact, the higher the flame temperature, the greater is the rate of pyrolysis and the tendency to soot.

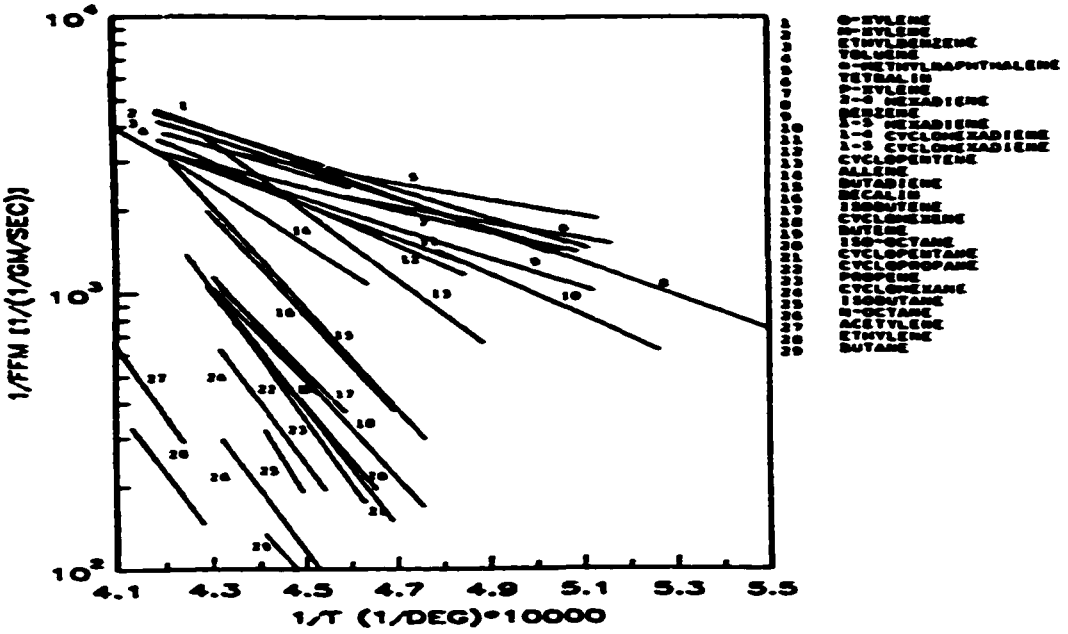

Figure 2-7: Sooting tendency of 29 hydrocarbon fuels plotted as the reciprocal of the fuel mass flow at the smoke height versus the reciprocal of the calculated adiabatic flame temperature [70].

Figure 2-7 also illustrates the effect of fuel structure. The sooting tendency generally increases with the carbon content for compounds of similar structure. For diffusion flames the order of the sooting tendency is [70]:

Aromatics > Acetylenes > Olefines > Paraffines > Alcohols

2.11 Influence of physical and chemical parameters on soot formation

The major physical effect on soot formation is the flame temperature. In fact, the temperature field of the flame determines the temperature-time history that the pyrolyzing fuel undergoes [20]. It plays an important role in the soot formation mechanism as the rate of fuel pyrolysis and polycyclic aromatic hydrocarbons (PAH) and C_2H_2 productions depend crucially on temperature. A review of critical temperature for soot formation draws the conclusion that the incipient particle formation controls the total mass of soot formed in any process [69]. The best approach to prevent soot formation and growth should then, prevent any soot particles from forming. However, it is the general complexity of the temperature, species and flow field in a diffusion flame that makes difficult to identify and control soot.

As regards the fuel molecular structure, the reciprocal value of the height at which a flame on a given burner starts to smoke and the limiting smoke-free fuel flow have been used to gauge the tendency of different fuels to smoke (the smoke point). This smoking tendency increases from paraffin to mono- and di-olefines, benzenes and naphtalenes. Generally the larger the molecule, the greater the smoke emission. Fuels with high sooting propensity produce smoke at low flow rates and short flame length, whereas low sooting fuels require higher flow rates to emit smoke [68, 70].

The effect of pressure on soot formation in diffusion flames has been investigated over a wide range of conditions. Generally speaking, low pressure reduces carbon formation while high pressure promotes it. In particular, in shock tubes, under high-

pressure conditions, the produced soot volume fraction is proportional to the square of the fuel partial pressure [68].

2.12 Influence of additives on soot formation

The effects of the addition of various gaseous compounds to the fuel flow have been investigated by many researchers. There are several means by which additives could affect the behavior of a diffusion flame. The most severe effect would be chemical reactions with the fuel, fuel pyrolysis products or with oxygen in competition with the fuel. Excluding chemical reaction, the additive can act basically through two mechanisms: The additive can participate in heat transport, which will be a diffusion process with thermal diffusivity and thermal conductivity as the important properties. It can also act as heat sink, in which case the specific heat (C_P) becomes the important parameter.

According to their ability to reduce or increase the sooting tendency of a diffusion flame, additives can be distinguished into two classes: soot suppressing and soot increasing. Most compounds are found to act as inert gases in decreasing the tendency to soot. Their effectiveness is found to be proportional to their molar specific heat (C_P).

Additives such as CO_2, SO_2 and water vapor reduce the sooting tendency of the flame purely thermally. Researchers have suggested that their influence is exerted primarily in the soot oxidation zone where these species probably promote soot burnout; a similar mechanism has been proposed also for SO_2; however, for the most part, reductions in sooting tendency are brought about thermally. If inert species are added to

the fuel, the greater their specific heat, the greater their effectiveness in soot reduction [69].

Additives such as N_2O and O_2 increase the sooting tendency when trace amounts are added to the fuel; halogens promote soot formation as well. Other compounds, such as SO_3, can suppress soot in diffusion flames but increase soot in diffusion flames [70]. Oxygen, added to the fuel stream of a diffusion flames causes an increase in temperature and a catalytic effect that leads generally to more soot production [72]. When soot suppressing additives are added to the fuel stream, as a function of the volumetric flow rate, even if there is no apparent change of the flame height, the behavior of the diffusion flame changes in the way that it can take an additional amount of fuel flow without more soot production. [72].

Striking effects on soot reduction are produced by various metal additives such as iron, nickel, manganese, and the alkaline earth metals [70, 69]. Although numerous researchers have been focusing on the effect of additives on soot formation, the mechanisms involved in soot suppression are not completely clear.

2.13 Fuel dilution effect

Particular attention in this study is given to fuel dilution and chemical additive effects on soot formation.

Inert addition has been employed as a useful technique for studying soot formation in diffusion flames [10, 69]. The addition of an inert to either or both the fuel and oxidizer streams modifies not only the flame temperature but also the reactive-

species concentration of the respective stream. Specifically, it was found that adding argon and nitrogen to a co-flow flame for the same adiabatic flame temperature, the argon-diluted flame had a lesser propensity to soot. Since a greater amount of argon dilution than nitrogen was required to reach the same adiabatic flame temperature, its smaller tendency to soot suggested that reduced fuel concentrations lowers soot formation [71]. The conclusion is that the amount of soot reduction with fuel dilution is due to the reduction in flame temperature and that fuel concentration can be a significant factor in influencing the soot production rate.

Experiments conducted in a counter-flow diffusion flame to isolate the temperature effect from the dilution effect showed that nitrogen addition to the fuel (ethylene) resulted in soot reduction as a consequence of both dilution and temperature reductions. Dilution has a significant influence on the soot production rate and its effect is primarily felt in the inception stage of the soot formation process [74]. Figure 2-8 shows the effect of dilution on soot formation for a counter-flow ethylene diffusion flame; the fuel is diluted with nitrogen in different percentages. As nitrogen % increases the soot volume fraction decreases.

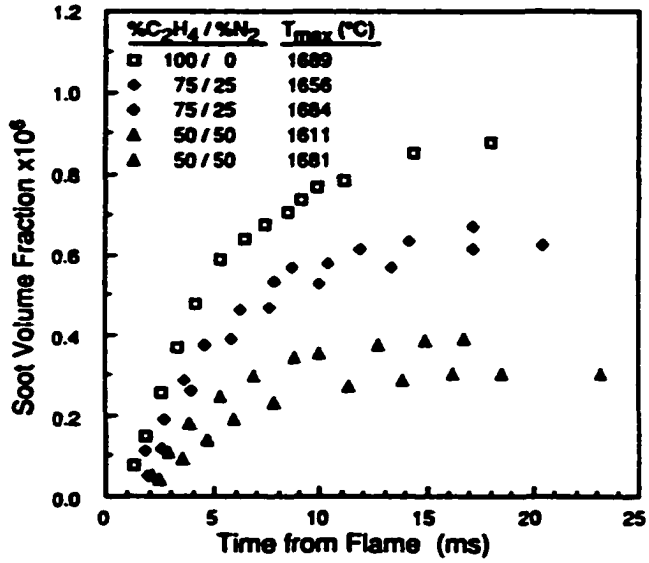

Figure 2-8: Soot volume fraction as function of time for the flame front [74].

2.14 Chemical effect

One of the most practical approach to soot reduction is to blend additives into the fuel to alter the soot nucleation and growth processes or to enhance soot oxidation [6].

Soot suppression by alcohol addition has been observed both in shock tubes and in flames [6]. The effects of ethanol (C_2H_5OH) and methanol (CH_3OH) addition to benzene flames have attributed the suppression effect to enhanced oxidation of soot and soot precursors by OH radicals generated from alcohol pyrolysis and removal of hydrogen atoms [75]. The most effective gaseous soot suppression additives appear to be sulfur compounds such as H_2S and SO_2 [6].

Other authors suggested that alcohol additions reduces soot by the same amount as other soot-controlling additives, indicating the dilution of the fuel concentration to be the dominant factor in soot reduction [76].

In the case of methanol (CH_3OH) and carbon disulfide (CS_2), added to ethane diffusion flames, researchers differentiated the chemical effects from the dilution and temperature effects. They concluded that methanol addition reduces the formation of soot particles by retarding the formation of the key soot precursors (PAH) or oxidizing them through OH attack [6]. In order to further understand the role of the hydroxyl group (OH) in alcohol addition, three other alcohols (ethanol, 1-propanol, and 2-propanol) were added to an ethane laminar diffusion flame; methanol, among the others, reduced soot significantly, while ethanol and propanol had less effect on the soot concentration. This was addressed to differences in methanol pyrolysis, according to the fact that methanol pyrolysis generates more OH radicals than ethanol; OH radicals can oxidize soot particles or soot precursors, reducing soot [6].

A hydrogen removal mechanism, to explain the effect of alcohol addition on soot formation, was also proposed by Frenklach and Yuan (1987). According to that, hydrogen atoms were removed through the following reactions:

$$H + ROH \rightarrow H_2 + RO$$

$$H + ROH \rightarrow H_2 + R'O$$

$$H + ROH \rightarrow OH + RH$$

Hydrogen atoms in fact, are believed to play a key role in the production of reactive radical species in the formation of soot precursors. Removal of hydrogen should slow down the reaction toward soot formation [75].

2.15 Additives in Diesel engines

In Diesel engines particulate emissions are in the form of complex aereosols consisting primarily of soot and volatile organics. The dimensions of these particles are very similar to those obtained from atmospheric diffusion flames of gaseous hydrocarbon fuels (from 10 to 1000 nm) [20]. Many studies have been focused on fuel additives as particulate reducers. Fuel additives can have substantial effects on the engine's fuel spray penetration, fuel-air mixing process, ignition delay, chemical reaction rates, and total heat release.

A variety of fuel additives have been proposed for soot reduction. Fuel additives used in diesel engines have been classified into four categories: the fuel injection deposit cleaning detergents, the cetane number improvers, the combustion process promoters and the oxygenates [19, 16, 18, 19].

The deposit cleaner acts as the anti-oxidant, which can block out the deposit surface oxidation process. These "cleaning detergents" are generally composed of organic compounds and are very effective on deposits. Good reductions have been found on smoke as well as CO and HC levels with their use, but increases in NO_x levels have been observed. Cetane number improvers such as DTBP (di-t-butyl peroxide) or EHN (2-ethylhexyl nitrate) reduce NO_x as well as smoke emissions.

Oxygenated additives such as methyl-tertiary-butyl-ether (MTBE) or dimethyl carbonate (DMC) act on the oxygen composition in the fuel-air mixture causing changes in diesel engine's combustion and emission characteristics. MTBE has long been

extremely effective on gasoline engine's exhaust emissions and, applied to diesel fuel, can lower smoke and NOx, but it has been criticized for causing human health problems.

Many authors have tested oxygenated compounds as diesel fuel additives. Specifically an investigation of the effect of eight kinds of oxygenated agent addition to fuels on diesel combustion (4-stroke cycle, single cylinder, DI diesel engine) has been carried out [15]. Results showed significant soot suppression. In particular, it was found that particulate emissions decreased linearly with increasing oxygen content in the fuel. The improvement in smoke and particulate emissions with the oxygenated agents was more significant for low volatility fuels. Dimethyl carbonate (DMC), among other oxygenated fuel additives, presented better reduction on smoke and NO_x. It is characterized by higher oxygen content, higher specific gravity and lower boiling point and molecular weight (see Table 2-4). DMC is also soluble in diesel fuels.

Table 2-1: Oxygenated Fuel Additives chemical characteristics [15].

Oxygenated additives	Oxygen content wt-%	Specific gravity (g/cm^3) at 15 C^0	Calorific value MJ/Kg	Boiling Point (C^0)
Dimethyl carbonate	53.3	1.079	20.2	90
Diethylene Glycol Dimethyl Ether	35.8	0.948	28.1	162
Ethylene Glycol Mono-n-butyl Ether	26.9	0.905	32.4	171
Ethylene Glycol Mono-t-butyl Ether	26.9	0.903	32.4	152
Di-n-butyl Ether	12.3	0.771	38.7	142
Propylene Glycol Mono-t-butyl Ether	24.2	0.879	33.5	-
2-Ethylhexyl Acetate	18.6	0.878	35.2	199
Ethylene Glycol Mono Butyl Ether Acetate	30.0	0.945	30.3	-

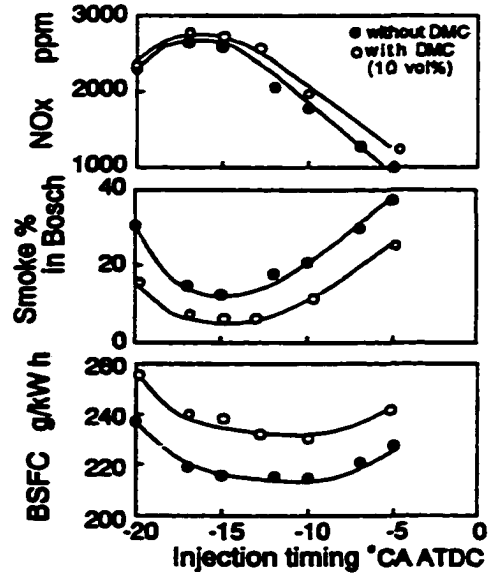

Fig.2-9: Effect of DMC addition for various fuel injection timings [15].

DMC added to fuel in 5% and 10% suppressed smoke and particulate significantly in comparison to other oxygenated additives in diesel engines; however, no analysis of the influence of the additive on combustion and soot evolution was done [15]. Oxygen in fuel produces lower flame luminosity and soot formation and faster oxidation process that pure diesel fuel. Results show that during the initial stage of the thermal cracking, the presence of oxygen reduces the formation of unsaturated compounds such as acetylene, ethylene, benzene, etc. [77]. Studies showed that the evolution of acetylene concentrations in diesel engines, is influenced by parameters such as fuel oxygen content and fuel cetane number; [77].

More recently, DMC has been added in the same amount (5% and 10% by volume) to diesel fuel [19]. Reduction has been registered on the exhaust gas temperature as well as on NOx, HC emissions and smoke opacity. The increase of DMC additive

dosage from 5% to 10% showed further reductions while other additives, including ethanol showed the opposite trend on NOx and HC emissions.

Ethanol added in 10% and 20% by volume in the same conditions showed particulate reductions as well. Figure 2-5 shows the effect of various fuel additives on the smoke opacity [19]. Best reductions were obtained with 20% ethanol addition on smoke opacity. Both DMC and ethanol showed better results when the dosage was raised.

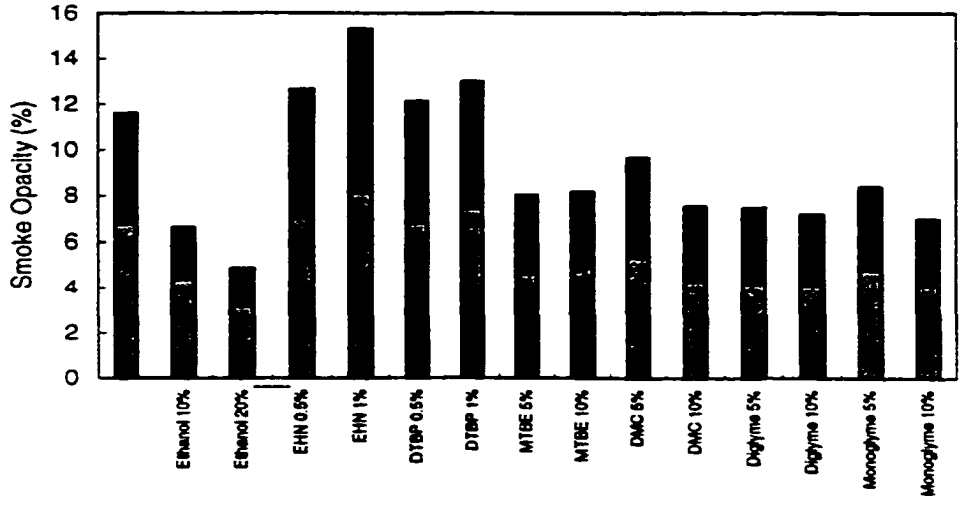

Figure 2-10: The average (engine load and engine speed) effects of various brand of fuel additives on smoke opacity [19].

Since ethanol as an additive is not naturally soluble in diesel fuel, changes of surface tension and viscosity (ethanol has low viscosity) of the mixture can cause substantial variation in the characteristics of fuel spray combustion patterns. Its mechanism on soot formation is then not completely clear.

2.16 Laboratory diffusion flames

From the previous discussion on soot characteristics for premixed and diffusion flames, soot mechanisms result more complicated in diffusion flames because of the important role of flow characteristics in the formation, growth and oxidation of soot. As a consequence the understanding of soot formation mechanisms is not as conclusive as that for premixed flames. In the case of diffusion flame, it is necessary to carefully examine the gas-phase flow field, particle path and species diffusion. Thermophoresis, caused by the temperature gradient, can also play a role in the examination of soot formation mechanisms for diffusion flames [36, 20, 41]. For this reason, easily controlled laboratory flames result more suitable for experiments on soot formation. Commonly used type of laminar diffusion flame burners for soot studies are:

- The co-flow burners
- The counter-flow burners

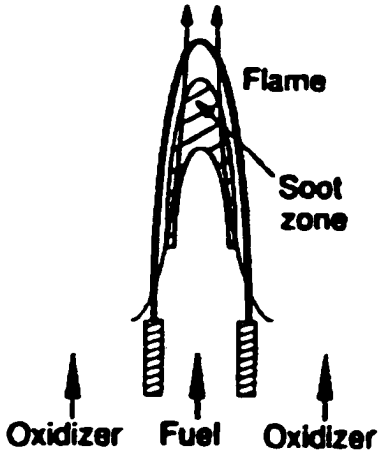

Fig. 2-11: Normal Co-flow diffusion flame burner [7].

Co-flow burner flames are radially axysimmetric two-dimensional flames with good stability (see Fig. 2-11). A normal co-flow flame surrounds the fuel stream ejecting from a center nozzle whereas an inverse co-flow flame surrounds the oxidizer stream ejecting from a center nozzle. Soot particles move toward the flame in normal co-flow while they move away from the flame for inverse co-flow. Most of the research work on soot formation and oxidation has been conducted on co-flow laminar diffusion flames. A schematic representation of soot aggregate evolution in the co-flow ethylene laminar diffusion flame is reported in Fig. 2-12.

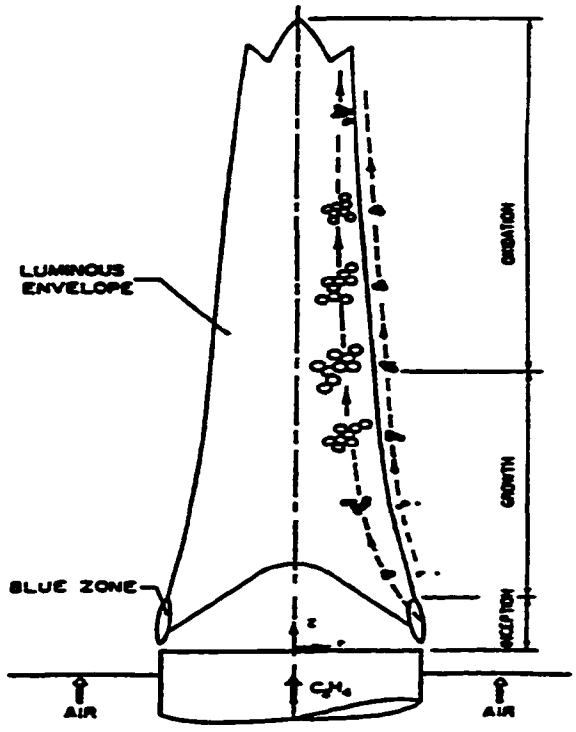

Fig 2-12: Local soot loadings in an n-hexane/air diffusion flame [69].

Counter-flow burners, although they may suffer from instability problems under certain flow conditions, produce a more convenient one-dimensional flame, as discussed below.

2.16.1 Counter-flow diffusion flames

The soot mechanism in co-flow diffusion flames is more difficult to interpret than the counter-flow configuration because of the complicated flow patterns and the intrinsically two-dimensional structure.

Counter-flow non-premixed flames result when reactant streams flow toward each other in a stagnation point flow, that is characterized by zero velocity in axial direction for both fuel and oxidizer (see Fig. 2-13). The great advantage of using such a burner is that the resulting flame structure is steady and one dimensional in temperature and species concentrations.

The stagnation point flow permits a similarity solution, facilitating mathematical analysis and computational simulation. The counter-flow configuration results particularly attractive for studies on soot formation because it provides a well-defined one-dimensional system convenient for both experiments and theoretical modeling [20,10, 4, 10, 78, 41, 67].

2.16.2 Sooting structure in counter-flow diffusion flames

The flat diffusion flame, established in the counter-flow burner, consists of an oxidant side and a fuel side, separated by a reaction zone and the hot products (Fig. 2-13).

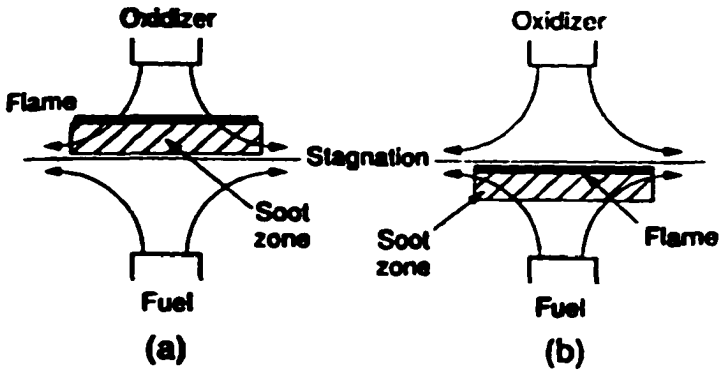

Figure: 2-13: Counter-flow diffusion flames located on the oxidizer side (a) and on the fuel side (b) [7].

The sooting characteristics for counter-flow flames can be significantly affected by the flame location. When a diffusion flame is located on the fuel side, the gas velocity is directed toward the flame and soot particles approximately follow the streamlines. When the flame is located on the oxidizer side, instead, the gas velocity is directed to the stagnation plane and soot particles move away from the flame. Soot particles are convected away from the flame by the gas flow and by the thermophoretic velocity, generated by the temperature gradient. When the flame is located on the fuel side, the convection velocity in the soot zone is toward the flame. The two velocity components of convection and thermophoresis are in opposition. It is because of this that the sooting characteristics of the two flames are expected to be quite different [7]. The criterion for the flame to be located on the fuel side is expressed as [7]:

$$\frac{Y_{O_0}\sqrt{Le_O}}{Y_{F_0}\sqrt{Le_F}} \rangle \sigma \qquad (1)$$

where Y_I is the mass fraction, σ the stoichiometric oxidizer to fuel mass ratio, Le is the Lewis number and subscripts F, O and 0 indicate fuel, oxidizer and free stream

respectively. In the case of propane as fuel (Le_F = 1.37, Le_O= 1), the criterion for the flame to be located on the fuel side is represented in terms of mole fraction X as

$$X_{O,0} > 4.3\, X_F. \qquad (2)$$

A schematic of the sooting structure for a methane counter-flow diffusion flame with preheated reactants is shown in Fig.2-13. In this work, a three-color flame with an extension of 1 or 2 mm was observed [60]. While traveling along the central streamline from the oxidizer side to the fuel side, first a blue flame is encountered in which the peak temperature (~ 1900 K) and primary combustion reactions occur. Next a bright yellow zone is encountered characterized by a temperature range of 1500 – 1800 K. A thin dark orange zone was also observed. They conclude that soot precursors are formed in the yellow zone but their concentration is not high enough for inception. Soot inception occurs at the diffusion interface between the yellow and orange zone; here the temperature is between 1200 K and 1600 K. This sooting structure is more simplified in comparison with the hexane co-flow diffusion flame reported in Figure 2-12 [69]. Therefore the investigation of additives on soot precursors is more suitable with the counter-flow diffusion flame configuration.

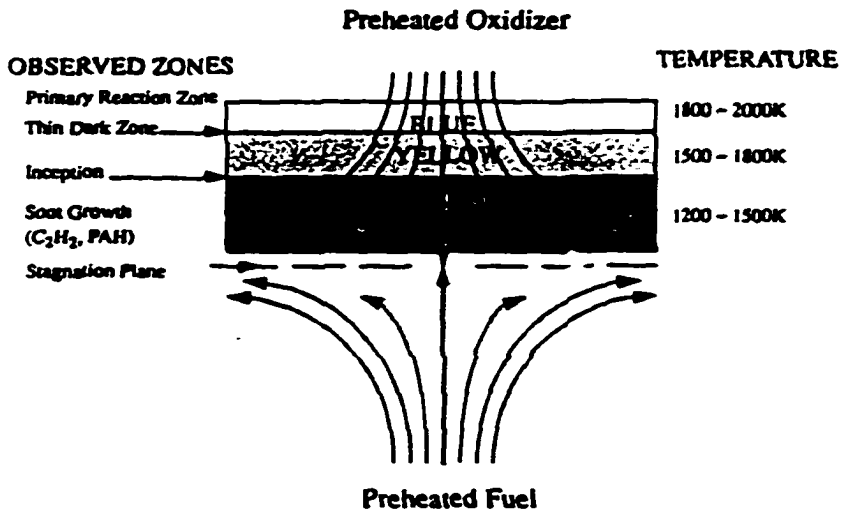

Figure 2-14: Schematic of the counter-flow diffusion flame structure for methane fuel [60].

2.17 Summary

The literature on soot formation shows that although this is a very complex process, it is possible to recognize the main paths that lead from soot precursors species to the final production of soot particles. Precursors formation, particle inception, particle growth and particle oxidation have been proposed to be the main steps of the soot formation process. Acetylene is the most important product of fuel pyrolysis in the sooting zone of a flame. As discussed before, acetylene is a key species in the formation of the first aromatic ring as well as in the formation and growth of PAHs through the HACA mechanisms.

Focus of this study is the formation of soot precursor species, such as acetylene and benzene. Because of the central role of acetylene as soot precursor, particular attention will be given to this compound within this study.

The counter-flow diffusion flame configuration simplifies the structure of the flame to a one-dimensional system. The result is that the sooting structure of the flame is easier to follow and a better understanding of soot precursor formation mechanisms is possible.

The investigation of the effects of oxygenated additives such as DMC and ethanol on soot precursors in counter-flow propane /air diffusion flame is conducted as they have been suggested from the literature to reduce soot in diesel engines.

CHAPTER 3: APPARATUS AND PROCEDURES

This chapter presents the experimental setup used for the analysis of the flame composition. It describes the counter-flow diffusion flame burner, developed and adopted in this study, the additive addition system, the sampling line for gas extraction across the flame and the methodology used for gas sample analysis. Sampling is accomplished using a quartz micro-probe, a micrometer for probe positioning and a vacuum pump, operating at low pressure to quench reactions in the probe tip. The additive is first vaporized, using a hot bath, and then added to the fuel stream. After extraction, gas samples are directly analyzed by a Gas chromatograph (GC) provided with Flame Ionization Detector (FID) and capillary column for extended analysis of hydrocarbons. Figure 3-1 shows a schematic of the experimental setup.

Experimental setup

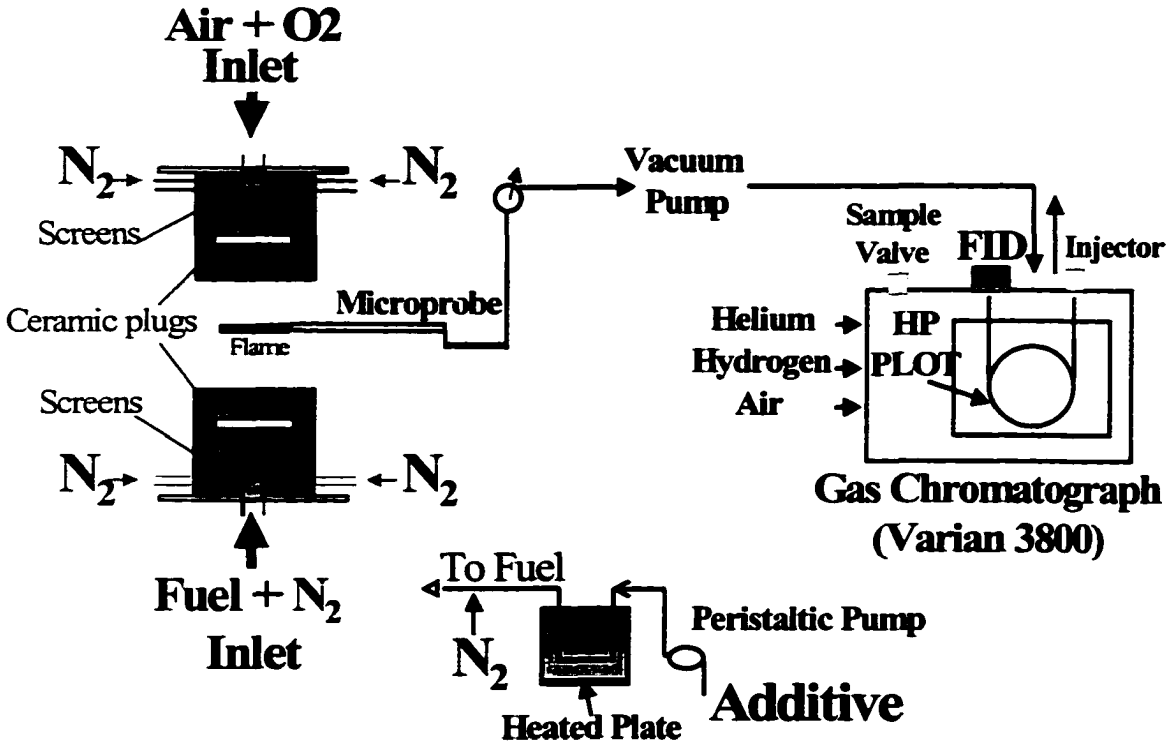

Figure 3-1: Schematic of the Experimental Setup; not to scale.

3.1 Burner Setup

Counter-flow non-premixed flames result when reactant streams flow toward each other in a stagnation point flow. As it simplifies the flame analysis to a one-dimensional system, a counter-flow non-premixed burner has been designed and adopted for this application.

The burner consists of two opposing identical stainless steel ducts that direct the fuel stream and oxidizer stream into a stagnation point flow. Two co-axial cylinders, with 2.2" and 2.62" inches inner diameter respectively, form an inner tube for the main flow (fuel or oxidizer stream), and an annulus for the nitrogen co-flow. The dimensions adopted for the cylinders minimize edge effects. The two cylinders are mounted co-axially. A schematic of the counter-flow diffusion flame burner is shown in Fig 3-2. The top duct is held in place by three stainless steel rods with threaded ends screwed into the support base of the bottom duct. The distance between the upper and lower duct is adjustable. Turning the rods allows both a fine adjustments of the burner lips separation and a minor tilting to obtain a horizontal flame.

In order to produce uniform, laminar flow, and to help quench the flame in the event of flashback, porous ceramic plugs (Hi Tech, porosity 0.80 PPI), 2-inch wide and 1-inch thick, are used [32, 33, 34]. They are placed in two small identical stainless steel cylinders (2.2 inches OD and 2.1 inches ID) located respectively inside each duct as shown in Fig. 3-2. Two identical metal devices, provided with very small holes along their cylindrical lateral surface, are located right at the outlet of the fuel and oxidizer streamlines (1/4" inches Swagelock) to spread the flow in the horizontal direction and

reduce turbulence. To ensure sufficiently flat velocity profiles at the duct exits, fine wire screens with same ID as the ducts are placed inside and on the top of each duct, [32, 33, 34].

This burner produces a steady and one-dimensional flame structure, approximately in the center of the two ducts. This flat profile for the flame is obtained by keeping the same velocity for both fuel and oxidizer streams and a fixed distance of 20-mm between the duct lips, [32, 33, 34, 35, 37]. The flame profile is stable regardless of the velocity chosen for the flow streams. A constant velocity of 10 cm/sec was adopted.

Chemically pure grade propane (Matheson, purity 99.95 % min.) is used as fuel. Propane has been chosen as a fuel because (1) it is a gas, (2) its detailed chemical kinetics is known and (3) it is an alkane like a substantial fraction of diesel fuel. Commercial nitrogen is used to dilute the fuel flow while oxygen (Matheson Extra Dry 99.6% min.) is added to the airflow to improve combustion. Propane mixed with nitrogen enters from the bottom of the lower duct, while the oxidizer, composed of air and oxygen, enters from the top duct (see Fig. 3-2). A surrounding annular shroud flow of nitrogen is also used to isolate and stabilize the flame such that entrainment and flame flickering are minimized [32, 33]. Gas flows are controlled by high accuracy calibrated rotameters (Matheson 605 and 603).

Burner Setup

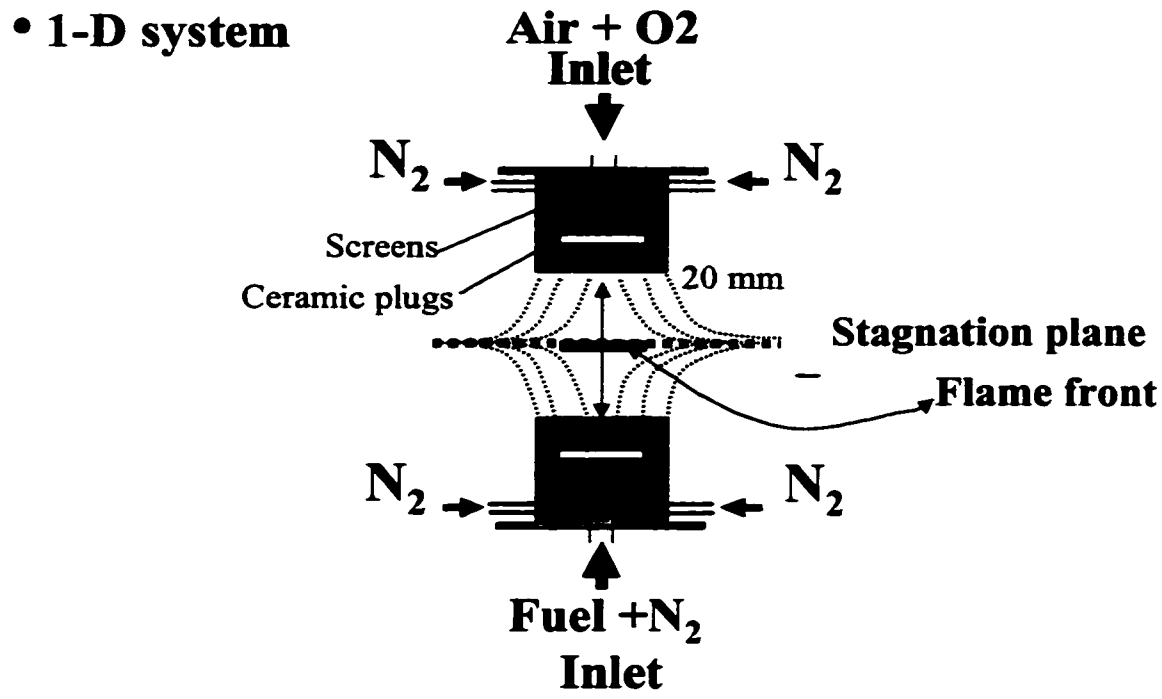

Fig 3-2: Schematic of the counter-flow diffusion flame burner.

The diffusion flame is located on the fuel side just below the stagnation plane. Usually counter-flow diffusion flames are located on the oxidizer side when pure hydrocarbon is the fuel; the flame can be located on the fuel or oxidizer side if inert gases are used in the fuel or oxidizer stream (see chapter 2). Sooting characteristics are also influenced by the flame location in the counter-flow and for a flame on the fuel side the gas velocity is directed toward the flame and soot particles approximately follow the gas-phase streamlines [36]. This is discussed in more details in chapter 2.

The flame is lightly-sooting (ϕ=1.79) and exhibits a yellow-orange luminosity; the size and the intensity of the luminous yellow and orange zone indicate the presence of higher molecular weight hydrocarbons and soot. The flow rate is kept constant on both fuel and oxidizer side. Flame characteristics are reported in Table 3-1.

Table 3-1: Flame Characteristics.

Equivalence Ratio (ϕ)	N2/O2 (mol basis)	Flow Velocity (cm/sec)	Flow-rate (SLPM)	Composition (mol basis) Oxidizer side %		Fuel side %	
1.79	3.03	10	13.46	O_2	30.1 %	N_2	83.7%
				Air	68.9%	C_3H_8	16.3%

A lightly-sooting flame with the characteristics above was chosen as it is more convenient for gas sampling. In fact, if the flame is very sooting, excessive soot levels can plug the probe orifice during sampling. In addition, soot formation can easily complicate flame sampling because of possible retention of PAHs on probe and soot surface [36]. On the other hand, with this flame condition, the flame temperature is not too high and quartz can be used for gas sampling [36, 34, 35].

The resulting flame is steady to the naked eye; measurements at the flame plane, using a micrometer, attest in fact that the flame front position moves slightly (order of a fraction of a millimeter).

3.2 Additive addition setup

Oxygenated additives are added to the fuel stream to evaluate their effects on soot precursor formation. Candidate oxygenated additives include dimethyl carbonate (DMC) and Ethanol. They are vaporized by flowing them through a heated bath of water. A schematic of the additive addition setup is reported in Fig. 3-3. The bath consists of a vessel containing ordinary water sitting on a heated plate. A peristaltic pump (Cole-Palmer/Masterflex) flows small amount of liquid additive (max 13 SLPM) through copper tubing immersed in the bath; this evaporates the additive. The additive boiling temperatures are below that of water (see Table 3-2). As soon as the additive evaporates, it mixes with N_2 and it is added to the fuel stream. The connection between the nitrogen line and the additive line is heated with heating tape to ensure that the additive is kept in the gas phase.

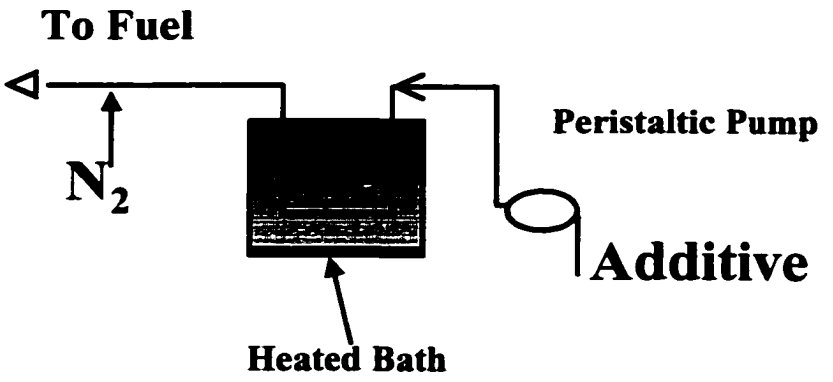

Figure 3-3: Additive addition set-up; not to scale.

Table 3-2: DMC and Ethanol chemical characteristics [15, 39, 40].

Species	Molecula structure	Molecular weight (g/mol)	Volume percent (%)	Boiling point (C^0)	Calorific value (KJ/mol)	Oxygen content (wt-%)	Specific gravity (g/cm^3)
DMC	$C_3H_6O_3$	90	10%, 15%	90	1818	53.33	1.369
Ethanol	C_2H_5OH	46.06	10%, 15%	78.5	1368	34.07	0.788

3.3 Gas sampling system

Experiments are conducted at atmospheric pressure using the flat flame burner previously described. Sampling is accomplished by continuously withdrawing gases from within the flame using a quartz micro-probe. Gases flow through Teflon lines to a filter, and a vacuum pump, which pushes the sample directly into a Gas Chromatograph (GC) provided with Flame Ionization Detector (FID) and capillary column for flame analysis (see Fig. 3-1).

The microprobe is characterized by a 1mm outer diameter at the tip and an orifice of a fraction of a millimeter (see Figure 3-5). Micro-probes, because of their small perturbation of flow fields, are of considerable utility in acquiring information on the concentrations of stable species in reactive systems such as flames [40, 41, 42, 44,45]. The effects of micro-probe size, shape, orifice diameter, and back-pressure on flame sampling have been investigated [40, 41, 42, 44,45]. These and related studies suggest that using smaller probes and low pressures, e.g. 50-100 Torr and below, provides accurate data on flame composition. In fact, rapid temperature drop is not a prerequisite for successful flame sampling; simultaneous reduction of pressure and the destruction of free radicals on the probe walls are sufficient to stop reactions [42]. Figure. 3-4 shows how important is pressure value during sampling. The dependence of CO measurements on probe pressure is reported for two flame conditions (ϕ =0.85, fuel-lean and ϕ =1.35, fuel-rich) in the pressure range (50- 500) Torr. The measured amount of CO increases as pressure in the probe decreases, for both quartz and water-cooled stainless probe [40] (see fig. 3-4).

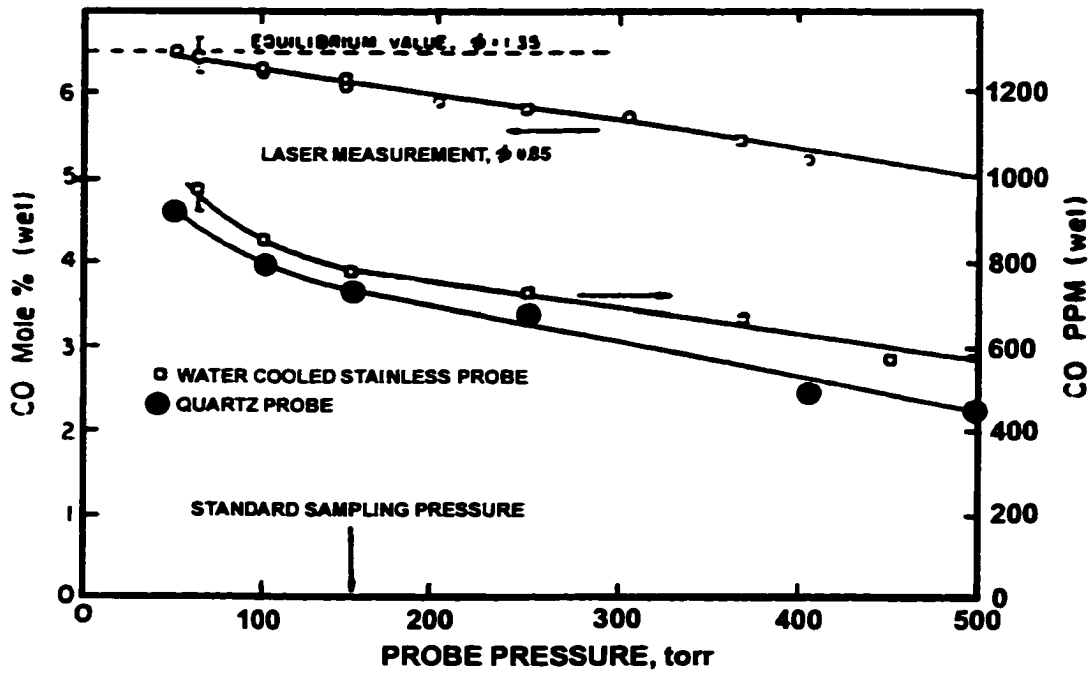

Figure 3-4: Dependence of CO measurements on probe pressure for two flame conditions (ϕ =0.85, ϕ =1.35) for two type of probes (water cooled stainless steel/quartz) and laser adsorption spectroscopy [40].

Thus, the back-pressure in the probe must be kept low in order that the chemical reaction are rapidly frozen on passing through the nozzle. A decrease in the sampling pressure increases the rate of recombination of active species such as OH, O and H, and reduces the residence time of the sampling in the hot region of the probe. Thus, quenching efficiency is dependent on sampling pressure [43, 40, 44].

Although sampling probes inherently interfere with the flow, the careful design of this micro-probe and its dimensions allow the acquisition of sample gases with low visible disturbance to the flame. Both cooled and uncooled quartz micro-probes have been tested in the flame but the uncooled one worked best. A schematic of the micro-probe used in this application is reported in Figure 3-5.

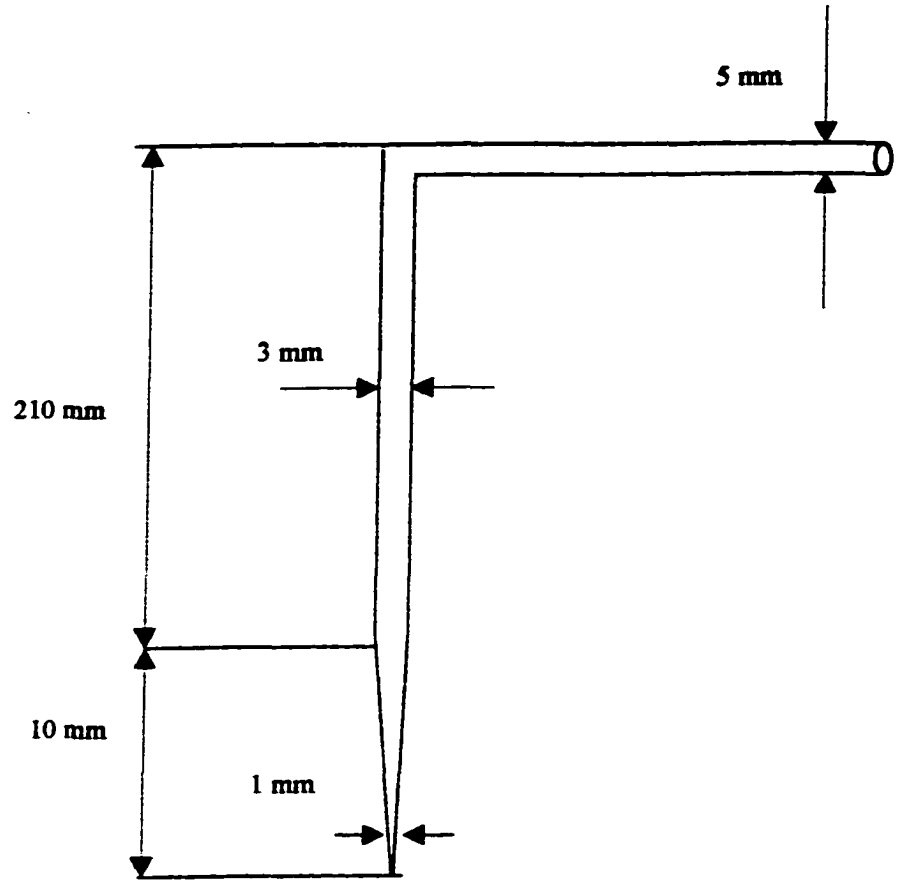

Figure: 3-5: Schematic of the quartz micro-probe; not to scale.

It is made of 3-mm outer diameter quartz; it narrows to 1-mm outer diameter over the last 10 mm of its length and it has a very small tip with inner diameter of fraction of a millimeter (0.73-mm). This orifice size, among others, better managed to resist soot clogging.

Quenching of reactions at the tip of the micro-probe is ensured, in this application, through the use of a dual stage heated head vacuum pump downstream from the sampling line. Rapid cooling in the probe tip, in fact, prevents reactions in the sampled gases. This vacuum pump (KNF UN035.3ST.11I) maintains low pressure in the

system to ensure quenching; at the same time, it pushes the sample directly into the GC for further analysis. It has a heated head to prevent any possible condensation. The performance characteristics of the dual stage heated head vacuum pump used are reported in Appendix A: Experimental set up.

After extraction the gas sample flows through Teflon lines (1/4 inches outer diameter) from the microprobe to the Gas Chromatograph (GC Varian 3800). Teflon tubing is used, as it is chemically inert and well suited for high-temperature work. A vacuum pressure gauge records the pressure at the probe outlet and soon after a filter traps any substance that can cause contamination downstream in the GC. The last part of the Teflon line, connecting the vacuum pump to the GC inlet, is heated to avoid condensation.

3.4 Measurement procedures

The burner remains stationary during measurements while the microprobe is moved by a high precision micrometer to obtain a profile of species across the flame. A micrometer holds and moves the probe with accuracy across the flame in the vertical as well as in the horizontal plane. The probe is positioned along the central axis of the burner. The distance between the two ducts is kept at 20-mm. The flame plane sits at 9 mm from the lower duct lip of the burner; this is used as a reference point during measurements. The value recorded by the pressure gauge during measurements across the flame is 23 in. Hg vac and it is constant during sampling.

Measurements are taken as follows: As soon as the flame with specified characteristics (see Table 3-1) is ignited we wait a few minutes until the gas flow rate has stabilized. The microprobe is fixed in the micrometer and it is always located along the central axis of the flame during sampling each time; it is then moved in the vertical direction to identify flame species profiles.

A baseline for the gas chromatograph analysis is conducted daily, before starting experiments, to make sure that the GC is functioning correctly. Flame plane position is daily controlled through micrometer for flame stability check. A value of 9-mm has been registered for the flame position in most of the cases except very small fluctuation (order of fraction of mm). Our reference point is the lower part of the burner (fuel side). This means that the flame sits 9-mm above the lower part of the burner. However, during the flame profile analysis other reference points are the flame plane and the upper part of the burner kept at the fixed distance of 20-mm from the lower part. Measurements have been taken in a random order at different positions. Experiments were repeated many times to check the reproducibility of the sampling technique adopted. Small scatter has been found (see chapter 4). During measurements, the probe is constantly maintained in the flame and the flame is kept on during the experiments. The sampling line is filled while keeping the probe in the same position in the flame for 22 minutes and using the vacuum pump specified before, to push the sample downstream toward the gas chromatograph for flame component analysis. This timing (22 minutes) is needed by the GC to analyze a sample with the temperature program adopted for the column (see Fig.3-6). During sample injection into the GC column, the vacuum pump is shut down to avoid any change in pressure. Low values in pressure during the GC analysis showed destabilization of the

FID (flame out) and differences in the size of the sample. Atmospheric pressure is then a necessary condition to guarantee the same volume of gas in the sample loop during injection. To get a profile of the species across the flame the following procedure is adopted:

The probe is moved to a different position across the flame (order of mm), soon after the valve switches to the sample loop fill position (0.5 min) (see Table 3.3). The sample loop is filled instantaneously and the probe is kept in this new position for all the time required by the GC to analyze the sample (22 minutes); This timing is enough to fill completely the sampling line. The vacuum pump is turned on as soon as the valve goes back to the initial position (5 minutes); this corresponds to the closure of the sample loop, which is now ready to be filled again with a new gas sample. Probe, kept across the flame for 22 minutes and vacuum pump on for the same time, provides the GC with a new gas sample. This procedure is repeated for each measurement.

3.5 GC method

Once the sample gas has been drawn from the quartz microprobe through the sampling line into the GC, it is carried by helium gas into a capillary column (HP-PLOT /AI 203) for extended analysis of C1-C10 hydrocarbons.

Gases are analyzed directly without any pre-concentration. This direct analysis approach permits accurate determination of the species contained in the sample and absolute concentration detection [2].The Gas Chromatograph is a GC Varian 3800, provided with STAR Chromatography Workstation 4.5 to run the GC through PC.

The type of column chosen and the column oven temperature program adopted permit the measurement of both low molecular weight compounds such as acetylene and higher molecular weight compounds such as benzene in 22 minutes. The column oven temperature program optimized for this analysis is shown in Figure 3-6. Three ramps have been chosen, 50, 110, 200 C^0, according to the specification of the column, maximum temperature 200 C^0, and the physical (boiling point) and chemical characteristics of the species. Temperature programming improves and accelerates the separation and identification of sample components, avoiding peak overlapping. A lower initial temperature is used to separate the more volatile species so that earlier peaks are well resolved. As the temperature increases, less volatile species are "pushed" out by the rising temperature. High boiling components instead are eluted earlier and as sharp peaks. Thus, temperature programming results in well-resolved peak and a total analysis time shorter than isothermal operation (see Fig. 3-11). The PLOT column used allows detection of C1-C10 species across the flame, its characteristics are reported in Appendices D.

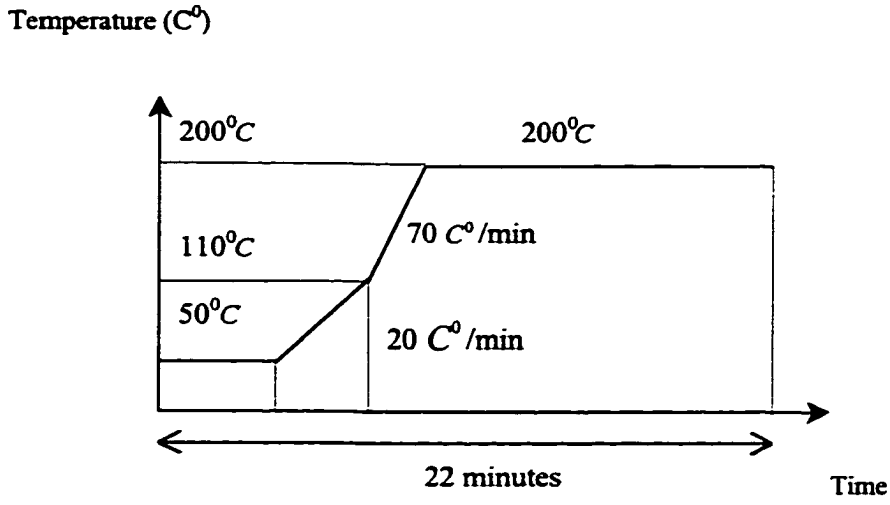

Figure 3-6: Column oven temperature program.

A pre-column is used to remove water and oxygen from the gas samples to avoid contamination while a rotary sample valve is used to trap the gases in a loop of constant volume (25 ml) and ensure identical analytical condition. The rotary sample valve timing is reported in Table 3-3.

Table 3-3: Rotary Sample Valve timing

Time (minutes)	Front Split	Gas Sampling Loop
Initial	ON (Split)	Fill
0.01	OFF (s/less)	Fill
0.50	OFF (s/less)	Inject
5.00	ON (Split)	Fill

3.6 GC equipment

3.6.1 Flame Ionization Detector

The Flame Ionization Detector (FID) has been adopted in this study as it allows hydrocarbon detection. A schematic of the FID detector is shown in Fig. 3-8. It is provided with a burner in which the effluent from the column is mixed with hydrogen and air and then ignited electrically [46, 50, 48].

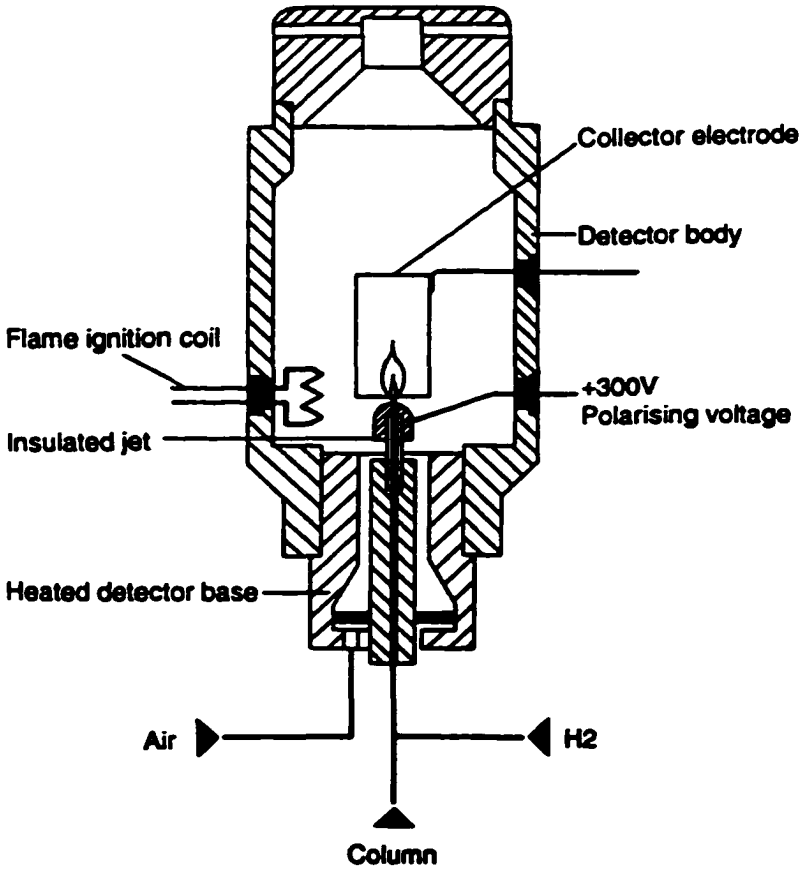

Figure 3-7: Schematic of Flame Ionization Detector [46].

Most organic compounds, when pyrolyzed at the temperature of a hydrogen-air flame, produce ions and electrons that can conduct electricity through the flame. The resulting current (10^{-12} A) is then directed into a high dependence operational amplifier for measurement. Because the FID responds to the number of carbon atoms entering the detector per unit of time, it is a mass sensive, rather than a concentration-sensive device. As a consequence, this type of detector has the advantage that changes in flow rate of the mobile phase have little effect on detector response. In addition it is insensitive toward non-combustible gases such as H_2O, SO_2, O_2, and NO_x [46, 50, 48].

According to the characteristics that an ideal detector should have, the FID detector exhibits a high sensitivity (10^{-13} g/s), large linear response range (10^7) and low noise. Generally the FID performance depends on the proper choice of gas flow rates. Good sensitivity and stability are obtained with a carrier gas flow of 30 ml/min (helium + make-up air), hydrogen flow of 30 ml/min and airflow of 300 ml/min. A disadvantage is that it is destructive of the sample [46].

3.6.2 Carrier Gas supply

Carrier gases, which must be chemically inert, include helium, nitrogen, carbon dioxide, and hydrogen. The type of detector dictates the choice of gases to use. Flow rates are controlled by two-stage pressure regulators and the inlet pressures lead generally to flow rates of 25 to 150 ml/min for packed columns and 1 to 25 ml/min for open-tubular capillary column; Carrier gas flow rates are established and controlled by simple soap-bubble meter. Helium has been chosen as carrier gas as a flame ionization detector (FID)

has been used for this study; its flow rate through the column is ~ 6 ml/min. In Table 3-4 are reported flow rates and values in pressure for helium (carrier), hydrogen and air.

Table 3-4: Gas supply specifications.

Gases	Specification	Flow-rate (ml/min)	Inlet Pressure (psig)
Helium	Purity 99.999% min.	30	80 psig
Hydrogen	Purity 99.995% min.	30	60 psig
Air	Ultrazero certified	300	40 psig

3.6.3 Injector system

Column efficiency requires the sample to be of suitable size and to be introduced as a "plug" of vapor. The most common method of sample injection involves the use of a micro-syringe to inject a liquid or gaseous sample through a silicone-rubber diaphragm or septum into a flash vaporizer port located at the head of the column. Our sample was injected through a rotary sample valve as discussed below.

3.6.4 Rotary sample valve

A 10 port rotary sample valve is used for sample injection into the GC. This setup is appropriately referred to as "gas sampling with backflash of precolumn to vent". A Sorbitol pre-column and a PLOT column are present. The Sorbitol pre-column adsorbs any water and oxygen present in the sample that can be harmful and contaminate the

PLOT column. When the valve is in the off position, the sample simply flows in and out of the sample loop to exhaust; when the valve switches to the on position, the sample is trapped in the 25 ml sample loop and it is flashed through the pre-column and the capillary column. Then the valve turns back to the off position. In the mean time the carrier gas (helium) that flows continuously through the column carries the sample down the column and to the FID. Fresh sample comes in and out the sample loop and the pre-column is purged to vent (i.e. blackflash). The switching time for the valve (see Table 3-3), is controlled automatically by STAR Chromatography Workstation, the PC software package provided by Varian to run the GC 3800. Due to the small flow through a capillary column (approximately 6/7 ml/m in this application), split mode is used. With split mode the amount of gas flowing down the column can be controlled. In fact the all sample contained in the valve sample loop (25 ml/m) would cause peak broadening of the column. Thus, split mode, is accomplished by establishing a second parallel route for the carrier gases that by-pass both the column and the detector. The splitting of the carrier gas (in this case a split ratio of 5 was used) allows adequate detection limits and reasonable temporal peak resolution.

3.6.5 Capillary columns

A PLOT column, (HP-PLOT /A1203), has been used in this application. Capillary columns operate at high efficiency and are particularly suitable for difficult sample separations such as a flame. In order to separate and analyze extremely small samples, their diameter is reduced to a small value. This is why packed chromatographic columns,

characterized by bigger diameter and less efficiency are not used as before (see Table 3-7). Capillary columns are made of glass, stainless steel, or nylon capillaries with an inner diameter between 0.25 and 1.0 mm. and lengths from 6 to 300 meters. The thickness of the liquid film of the stationary phase is between 0.4 and 2 microns.

Capillary columns can be divided into two types: WCOT wall coated open tubular columns and SCOT support coated open tubular columns and related PLOT columns (Porous Layer Open Tubular Columns). Characteristics and specifications of our PLOT column are reported in Appendix D.

3. 7 Quantitative Analysis

Quantitative column chromatography is based upon a comparison of either the height or the area of the analyte peak with that of one or more standards. The height of a chromatographic peak is obtained by connecting the base lines on either side of the peak by a straight line and measuring the perpendicular distance from this line to the peak. It is important to note however that accurate results are obtained with peaks heights only if variations in column conditions do not alter the peak widths during the period required to obtain chromatograms for sample and standards. Peak areas are instead independent of broadening effects due to the variables mentioned before and therefore areas are a more satisfactory analytical parameter than peak heights. Motivated by the previous observation, chromatographic peak areas are taken into account for this analysis.

3.7.1 Calibration and standards

The most straightforward method for quantitative chromatographic analyses involves the preparation of a series of standard solutions that approximate the composition of the unknown. Chromatograms for the standards are then obtained and peak areas are plotted as a function of concentration. A plot of the data should yield a straight line passing through the origin; analyses are based upon this plot.

The most important source of error in analyses by the method just described is usually the uncertainty in the volume of the sample; ordinarily samples are small (~1microliter) and the uncertainties associated with injection of a reproducible volume of

this size with a micro-syringe may amount to several percent relative. Errors in sample volume can be reduced using a rotary sample valve, in which a reproducible volume of sample is introduced each time. This is the reason why we adopted a 10 ports sample valve for this application. Other possible source of errors are sample adsorption or decomposition in the chromatogram, in which compounds can be decomposed or adsorbed in the injector port, on the column, or in the detector. Detector performance can change as operating conditions change; for accurate and reproducible analysis, the purity of carrier gas, gas flow rate, detector temperature, filament current, filament resistance and pressure inside the detector must remain constant. Recorder performance, integration technique of the chromatographic peaks and peak area calculation can be also source of errors during quantitative analysis. In fact, different compounds have different detector response [46].

All the species detected in this study are reported with correspondent retention times in Table 3-5. Species across the flame have been identify and quantify using standard calibration gas mixtures that are reported in Table 3-6, 3-7; here there are listed concentrations (PPM) and chromatographic retention times of each species. Each component requires its own calibration curve, since it has a unique detector response The calibration curves for all the species detected are reported in Appendix D. Calibration curves are calculated through STAR Chromatography Workstation; the standard peak area is plotted as function of its concentration. The retention times of some species were also calculated through liquid sample injections using a 25-liter sample bag, provided with an inlet for syringe injection.

Table 3-5: C1-C6 species identified through gas chromatography.

Species	Retention Time (min)
Methane	7.19
Ethane	7.42
Ethylene	7.67
Propane	8.12
Acetylene	8.93
N-Butane	9.34
Propylene	9.69
N-Pentane	10.8
Propyne	11.2
N-Hexane	12.30
Benzene	16.44

Table 3-6: Supelco Gas Mix 236 (Cat. No. 501832)

Species	Concentration (PPM)	Retention Time (min)	Area (counts)
Methane	999	7.196	23861
Ethane	1008	7.403	35650
Propane	1005	8.097	42063
N-Butane	992	9.378	48207
N-Pentane	995	10.871	51412
N-Hexane	1000	12.305	55132

Table 3-7: Supelco Gas Mix 54 (Cat. No.2-3470-U)

Species	Concentration (PPM)	Retention Time (min)	Area counts
Methane	14.85	7.196	677
Ethane	14.67	7.403	1252
Ethylene	15.36	7.676	1259
Propane	16.03	8.097	1645
Acetylene	15.99	8.937	1682
N-Butane	15.94	9.378	2163
Propylene	15.41	9.677	1136
Propyne	15.94	11.213	2492

Chapter 4: Results and Discussion

4.1 Flame and intermediate species

A propane non-premixed flame has been used as baseline for oxygenated fuel additive experiments. The flame is formed from a fuel stream consisting of high purity propane (~17%) and nitrogen (~84%). The oxidizer stream includes 31% oxygen and ~69% air. The overall mixture is fuel-rich, with an equivalence ratio of 1.79; the ratio between nitrogen and oxygen (N_2/O_2) is 3.03, a value that is close to that of air (3.76).

To establish flat flame conditions in the counter-flow burner, a velocity of 10 cm/sec has been chosen for both fuel and oxidizer streams. However, higher velocities didn't show flame instability. The flame characteristics are summarized in Table 4-1.

Table 4-1: Flame characteristics with and without additive addition.

Case	Stream Velocity (cm/s)	Equivalence ratio (ϕ)	N_2/O_2 (mole fraction)	Flame composition (mole fraction)			
				Fuel side %		Oxidizer side %	
				C3H8	N2	Air	O2
No Additive	10	1.79	3.03	16.3	83.7	69.0	31.0
DMC 10 %	10	1.68	3.03	14.7	83.7	69.0	31.0
DMC 15 %	10	1.63	3.03	13.8	83.7	69.0	31.0
Ethanol 10 %	10	1.70	3.03	14.7	83.7	69.0	31.0
Ethanol 15 %	10	1.67	3.30	13.8	83.7	69.0	31.0

Additive addition in 10% and 15% by volume, produces small changes in equivalence ratio and N_2/O_2 ratio compared to the pure fuel case (see Table 4-1). This is due to differences in molecular structure between the two additives, having respectively 2 and 3 carbon atoms (see Table 4-2). Additives are added to the fuel stream keeping constant the volumetric flow rate and the fuel velocity; this ensures same flame size and shape, Gupta and Santoro [6].

Table 4-2: DMC and Ethanol chemical characteristics [15, 38, 39].

Species	Molecular structure	Molecular weight (g/mol)	Volume percent (%)	Boiling point (C^0)	Calorific value (KJ/mol)	Oxygen content (wt-%)	Specific gravity (g/cm^3)
Propane	C_3H_8	44.09	100	36.07	2220.9	0	1.79
DMC	$C_3H_6O_3$	90	10, 15	90	1818.0	53.33	1.069
Ethanol	C_2H_5OH	46.06	10, 15	78.5	1368.0	34.07	0.788

The flame appears steady and one-dimensional to the naked eye. Its structure is similar to a disk, with a thickness of few mm and a diameter similar to that of the burner ducts. It exhibits a yellow-orange luminosity that doesn't change with time. As regards the flame position, it is at ~ 9 mm from the lower duct, just below the stagnation plane, on the fuel side; a micrometer has been used to detect the flame position; no more accurate measurements were available. However, only small fluctuations (order of fraction of mm) are observed for the flame plane level. The flame, when located on the fuel side, is more convenient for the analysis. In fact, the sooting characteristics for counter-flow diffusion flames can be significantly influenced by the flame location and this can cause problems during sampling. When a diffusion flame is located on the fuel side, the gas velocity is directed toward the flame and the soot particles approximately follow the gas-phase streamlines. On the other hand, when the flame is located on the oxidizer

side, the gas velocity is directed to the stagnation plane and soot particles move away from the flame [7] (see chapter 2). Figure 4-1 is a schematic of the soot zone structure for methane counter-flow diffusion flame located on the oxidizer side (a) and fuel side (b) [7].

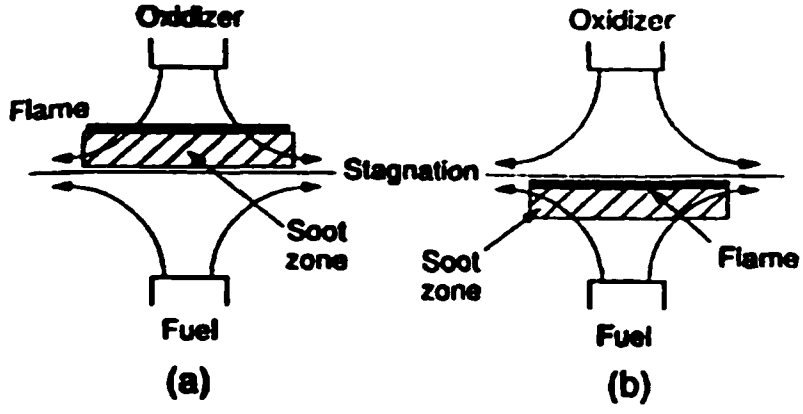

Figure 4-1: Sooting structure of counter-flow diffusion flames with flame located on the oxidizer side (a) and fuel side (b) [7].

From the criteria on the flame location, illustrated in chapter 2, we would expect a flame on the oxidizer side, instead, the flame sits very close to the stagnation plane, slightly on the fuel side (9-mm). Pictures of the flame are taken with a digital camera (Kodak DC120 Zoom Digital Camera). The flame is thin and yellow-orange in color. Figure 4-2, (a) shows color and position of the baseline flame used in this study; Figure 4-2 (b) zooms in on the probe position across the flame during sampling. An increase in oxygen from the oxidizer side results in a very bright color for the flame and higher temperature as shown in Figure 4-4. An increase in nitrogen from the fuel side results, instead, in an intense blue-color flame (Figure 4-3). The color of the luminous zone changes with fuel-air ratio; for hydrocarbon-air mixtures that are fuel lean, the flame is a deep violet color due to excited CH radicals [70]. The yellow luminosity has been

associated with the presence of soot precursors [60], while the yellow-orange zone with the particle inception step of the overall mechanism of soot formation (see chapter 2). A blue zone (peak flame temperature) can be still recognized with the yellow and orange color of the flame but it is difficult to isolate because of the very thin flame layer. The luminous zone, in fact, is only 2-3 mm thick.

Figures 4-3 and 4-4 show changes in shape and color of the flame with an increase in the oxygen level (4-4) and the nitrogen level (4-3). Small edges can be still recognized in the flame shape; this is probably due to buoyancy effects. However, the fact that the micro-probe tip is in the central part of the flame during the analysis, ensures stable sampling conditions.

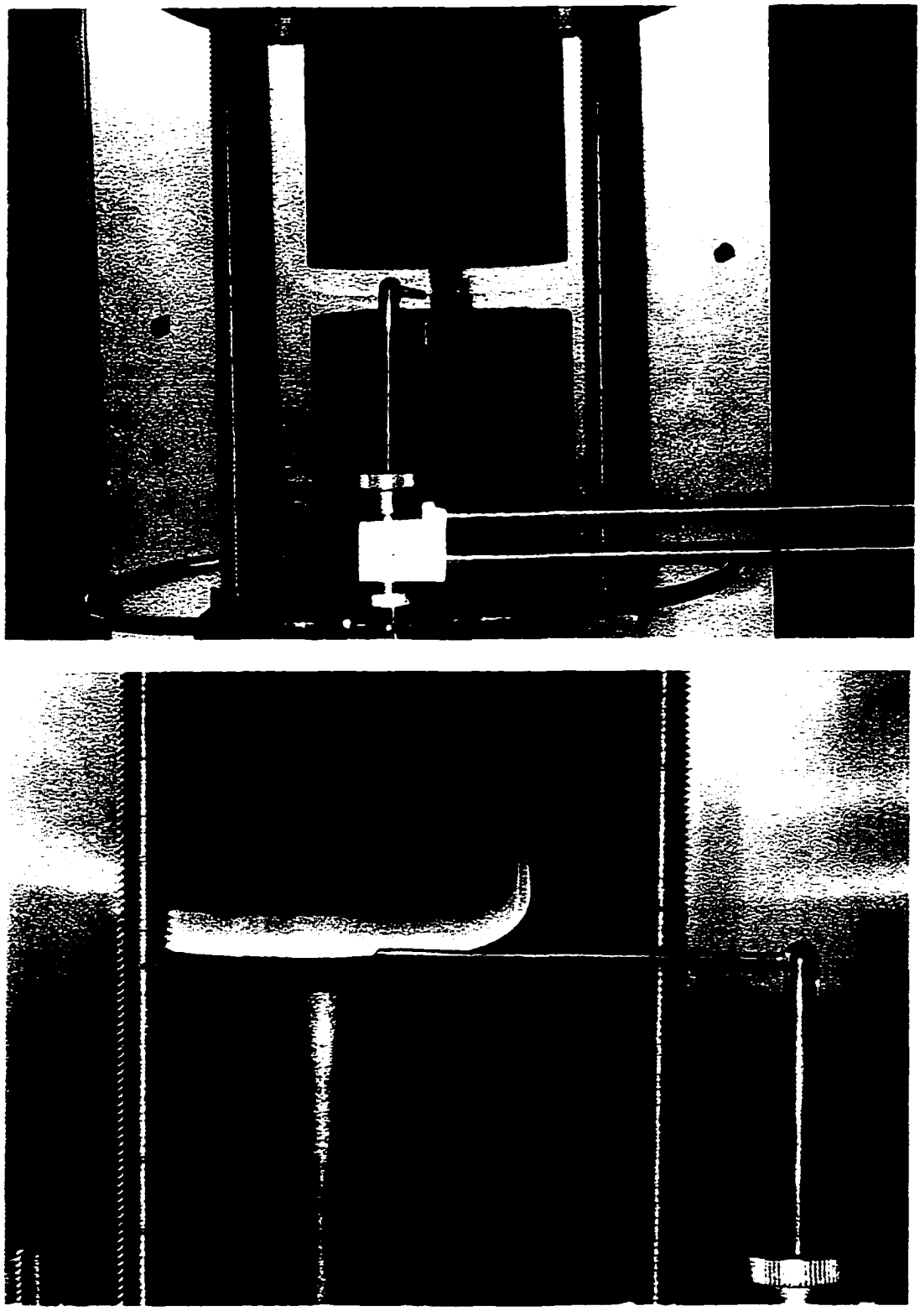

Figure 4-2 (a),(b): Pictures of the flame used as baseline for additive investigation.

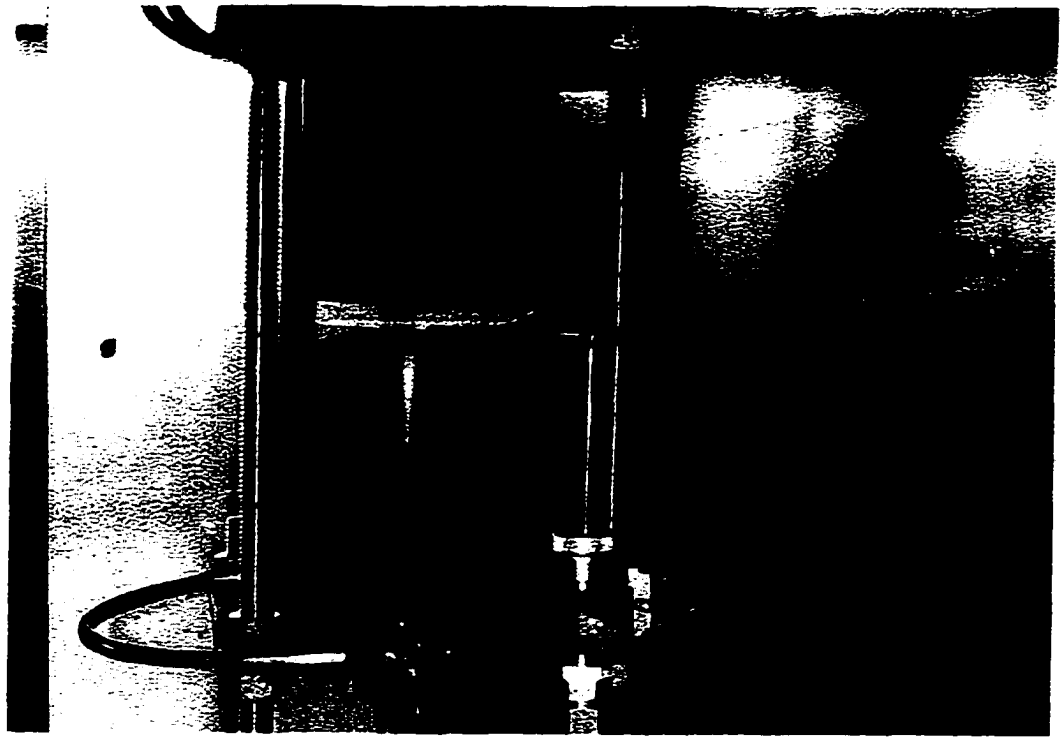

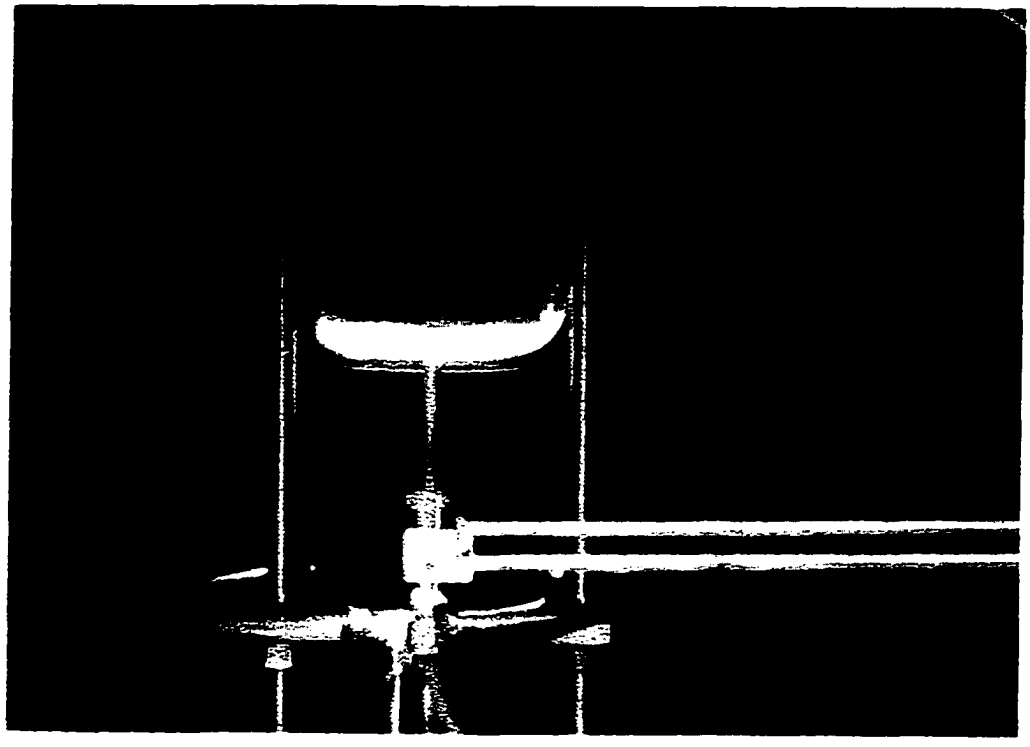

Figure 4-3, 4-4: Flame shape and color increasing N_2 in the fuel stream (4-3) and oxygen in the oxidizer stream (4-4).

The typical profile of propane, when injected without additives is reported in Fig. 4-5. The fuel profile is taken across the flame by moving the quartz microprobe in the vertical direction, along the opening that separates the upper duct (oxidizer side) from the lower duct (fuel side) of the burner. This distance is kept at 20-mm. Propane levels across the flame, in PPM, are plotted versus the distance (in mm) of the opening that goes from the fuel side to the oxidizer side of the burner. As expected, the fuel levels decrease rapidly as we approach the luminous zone (9-mm). Here, pyrolysis occurs and a pool of intermediate species is generated.

Propane consumption is mainly due to thermal decomposition and reaction with H radicals. Major species of its breakdown reactions are ethylene and acetylene. Ethylene is mainly produced through the decomposition of ethyl and n-propyl radicals (see chapter 2); acetylene is the major product of ethylene consumption in diffusion flames. Figure 4-6 shows the major species detected across the flame, which sits at 9-mm above the lower duct of the burner. Species such as ethane and methane, formed mainly through the recombination of methyl radicals in the fuel-rich region of the flame, show similar profiles but differences in levels (Figure 4-6). Methane presents higher concentrations than ethane in the flame. However these levels, as expected, are much lower than those of ethylene (Figure 4-6). Propylene shows a profile similar to acetylene in shape but lower in value. A burner preheating effect is probably responsible of the values measured at the zero mm position. All the major species of propane pyrolysis start to increase just below the flame plane (9-mm) to reach highest levels at this location and decay few mm above (12 mm) with a smooth profile. Accordingly, propane is consumed rapidly on the fuel rich side of the flame and reaches zero levels at the same height (12-mm). Minor intermediate species such as n-hexane, n-butane and benzene, measured across the flame in the same conditions are shown in Figure 4-7.

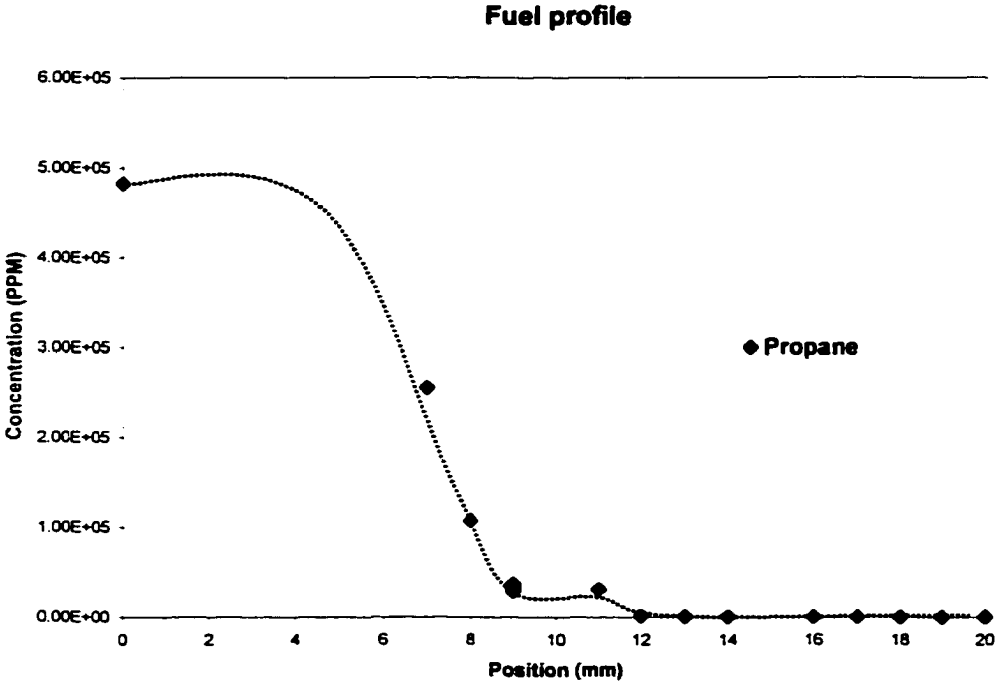

Figure 4-5: Propane profile across the flame.

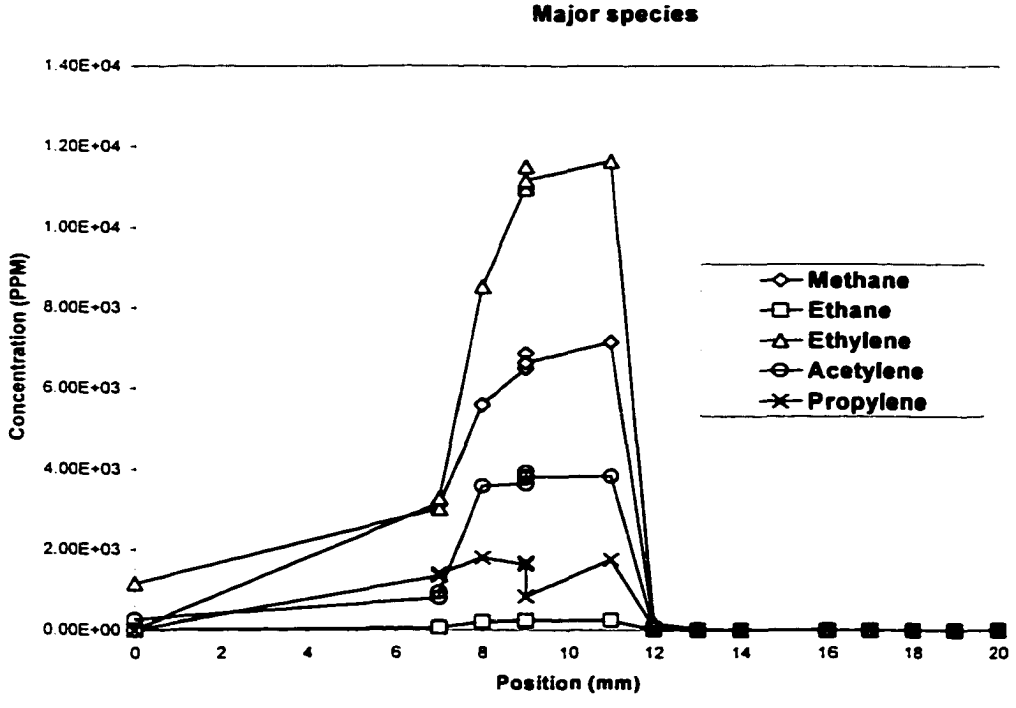

Figure 4-6: Major species profile across the flame.

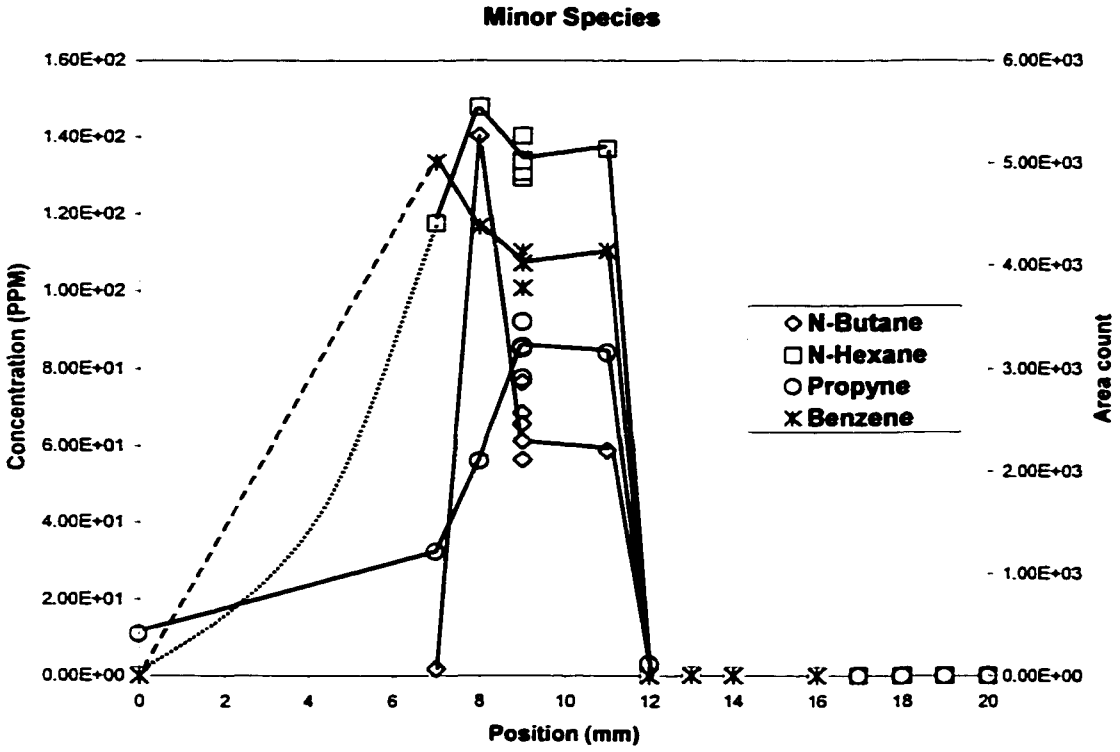

Figure 4-7: Minor species profile across the flame.

The previous figures (Fig. 4-5, 4-6 and 4-7) show the typical profile of the fuel and intermediate species across the flame obtained for a typical day. Measurements were taken several times and with randomized position order across the flame, to prove the reproducibility of the experiment.

Similar values are registered for same experimental conditions for each day of measurements. The scatter of the two most significant species, ethylene and acetylene, is reported in Figure 4-8 and 4-9. The ethylene and acetylene raw data (in area count) are plotted versus each day of measurements. Average value, standard deviation and standard error are shown for both species. A standard error of approximately 2% is found for both acetylene and ethylene data; this looks reasonable, although minor species detected have a larger error.

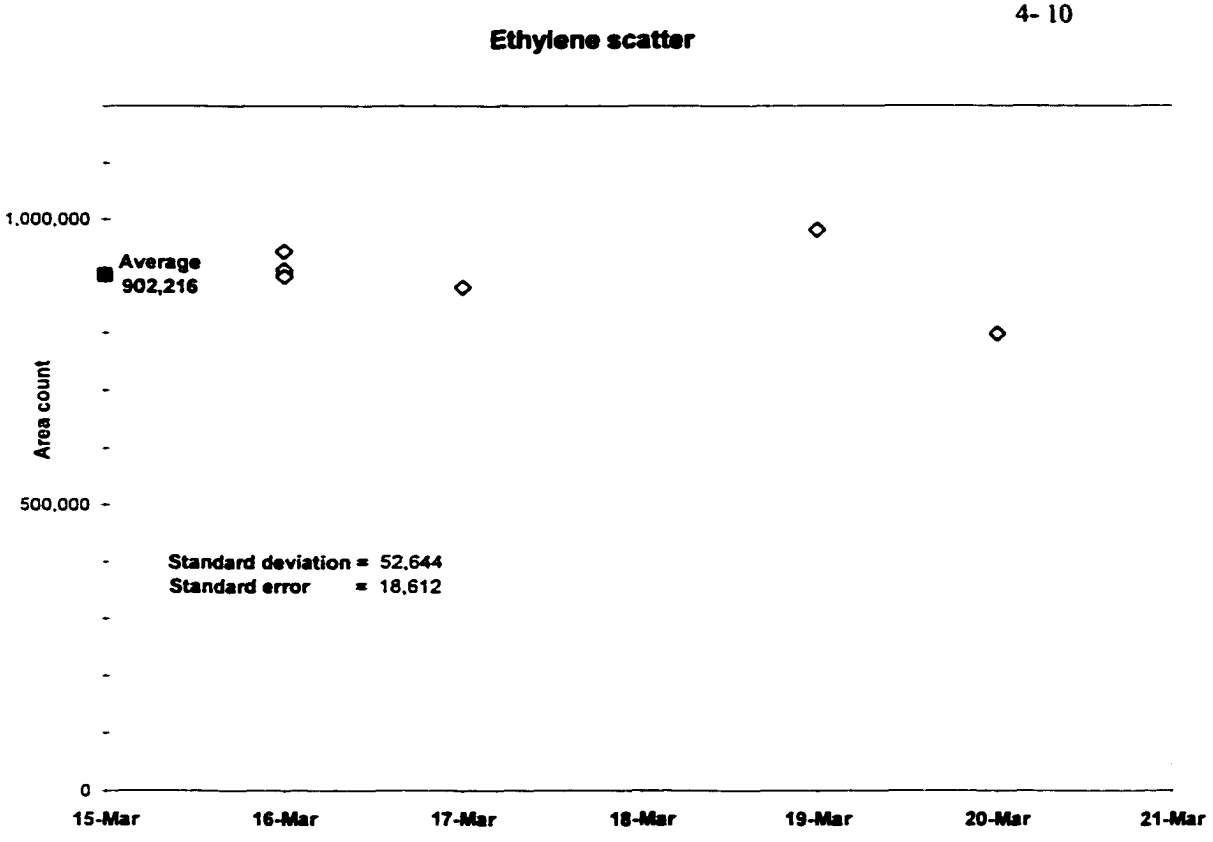

Figure 4-8: Ethylene scatter at flame plane for different days; all available data has been plotted.

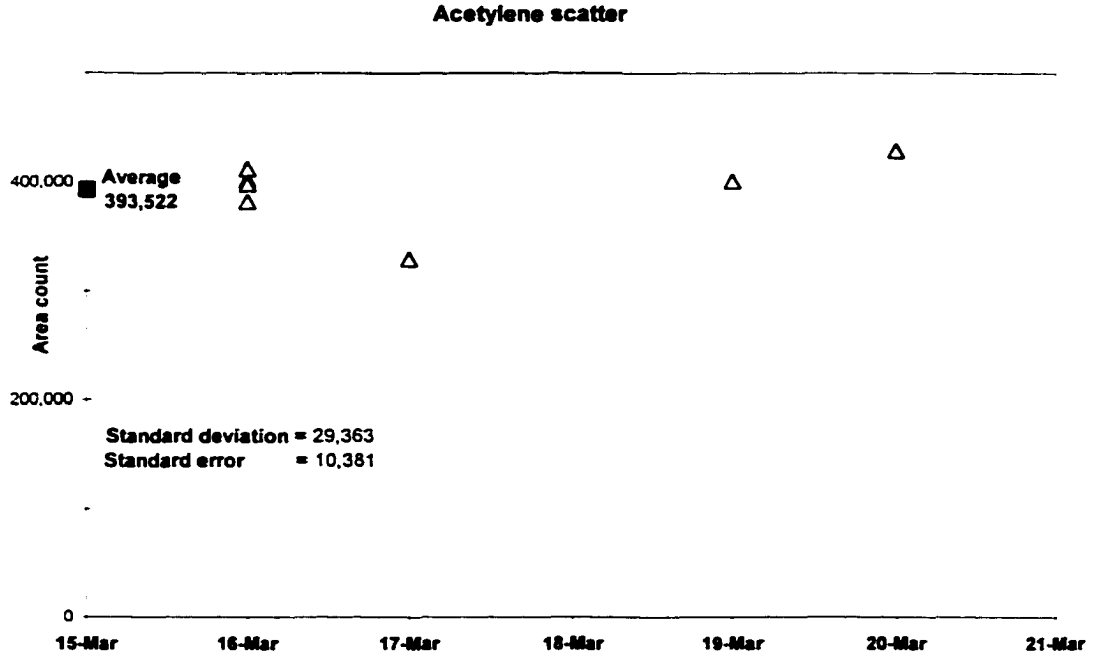

Figure 4-9: Acetylene scatter at flame plane for different days; all available data has been plotted.

In this study, particular attention is given to acetylene as a soot precursor species. As discussed before (see chapter 2), acetylene acts in the formation of the first aromatic ring and in the formation and growth of PAHs and it has a crucial role in the soot production mechanisms. Therefore, decreases in acetylene levels most likely lead to soot level reductions, in the last stage. Reactions with O atoms are acetylene's major consumption path during oxidation but large production of OH radicals can result in a major acetylene consumption path through oxidation that can then lead to soot reduction.

4.2 DMC Addition

DMC ($C_3H_6O_3$) is added in 10% and 15% by volume to the fuel stream. No significant differences in flame color have been noticed with DMC addition. Changes in flame characteristics are reported in Table 4-1, while the additive chemical and physical characteristics are listed in Table 4-2. Figure 4-10 and 4-11 show results obtained, for a typical day of measurement, at the flame plane with 10% and 15% by volume DMC addition on all the species detected across the flame.

DMC added in 10% by volume significantly reduces soot precursor levels such as acetylene (~ 15%) and mostly all the other species detected across the flame. Only methane shows a slight increase (~ 3%) probably due to the molecular structure of the additive itself ($C_3H_6O_3$), containing two methyl groups.

Higher DMC dosage (15% in volume) results in higher reduction for acetylene (~ 28%), benzene levels (~50%) and many other species such as methane, ethane, ethylene, pyrene and n-hexane (see Figure 4-11).

In Figure 4-12 are reported only acetylene levels with 10% and 15% DMC addition from Figure 4-10 and 4-11. It is clear from the percentage of reductions that DMC significantly reduces soot precursors such as acetylene in counter-flow propane/air diffusion flames. An increase in DMC dosage leads to a higher reduction in acetylene levels at flame plane. The same trend has been registered with benzene. Benzene level reductions with 10% and 15% DMC addition are reported in Figure 4-13.

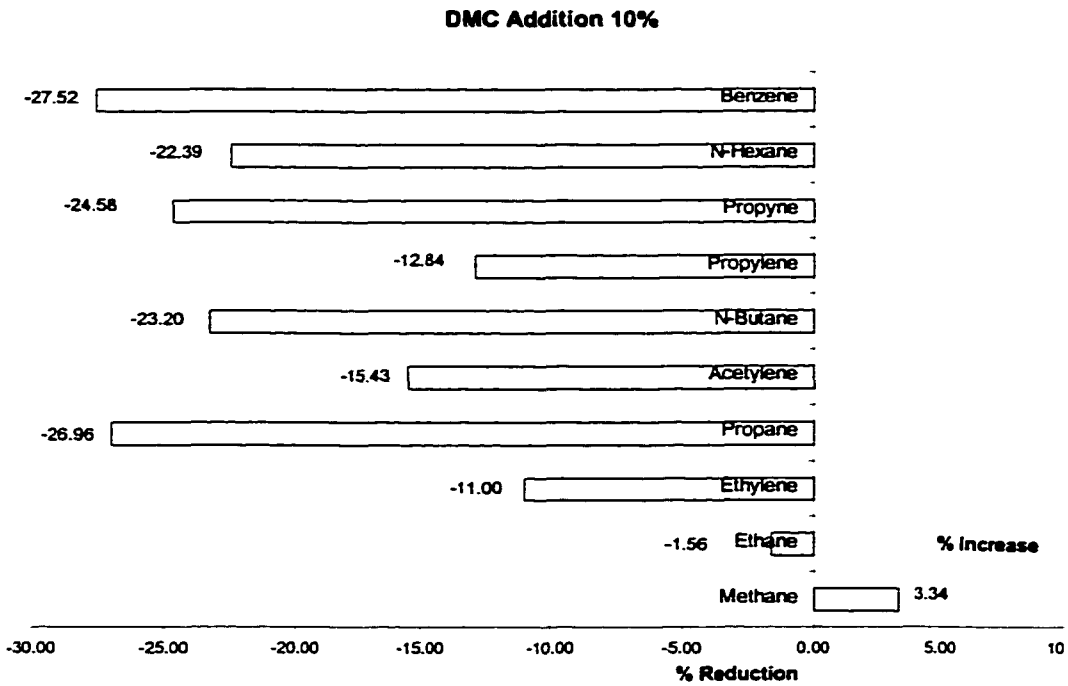

Figure 4-10: DMC addition 10% by volume.

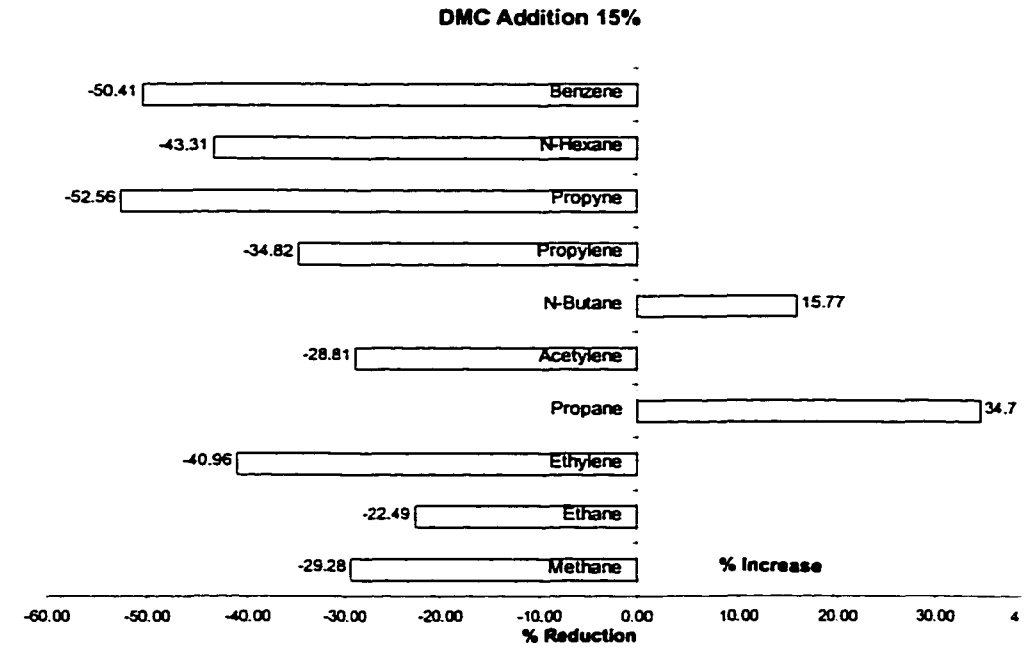

Figure 4-11: DMC addition 15% by volume.

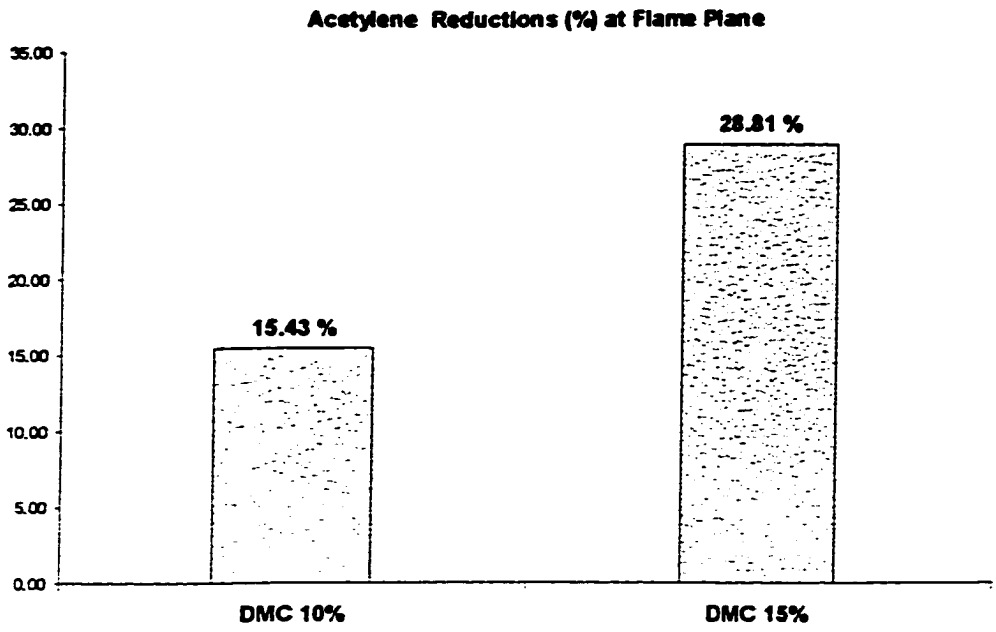

Figure 4-12: Reduction in Acetylene levels with DMC 10% and 15%.

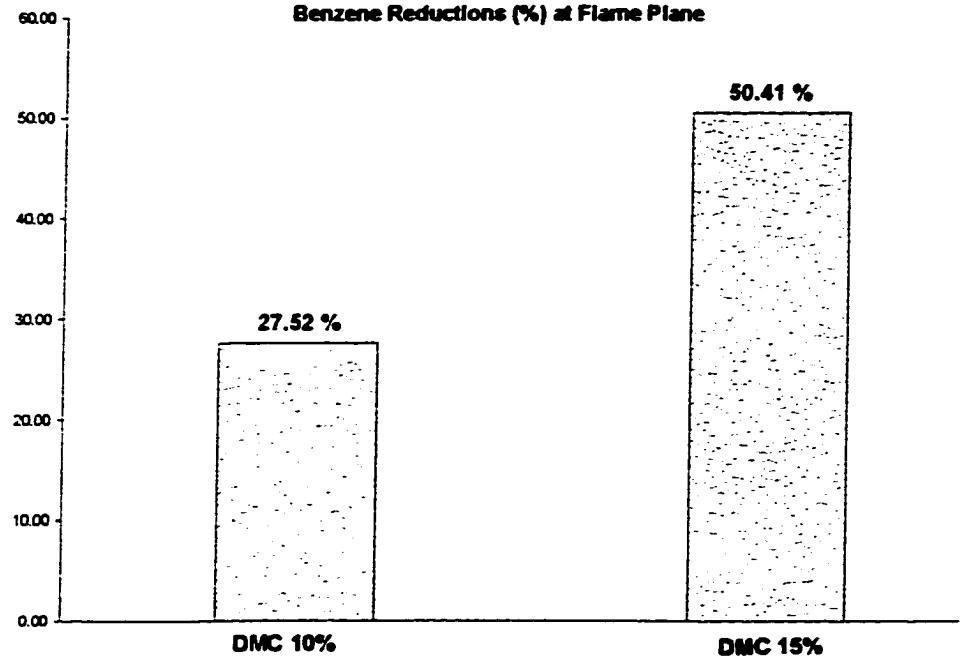

Figure 4-13: Reduction in Benzene levels with DMC 10% and 15%.

DMC has been applied in this study because it has already shown promising results on soot reduction in diesel engines. Our results suggest good agreement with that data [15, 19] and in particular we register the same trend on soot precursors such as acetylene and benzene, with an increase in the additive dosage.

For a high additive dosage such as in this case study, the chemical characteristics of the additives (molecular structure, density, molecular weight, heating value, and C/O ratio) can affect the global chemical reaction pattern substantially. DMC, among other oxygenated fuel additives (see chapter 2), presents higher oxygen content, higher specific gravity and lower boiling point and molecular weight (see Table 4-2). DMC is also soluble in diesel fuel. Therefore, it is easy to handle and convenient for experimental purposes.

Miyamoto et al. [15] have shown that DMC addition to fuel suppresses smoke and particulate significantly in diesel engines, but no analysis of the influence of the additive on combustion and soot evolution was done. It was demonstrated, however, that its effect on soot was not due to its lower boiling point [15]. This probably suggests that the reductions seen on soot precursors in this study most likely are due to chemical mechanisms, although dilution effects can play an important role at the same time.

More recently, Kuo and Shih [19] have added DMC in 5% and 10% by volume to diesel fuels. DMC has shown reduction on the exhaust gas temperature as well as on NOx, HC emissions and smoke opacity (see chapter 2). The increase of DMC additive dosage from 5% to 10% showed further reductions while other additives, including ethanol, showed higher NOx and HC emissions.

4.3 Ethanol addition

Ethanol (C_2H_5OH) is added in the same dosage as DMC, 10% and 15% by volume. No differences in flame color are noticed. Ethanol chemical and physical characteristics are reported in table 4-1. It is an alcohol; its molecular structure (2 carbon atoms and one C-C bond) is different and its oxygen content (~30 wt-%) is much lower than DMC (~50.3 wt-%). Figure 4-14 and Figure 4-15 show results for 10% and 15% by volume ethanol addition.

Ten percent (10 %) ethanol addition shows more modest reductions than DMC. On soot precursors such as acetylene we register only ~ 8% reduction at the flame plane. Benzene and n-hexane have a small increase. However, reductions are found for all the other species such as n-butane, propane, propylene, propyne and ethylene. A modest reduction (~ 4%) is registered for methane while a small increase is caused by DMC, added in the same percentage (10%).

Higher Ethanol dosage (15% in volume) results in higher reduction above all for n-butane, propane and propyne (order of 22-24%); more modest reductions are registered for acetylene (~ 13%), ethane (~ 10%) and n-hexane. Benzene levels decrease with increasing ethanol dosage as shown in Figure 4-15.

Results for 10% and 15% ethanol addition on acetylene and benzene, for a typical day of measurement are shown in figure 4-16 and 4-17. These results suggest that ethanol reduces key soot precursors such as acetylene and benzene in counter-flow propane/air diffusion flames.

However, this effect is modest compared to DMC addition in the same percentages (Figure 4-12, 4-13). An increase in ethanol dosage leads to more modest reductions than in the DMC case.

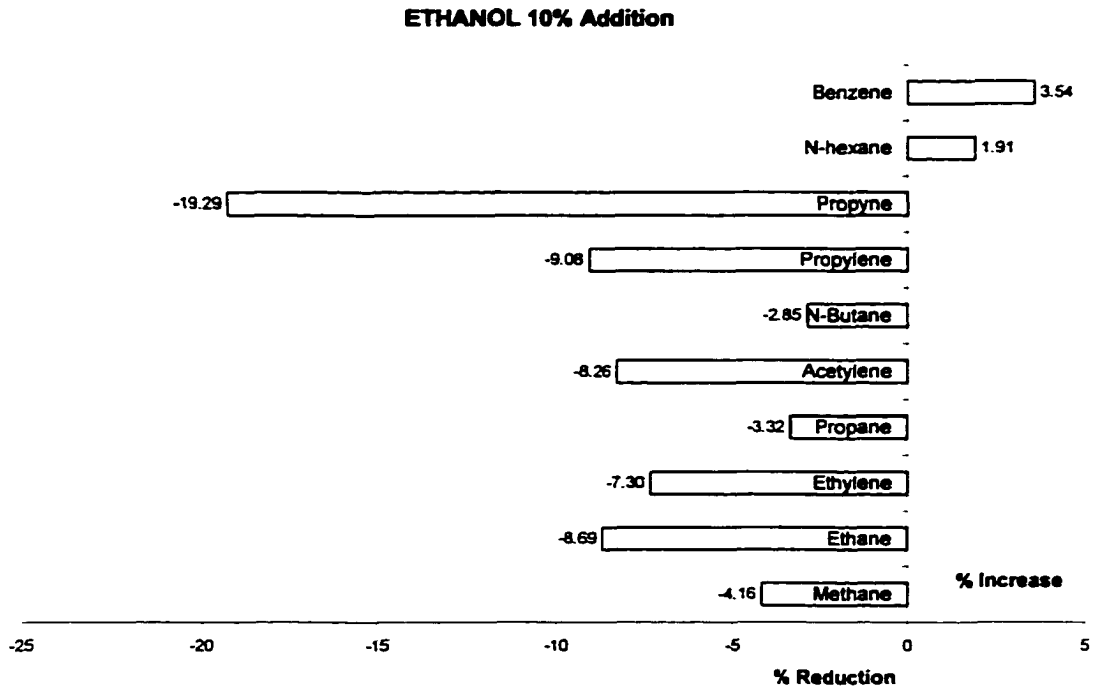

Figure 4-14: Ethanol addition 10% by volume.

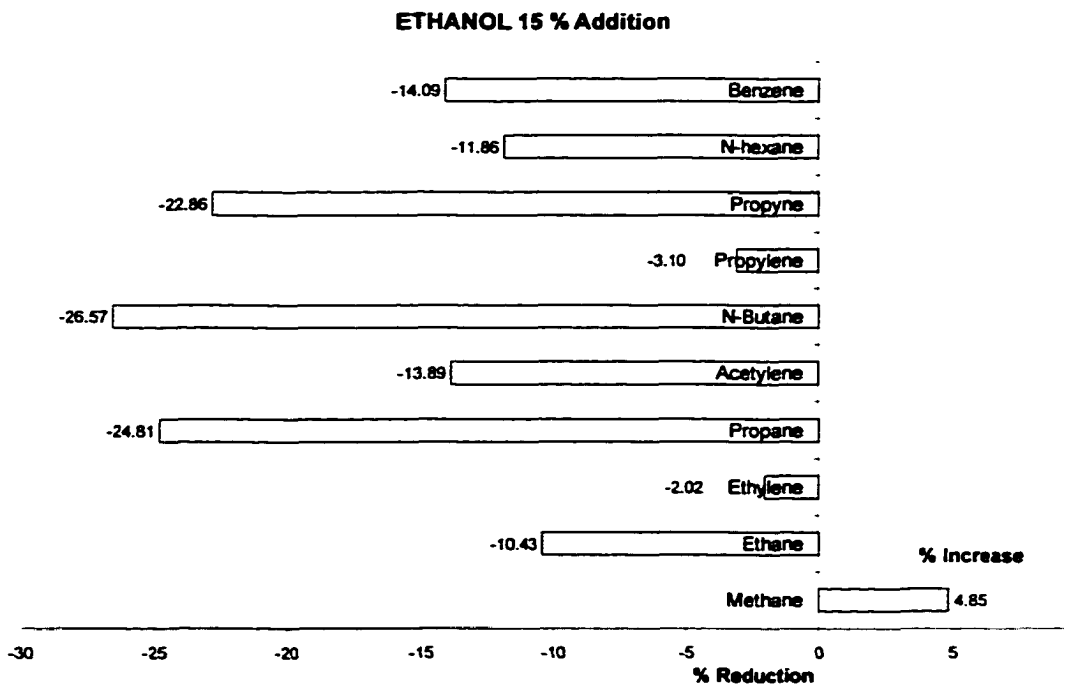

Figure 4-15: Ethanol addition 15% by volume.

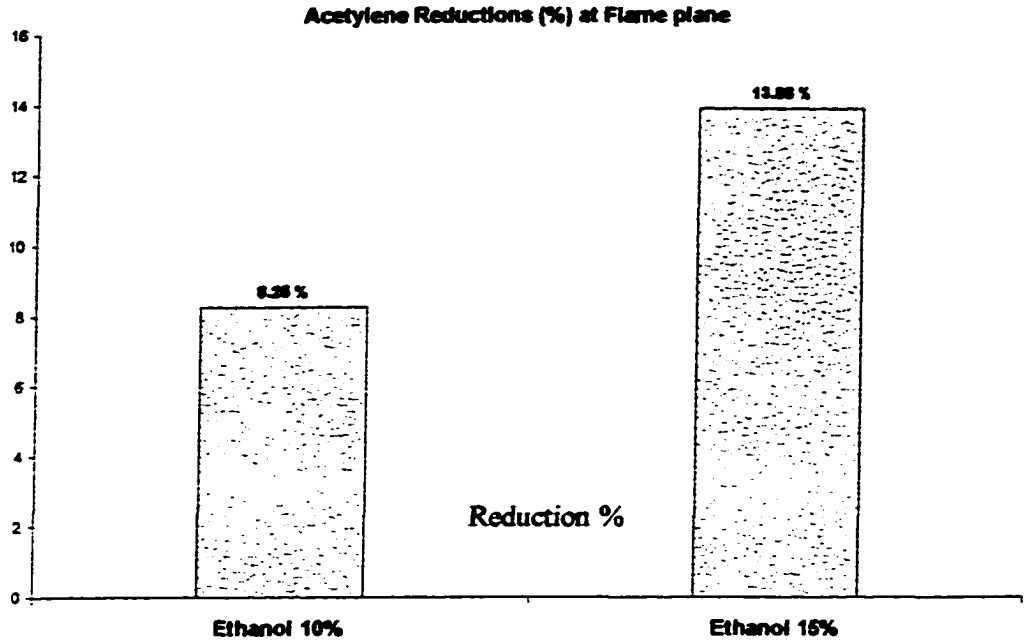

Figure 4-16: Acetylene reduction with ethanol addition 10% and 15% by volume.

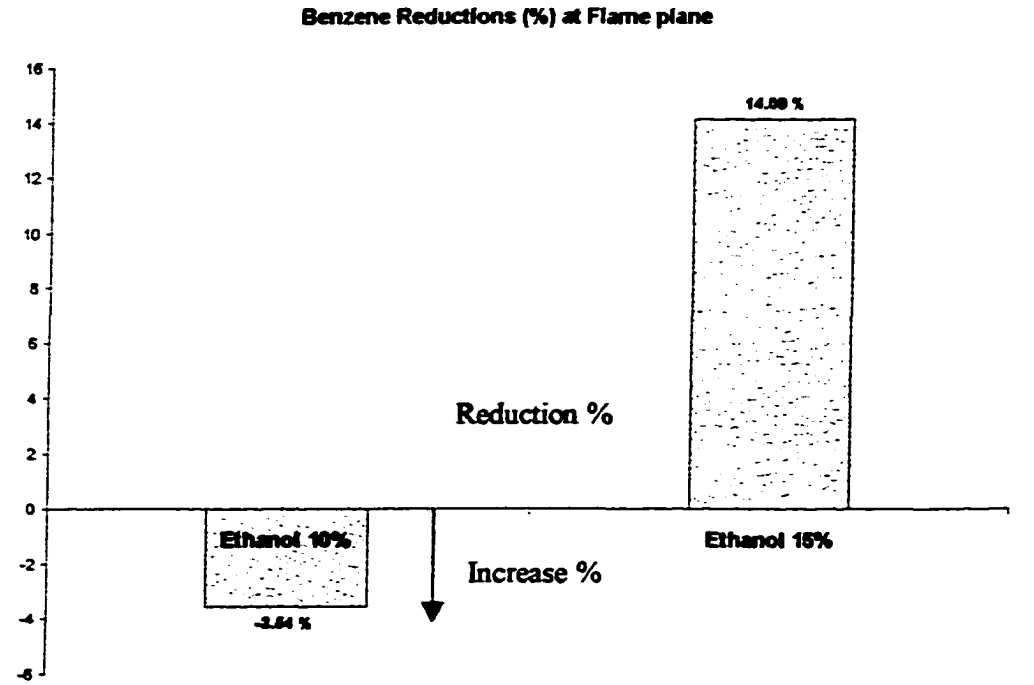

Figure 4-17: Benzene levels with ethanol addition 10% and 15% by volume.

Ethanol, like DMC, has been already used as an additive in diesel engine applications [19]. Our reductions on soot precursors, agree with the fact that ethanol reduces soot levels in diesel engines. Ethanol added in 10% and 20% by volume by Shih et al., [19], showed reductions in smoke opacity and exhaust temperature, but increases in NOx and HC levels.

Since ethanol, as an additive, is not naturally soluble in the diesel fuel, the changes of surface tension and viscosity (ethanol has low viscosity) of the mixture can cause substantial variation in the characteristics of fuel spray combustion patterns. Our results can help to understand its chemical mechanism of action on soot formation.

Ethanol, added in ethene laminar diffusion flames, showed less effective reductions than methanol on soot concentrations (see chapter 2). A possible explanation proposed by Gupta and Santoro [6] was that the pyrolysis of methanol generates OH radicals, which can oxidize soot particles or soot precursors, while the main pyrolysis product of ethanol is ethene and water.

The more modest reductions on soot precursors such as acetylene, with 10% and 15% ethanol addition, found in this study, can be probably due to differences in the additive pyrolysis. On the other hand, the hydrogen removal mechanism suggested by Frenklach and Yuan [23] (see chapter 2) can be also responsible of the ethanol effect on soot precursors.

4.4 Comparison of the additive effects

The two additives, ethanol and DMC, can be compared for their effect on soot precursor species. This comparison is made on the basis of equal percent by volume in the fuel.

Ten percent (10%) DMC significantly reduces intermediate species detected across the flame (Figure 4-10; 4-11) and in particular soot precursor such as acetylene and benzene (Figure 4-12, 4-13). Ethanol, instead, shows more modest reductions on acetylene and benzene (Figure 4-16, 4-17) as well as on many of the other species (Figure 4-14, 4-15).

Figure 4-18 summarizes the effect of DMC and Ethanol on acetylene levels while Figure 4-19 on benzene levels. As their dosage level increases, both DMC and Ethanol show higher reductions for almost all the species detected and in particular for acetylene and benzene. In particular, when the DMC dosage is increased from 10% to 15%, the reduction in benzene and acetylene levels approximately doubles. Ethanol shows more modest effect.

Myamoto [15] and Shih [19] have measured soot reductions in diesel engines with the use of DMC and ethanol as fuel additives. In particular Shih, has compared both DMC and ethanol effects on diesel engine emissions (see chapter 2). Results suggested that smoke opacity decreases as the DMC and ethanol dosage increases. This seems to agree with the trend observed in our study on soot precursors such as acetylene and benzene. Shih measured similar reductions (~39% and ~34%) in smoke opacity with the same amount (10%) of ethanol and DMC, respectively.

Our measurements in a counter-flow propane/air diffusion flame suggest that, at 10% by volume, DMC has a stronger effect than ethanol on soot precursors (i.e. acetylene) (Fig. 4-18).

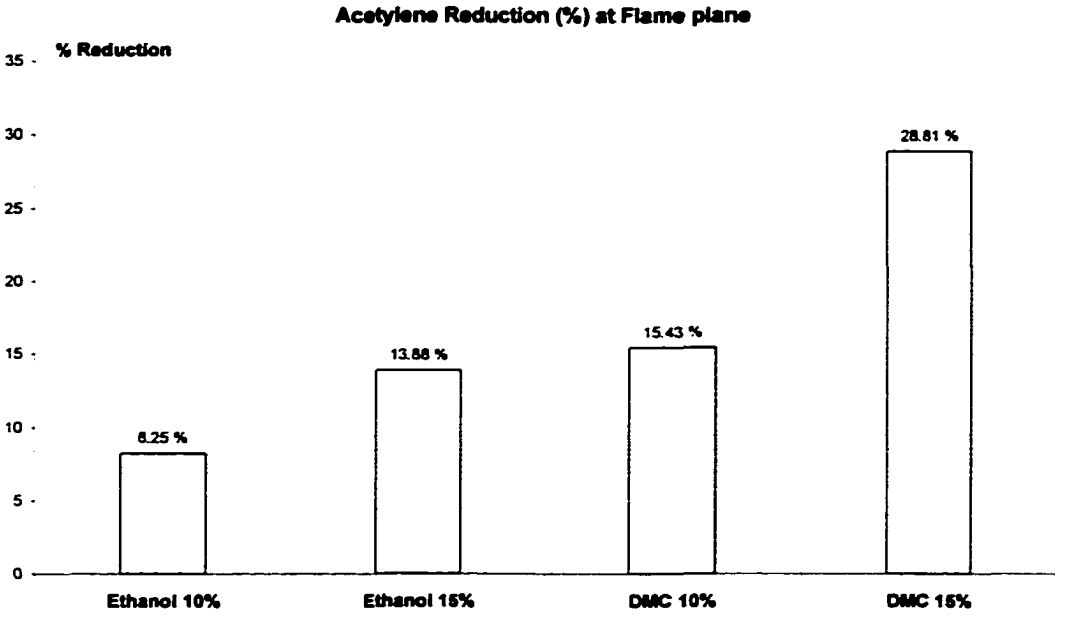

Figure 4-18: Ethanol and DMC effects in 10% and 15% on acetylene levels.

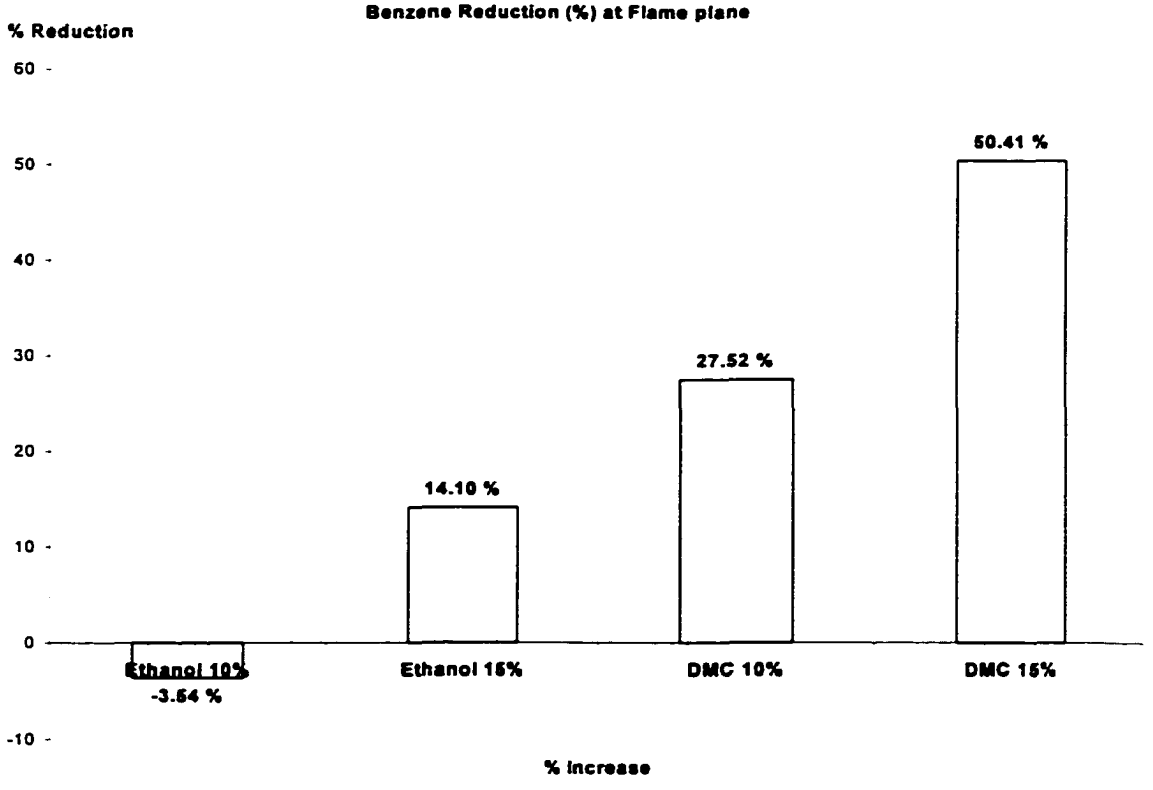

Figure 4-19: Ethanol and DMC effects in 10% and 15% on benzene levels.

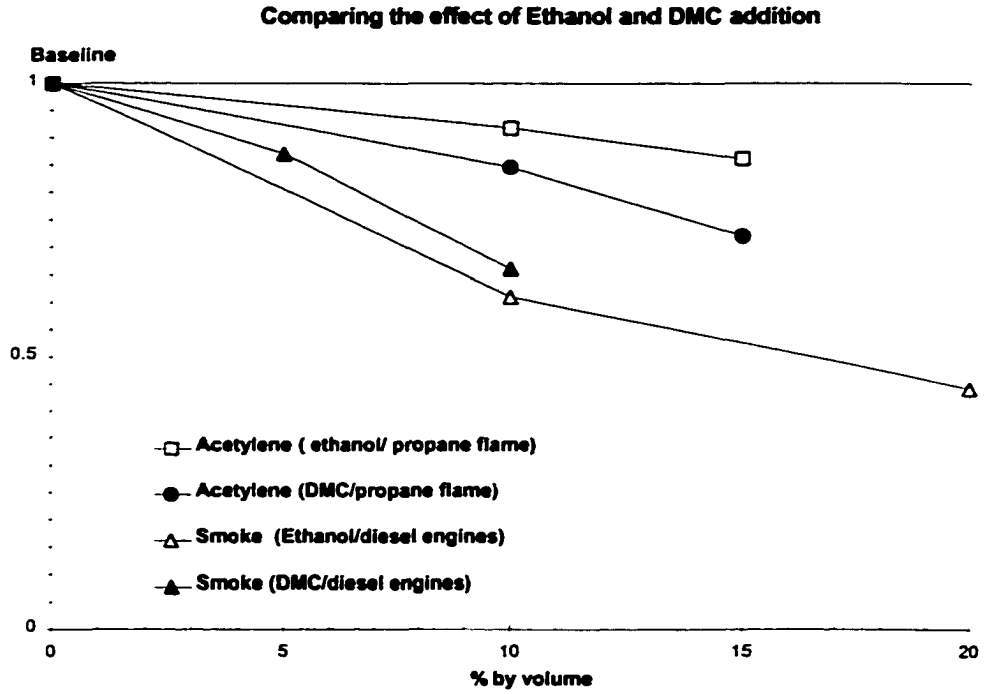

Figure 4-20: Comparison of Ethanol and DMC effects in 10% and 15% by volume on acetylene (counter-flow) and smoke (diesel engines)[19].

In Figure 4-20, our results on acetylene, with 10% and 15% by volume ethanol and DMC addition, are compared with those found by Shih [19] on smoke opacity in diesel engines, using similar dosage (5%, 10%, 20% by volume).

Figure 4-20 shows that 10% DMC addition is more efficient than ethanol in reducing soot precursors such as acetylene in counter-flow propane/air diffusion flame; the same dosage, instead, shows DMC be less efficient than ethanol in reducing smoke in diesel engines. However, we observe the same trend in reduction for both smoke and acetylene with higher DMC and ethanol dosage.

4.5 Potential mechanisms of acetylene reduction

In this section, we will discuss the most important factors that control the observed reductions in acetylene levels with the addition of oxygenated additives such as DMC and ethanol to the fuel stream of a propane /air diffusion flame.

The major physical effect on the soot formation process and soot precursor formation is the flame temperature. As discussed before (see chapter 2), it is a determinant factor of the rate of fuel pyrolysis and soot precursor formation [20]. Another physical factor that may affect fuel pyrolysis is dilution of the fuel stream. Chemical mechanisms may also play an important role. The presence of oxygen on the fuel side of the flame with additive addition can affect the fuel pyrolysis chemical pathways.

4.5.1 The influence of the flame temperature on acetylene levels

As discussed in detail in chapter 2, the flame temperature plays an important role in the rate of fuel pyrolysis and acetylene formation. When an oxygenated hydrocarbon is added to the fuel stream, it changes the flame temperature due to its different heat of combustion and its effect on the gas composition in the flame.

To evaluate the temperature effect of additive addition on soot precursor such as acetylene, the adiabatic flame temperature has been calculated. The adiabatic flame temperature is the maximum temperature achieved in the combustion process. It can be calculated by applying the first law of thermodynamics to an adiabatic combustor. The first law of thermodynamics can be written as [70, 79]:

$$\sum_{i,prod} n_i (h(T_2) - h(T_0) + \Delta H^0_f)_i - \sum_{j,react} n_j (h(T_1) - h(T_0) + \Delta H_f{}^0)_j = Q - W_x \qquad (1)$$

For adiabatic condition there is no heat released (Q) or work transferred (W_x). Using the linear approximation for the temperature dependence of the specific heats, $c_{pi}=a_i+b_iT$, we have [70, 71]:

$$h_i(T) - h_i(T_0) = a_i (T-T_0) + b_i/2 (T^2-T^2_0) \qquad (2)$$

The reactant temperature (T_1) is set equal to T_0. The problem can be further simplified by considering the case of isothermal reaction ($T_1=T_2=T_0$). For this case,

$W_x=0$, $Q=-\Delta h_c^0(T_0)$

$$\sum_{i,prod} n_i (\Delta H^0_f)_i - \sum_{j,react} n_j (\Delta H_f{}^0)_j = Q=-\Delta h_c^0(T_0) \qquad (3)$$

where $\Delta h_c^0(T_0)$ is the heat of combustion of the reactants at $T=T_0$. The heats of combustion of fuel and additives are reported in Table 4-2. Dissociation of the combustion products is not significant, as the temperatures are less than 2200 K [70, 79]. If we substitute equation (2) and (3) in equation (1), we can solve for the adiabatic flame temperature T_2:

$$\sum_{i,prod} n_i \left[a_i (T_2 - T_0) + \frac{b_i}{2} (T_2^2 - T_0^2) \right] = \Delta h_c^0(T_0) \qquad (4)$$

The adiabatic flame temperature has been calculated for five different cases: no additive, DMC 10% and 15% by volume, ethanol 10% and 15% by volume. Figure 4-21 shows the concentration of acetylene in PPM versus the adiabatic flame temperature for all these different cases.

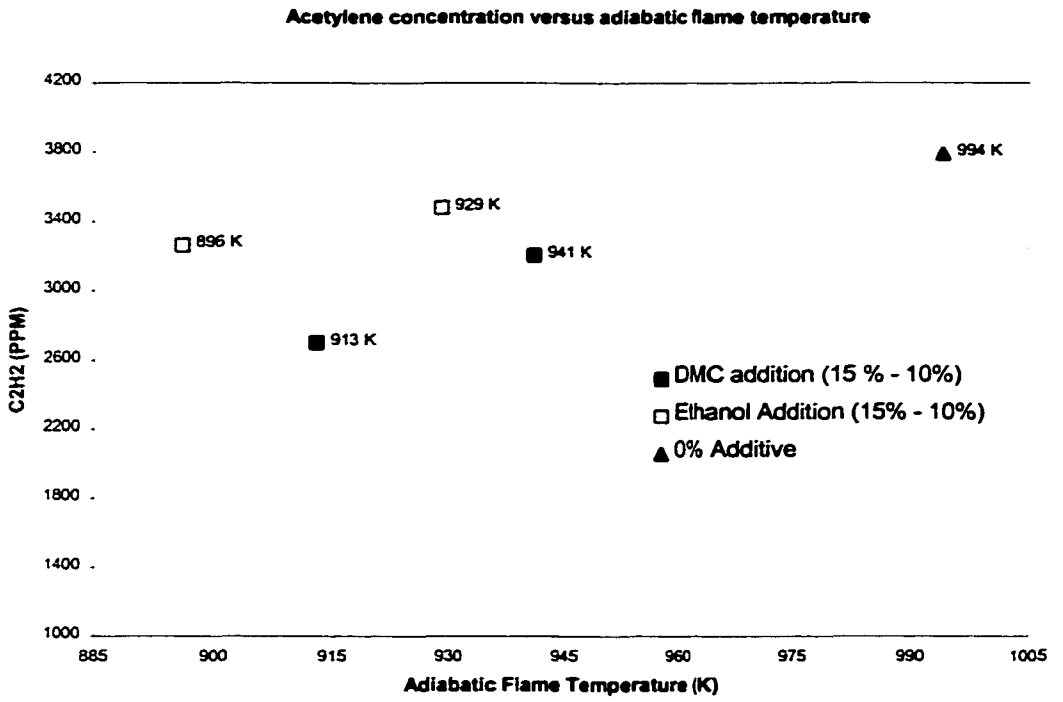

Figure 4-21: Acetylene concentration versus adiabatic flame temperatures with and without additive addition.

As expected, the adiabatic flame temperature decreases from the case with 0% additive (994 K) as we add DMC and ethanol to the fuel stream. We observe that the adiabatic flame temperature changes from 994 K to 929 K with 10% by volume ethanol addition and from 994 K to 941 K with 10% by volume DMC addition according to the different thermal properties of the two additives (see Table 4-2).

As we add DMC in 10% and 15% by volume, we observe higher reductions in acetylene levels than with ethanol addition although the adiabatic flame temperature for the DMC case is

higher than for the ethanol case. This suggests that the thermal effect produced by DMC addition is not a dominant effect for soot precursor reduction. The thermal effect alone cannot explain the higher reductions observed for the acetylene levels with DMC addition. In fact, for the same amount of additive, ethanol presents lower adiabatic flame temperatures but higher acetylene concentrations. Therefore, a thermal effect does not seem to be the most dominant mechanism of the higher acetylene reductions with DMC addition.

4.5.2 The influence of fuel stream carbon content on acetylene levels

The fuel pyrolysis in diffusion flames is related to the flame temperature but also to other parameters such as chemical structure and overall fuel carbon content. Neglecting the flame temperature effect, we would expect that a reduction in the overall carbon content in the fuel stream would lead to a reduction in acetylene levels. This is the case with ethanol addition, which has a lower carbon content than propane. However, the DMC addition tests this hypothesis as it has the same carbon content as propane. As DMC reduces acetylene levels without effecting the carbon content, this effect is not dominant.

4.5.3 The influence of fuel oxygen content on acetylene levels

From the literature (see chapter 2), the additive oxygen content is known to be an important factor for soot reductions [15, 19]. Figure 4-22 shows the relationship between acetylene concentrations across the flame and the O/C ratio with 10% and 15% by volume additive additions. From this plot of data, we can recognize a trend that leads to a decrease in acetylene levels with increases in the additive oxygen content, as already suggested from the literature [15, 19].

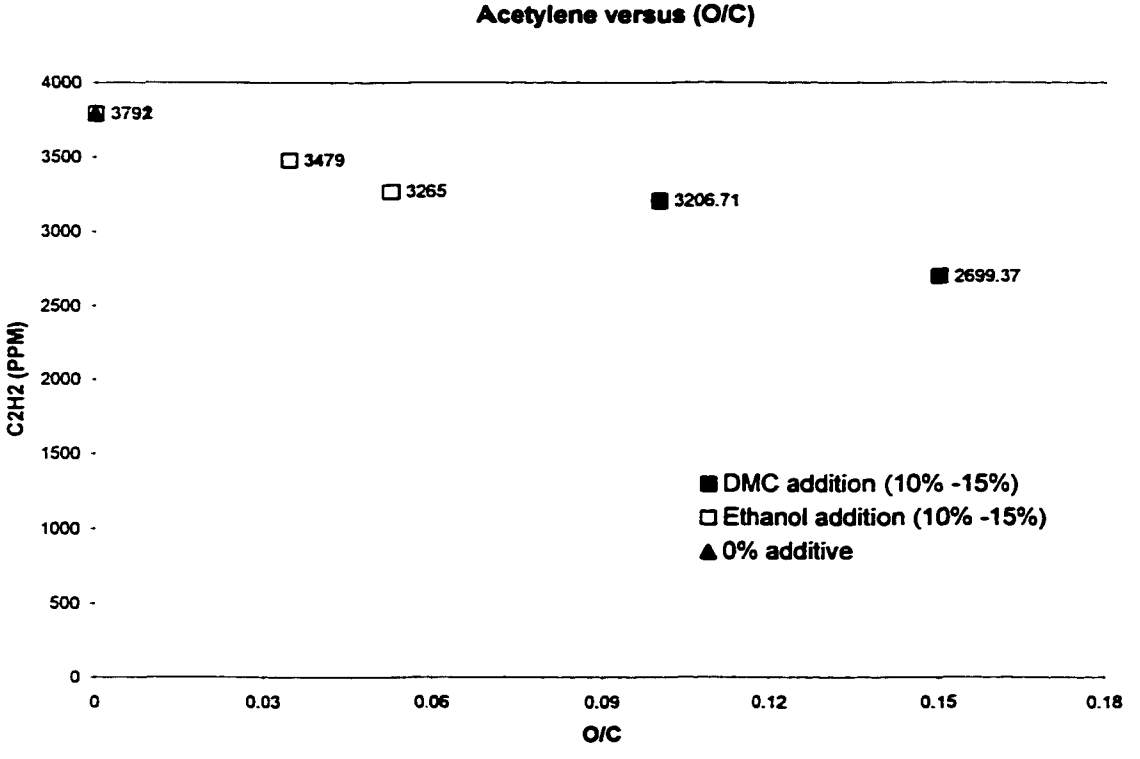

Figure 4-22: Acetylene concentration versus oxygen/carbon ratio.

From the previous observations, this reduction effect is probably due to the addition of oxygen atoms to the fuel rich side of the flame. This oxygen is generated by additive pyrolysis and it can form O and OH radicals. These radicals can attack acetylene and propane enhancing their oxidation. The O and OH radicals, competing with H atoms that play a key role in fuel pyrolysis, can then modify the path of propane pyrolysis toward less acetylene production.

In Figure 4-23, it is shown the relationship between C-C content and acetylene concentrations for both the cases with and without additives.

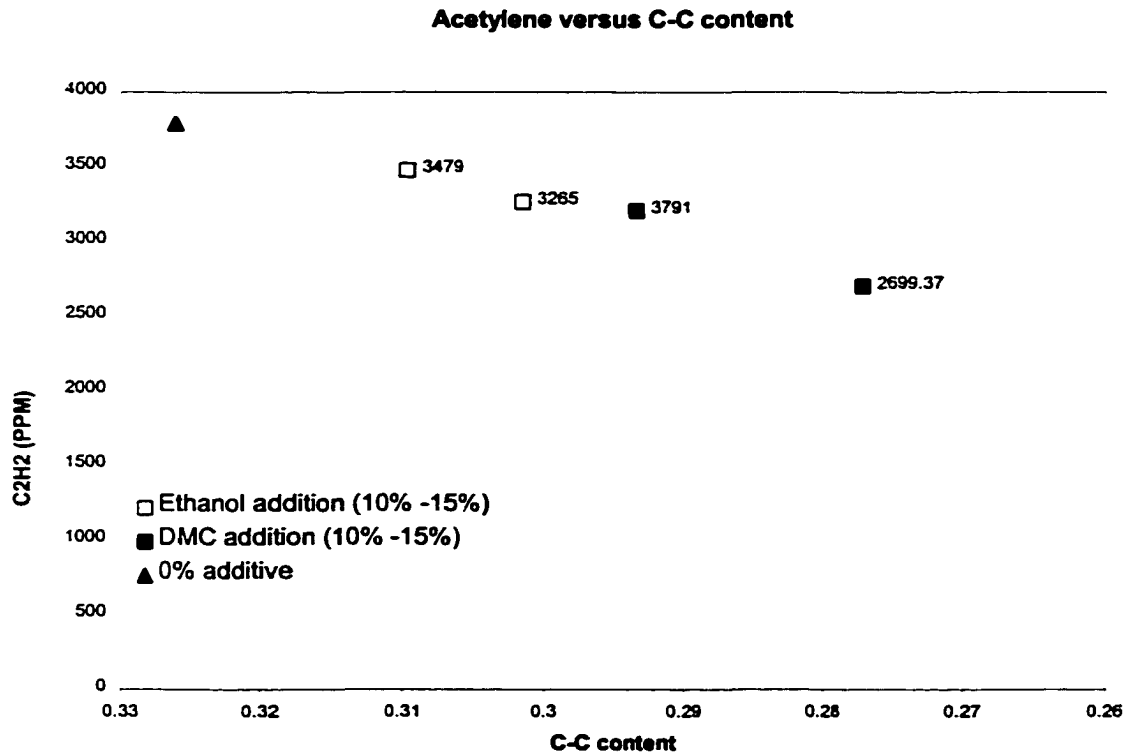

Figure 4-23: Acetylene concentration versus C-C content.

Similarly to Figure 4-22, the acetylene concentration decreases as the C-C content of the fuel stream decreases.

However, more data points (additive with different chemical structures and in different percentages) are needed to better highlight this effect and relate not only the oxygen content but also the chemical structure of the additive to acetylene and other soot precursor reductions.

Chapter 5: Conclusions and Recommendations

5.1 Conclusion

The objective of this research was to investigate the fundamental mechanisms by which oxygenated additives act on soot precursor formation in a counter-flow propane/air diffusion flame at atmospheric pressure. Particular attention was given to acetylene, as it is a key precursor species for soot particle formation. Experiments were carried out using a counter-flow diffusion flame burner as it simplifies the analysis of the soot formation mechanisms to a one-dimensional system [7,11]. From the experiments the following conclusions can be made:

1. The structure of the counter-flow diffusion flame was flat, steady and one-dimensional. The flame was sitting just below the stagnation plane, on the fuel side. Flow rate and stream velocities for both fuel and oxidizer were kept constant (10 cm/sec) and the distance between the two ducts of the burner was fixed at 20-mm.
2. Sampling was accomplished by continuously withdrawing gases from within the flame using a quartz micro- probe. C1-C6 species have been detected across the flame using a Gas Chromatograph (GC) provided with a flame ionization detector (FID) and a capillary column.
3. Repeatability of experimental measurements has been demonstrated.
4. The oxygenated additives, dimethyl carbonate (DMC) ($C_3H_6O_3$) and ethanol (C_2H_5OH), were added to the fuel stream of the burner in different dosages, keeping the total

volumetric flow rate constant, in order to ensure similar flame sizes and shapes [6]. Additives were first evaporated and soon after added in 10% and 15% by volume to the fuel stream.

5. Results showed 10 vol% DMC significantly reduces soot precursor levels such as acetylene (~ 15%) and benzene (~ 27%) and most of the other flame products at the flame plane.
6. Ethanol addition (10 vol%) showed, instead, more modest reductions for acetylene (~ 8%) and most of the other species except benzene, which increased slightly.
7. Higher dosages for both additives (15 vol%) generally gave higher precursor reductions. In particular, acetylene (C_2H_2) was reduced by 15% and 28% with 10% and 15% DMC addition, respectively, while by ~ 8% and ~13 % with ethanol addition. DMC also consistently reduced benzene (27% and 50%) while ethanol had a modest effect (14%) that was evident only at the higher dosage (15% by volume).
8. Our results on the effects of oxygenated additives on soot precursor formation are analogous to those found on soot emissions in diesel engines using DMC and ethanol [19]. Soot reductions have been observed with both DMC and ethanol in diesel engines. This effect increases with additive content. However, in diesel engines, complexities due to many simultaneous parameters (i.e. fluid flow, vaporization and chemical processes) limited the ability to determine how these additives operate. This supports our view that laboratory scale experiments such as a counter-flow configuration can provide useful insight into soot formation mechanisms and additive effects.
9. The temperature effect of additive addition has been investigated through the calculation of the adiabatic flame temperature. In the DMC case, although the adiabatic flame

temperature decreases because of its lower heat of combustion, the thermal effect does not seem to be significantly related to the reductions in acetylene levels.

10. The investigation of the fuel stream carbon content on acetylene levels suggests that this effect is not a determinant parameter for explaining acetylene reductions. However, a linear relationship between additive oxygen content and acetylene concentrations has been found.
11. Results suggest that DMC and ethanol may act chemically on soot precursor formation (i.e. acetylene and benzene) in counter-flow propane/air diffusion flames.

5.2 Recommendation

In order to improve our understanding of how additive affects soot formation mechanisms, more flame parameters need to be measured:

1. Flame temperature is a key factor in soot formation mechanisms. Platinum-Rhodium thermocouples, provided with fine coating to avoid appreciable conduction losses, represent an example of device that could be used for temperature measurements across the flame, although problems can arise in a sooting flame because of possible soot deposition. The advantage of taking temperature measurements is that we can more easily follow any changes in the flame temperature due to additive additions. One approach is to isolate the effect of temperature by keeping it constant during additive addition in order to investigate the chemical mechanisms by which additives act on soot formation.
2. Measurements of soot concentrations through laser techniques (i.e. light extinction) and PAH, through gas chromatography and mass spectrometry (GC/MS) could give a better picture of the link between soot precursor levels and soot formation.
3. The use of a microprobe for sampling, although it doesn't significantly affect the flame due to its small dimensions, represents an intrusive sampling technique that can lead to disturbance and error during measurements. A laser technique would overcome this problem.

Flame conditions could resemble more closely those within actual diesel engines:

1. Pressure is known to affect soot formation mechanisms. Tests could be conducted at high pressure.
2. Heavier fuels could be used to replace propane.

Further studies can deepen our understanding of the effect of additives on soot formation:

1. The counter-flow diffusion flame burner is a suitable device for numerical modeling. This can provide us with a more detailed knowledge of the combustion chemistry of oxygenated additives in flames. Kinetic models in fact are available for both propane and ethanol oxidation and can be easily implemented to model our experimental data.
2. More investigations are needed into the link between the additive's chemical structure and its effect on soot formation. One study could compare the effect of additives with the same number of carbon atoms as for the fuel, but slightly different in structures. The idea is to highlight chemical mechanisms that can reduce soot levels promoting soot oxidation or acting as soot precursor inhibitors.

References

1. Browner M.C., "Smog and Soot: Updating Air quality Standards", *Public Health Reports*, 112: 366-367 (1997)
2. Castaldi M.J., Vincitore, A.M. and Senkan, S.M., "Micro-Structure of Premixed Hydrocarbon Flames: Methane", *Combust. Sci. Tech.*, 107: 1-9 (1995).
3. D. C. Siegla and G. W. Smith, eds., *Particulate carbon: Formation during combustion.* Plenum Press, New York, 1981.
4. Vincitore, A.M. and Senkan, S.M., "Polycyclic Aromatic Hydrocarbon Formation in Opposed Flow Diffusion Flames of Ethane", *Combust. Flame*, 114: 259-266 (1998).
5. McKinnon, J.T. and Howard, J.B., "The Role of PAH and Acetylene in Soot Nucleation and Growth", *XIV th Symp. (Int.) on Combust.*, The C. I., pp 965-971 (1992).
6. NI, T, Gupta, S.B. and Santoro, R.J., "Suppression of Soot Formation in Ethene Laminar Diffusion Flames by Chemical Additives", *XV th Symp. (Int.) on Combust.*, The C. I., pp 585-592 (1994).
7. Kang, K.T, J.Y. Hwang, S.H. Chung, and W. Lee, "Soot Zone Structure and Sooting Limit in Diffusion Flames: Comparison of Counter-flow and Co-flow Flames", *Combust. Flame*, 109: 266-281 (1997).
8. Colket, M.B. and Hall, R.J., "Mechanism Controlling Soot formation in Diffusion Flames" Annual Report for AFOSR Contract F49620-94-C-0059, August (1995).
9. McEnally, C.S. and Pfefferle, L.D., "Aromatic and Linear Hydrocarbon Concentration Measurements in Non-Premixed Flame", *Combust. Sci. Tech.*, 116-117: 183-209 (1996).

10. Marinov, N.M, Pitz, W.J., C.K.Westbrook, Lutz, A.E., Vincitore, A.M. and Senkan, S.M. "Chemical Kinetic Modeling of Methane Opposed Flow Diffusion Flame and Comparison to Experiments", Lawrence Livermore National Laboratory, Pub. # 2 DO5.

11. Gomez, A. and Rosner, D.E., "Thermophoretic Effects on Particles in Counter-Flow Laminar Diffusion Flames", *Combust. Sci. Tech.*, 89: 335-362 (1993).

12. Shyan-Lung Chung and Katz, J.L, "The Counter-Flow Diffusion Flame Burner: A New Tool for the study of Nucleation of Refractory Compounds", *Combust. Flame* 61: 271-284 (1985).

13. Liu, G.E, Ye, Z.Y., and Sohrab, "On Radiative Cooling and Temperature Profiles of Counter-Flow premixed Flames", S.H., *Combust. Flame* 64: 193-201 (1986).

14. Wang, H., D.X. Du., C.J. Sung and C.K. Law, "Experiments and Numerical Simulation on Soot Formation in Opposed-Jet Ethylene Diffusion Flames", *XIV th Symp. (Int.) on Combust.*, The C. I., pp. 2359-2368 (1996).

15. N. Miyamoto, Hideyuki Ogawa, and Teruyoshi Arima, "Improvement of Diesel Combustion and Emission with Addition of Various Oxygenated Agents to Diesel Fuels", SAE Paper No.962115.

16. Lipkea, W.H., Johnson, J.H. Vuk C.T., "The Physical and Chemical Character of Diesel Particulate Emissions-Measurement Techniques and Fundamental Considerations", SAE Paper No. 780108, USA.

17. Leung, K.M., and Lindstedt, R.P., "A Simplified Reaction Mechanism for Soot Formation in Non-Premixed Flames", *Combust. Flame* 87: 289-305 (1991).

18. Kittleson, D.B., Imad S. Abdul-Khalek, Yong Chen, Cao-Jian Du, David J. Haugen, and Eivind Stenersen, " Influence of a fuel additive on the performance and emissions of a Medium-duty Diesel Engine" SAE Paper No. 941015.

19. Leonard Kuo-Liang Shih, "Comparison of the Effects of Various Fuel Additives on the Diesel Engine Emissions" SAE Paper No. 982573.

20. Omer L. Gulder, "Soot Particulate Formation and Characterization in Combustion", *Combustion Research Group*, National Research Council Canada 1996.

21. Calcote H.F., "Mechanisms of Soot Nucleation in Flames – A Critical Review", *Combust. Flame* 42: 215-242 (1981).

22. Kennedy I.M., "Models of Soot Formation", Prog. Energy Combust. Sci. 23: 95-132, 1997.

23. Frenklach M., "On Surface Growth Mechanism of Soot Particles", *Twenty-Sixth Symposium (International) on Combustion*, p. 2285-2293, The Combustion Institute, 1996.

24. Sung C.J. et al., "Structure and Sooting Limits in Counterflow methane/Air and propane/Air Diffusion flames from 1 to 5 Atmosphere" *Twenty-Seventh Symposium (International) on Combustion* The Combustion Institute, Publication No. 1DO7.

25. E. Muller and M. Zillmer, "Modeling of Nitric Oxide and Soot Formation in Diesel Engine Combustion", SAE Paper No. 982457.

26. Herbstman, S., and Virk K., 1991, "Use of Dispersan/Detergents in Diesel Injector Keep Clean and Clean Up Studies," SAE Paper No. 912330.

27. Li, H, Prabhu, S.K., Miller D., and Cernasky, N., 1994, "The Effects of Octane Enhancing Ethers on the Reactivity of Primary Reference Fuel Blend in Motored Engine," SAE Paper No. 940478.

28. Du, D.X., H. Wang, and C.K. Law, "Soot Formation in Counter-Flow Ethylene Diffusion Flames from 1 to 2.5 Atmospheres", *Combust. Flame* 113: 264-270 (1998).

29. H. Bockhorn (Ed.), 1994, *Soot Formation in Combustion*, Springer-Verlag, Berlin.

30. Frenklach, M., M. Clary, D.W. Gardiner, W.C. Jr., and Stein, S.E. *Twentieth Symposium (International) on Combustion*, p. 887-901, The Combustion Institute, 1984.

31. Puri, I.K. and Seshandri, K., "The extinction of Diffusion Flames Burning Diluted Methane and Diluted Propane and Diluted Air", *Combust. Flame* 65: 137-150 (1986).

32. Liu, G.E, Ye, Z.Y., and Sohrab, "On Radiative Cooling and Temperature Profiles of Counter-Flow premixed Flames", S.H., *Combust. Flame* 64: 193-201 (1986).

33. Xu F. Sunderland P.B. and Faeth G.M., "Soot Formation in Laminar Premixed Ethyelene/Air Flames at Atmospheric Pressure", *Combust. Flame* 108: 471-493 (1997).

34. Shyan-Lung Chung, and Katz, L.J., "The Counter-Flow Diffusion Flame Burner: A New Tool for the Study of the Nucleation of Refractory Compounds", *Combust. Flame* 61: 271-284 (1985).

35. Bachmann, M., Wiese, W and Homann, K.H., "PAH and Aromeres: Precursors of Fullerenes and Soot", *Twenty-Sixth Symposium (International) on Combustion*, pp. 2259-2267, The Combustion Institute, 1996.

36. Senkan, S. and Castaldi, M., "Formation of Polycyclic Aromatic Hydrocarbons (PAH) in Methane Combustion: Comparative New results From Premixed Flames", *Combust. Flame* 107: 141-150 (1996).

37. Kang, K.T, J.Y. Hwang, S.H. Chung, and W. Lee, "Soot Zone Structure and Sooting Limit in Diffusion Flames: Comparison of Counter-flow and Co-flow Flames", *Combust. Flame*, 109: 266-281 (1997).

38. H.Y. Afeefy, J.F. Liebman, and S.E. Stein, "Neutral Thermochemical Data" in NIST Chemistry WebBook, NIST Standard Reference Database Number 69, Eds. W.G. Mallard and P.J. Linstrom, November 1998, National Institute of Standards and Technology, Gaithersburg MD, 20899.

39. Weast, R.C., "CRC Handbook of Chemistry and Physiscs', CRC Press Inc., 1979.

40. Schoenung, S.M. and Hanson, R.K., "CO and Temperature Measurements in a Flat Flame by Laser Absorption Spectroscopy and Probe Techniques", *Combust. Sci. Tech.*, 24: 227-237 (1981).

41. Cor, J.J. and Branch, M. C., "Studies of Counter-Flow Diffusion Flames at Low Pressure", *Combust. Sci. Tech.*, 127: 71-88 (1997).

42. Kassem, M., M. Qun, and S.M. Senkan, "Chemical Structure of Fuel-rich 1,2-$C_2H_4Cl_2/CH_4$/Ar Flames: Effects of Micro-Probe Cooling on the Sampling of Flames of Chlorinated Hydrocarbons", *Combust. Sci. Tech.*, 67: 147-157 (1989).

43. Frimstom, R.M., "Comments on Quenching Mechanisms in the Microprobe sampling of Flames", *Combust. Flame* 50: 239-242 (1983).

44. Bowman, C.T., "Probe measurements in Flames", 1976.

45. Malte, C.P., and Kramlich John C., "Further Observations of the Effect of Sample Probes on Pollutant Gases Drawn from Flame Zones", *Combust. Sci. Tech.*, 22: 263-269 (1980).

46. McNair, H.M. & Bonelli, E.J., "Basic Gas Chromatography", Varian, 1968.

47. Kramlich, C.J. and Malte, C.P., "Modeling and Measurement of Sample Probe Effects on Pollutant Gases Drawn from Flame Zones", *Combust. Sci. Tech.*, 18: 91-104 (1978).

48. W. Jennings, *Analytical Gas Chromatography* Orlando, FL: Academic Press, 1987.

49. Varian " Chromatography Systems", Varian Associated, Inc. 1996.

50. M.L. Lee, F. Yang, and K. Bartle, *Open Tubular Gas Chromatography: Theory and practice*. New York: Wiley, 1984.

51. R. Schill and Freeman, in *Modern Practice of Gas Chromatography*, 2 nd. ed. New York: Wiley, 1985.

52. De Nijs, R.C. and De Zeeuw, J., "Aluminum Oxide-Coated Fused-Silica Porous-Layer Open Tubular Column for Gas Solid Chromatography of C_1-C_{10} Hydrocarbons", *Journal of Chromatography*, 279: 41-48 (1983).

53. Xu F. Sunderland P.B. and Faeth G.M., "Soot Formation in Laminar Premixed Ethylene/Air Flames at Atmospheric Pressure", *Combust. Flame* 108: 471-493 (1997).

54. D.J. Hucknall, *Chemistry of Hydrocarbon Combustion*. London New York: Chapman and Hall, 1985.

55. Zang, J., and Megaridis, M.C., "Soot Suppression by Ferrocene in Laminar Ethylene/Air Non-Premixed Flames", *Combust. Flame* 105: 528-540 (1996).

56. Schug K.P., Y. Manheimer-Timmat, P. Yaccarino, and I. Glassman, "Sooting Behavior of Behavior of Gaseous Hydrocarbon Diffusion Flames and the Influence of Additives", *Combust. Sci. and Tech.*, 22: 235-250 (1980).

57. Du J., and Axelbaum, R.L., "The Effect of Flame Structure on Soot Particle Inception in Diffusion Flames", *Combust. Flame,* 100: 367-375 (1995).

58. Smooke M.D., "Mechanisms controlling soot formation in diffusion flames", ASFOSR Contract F49620-94-C-0059, 1997.

59. Frenklach M. and Yuan T., *Sixteen International Symposium on Shock Tubes and Waves*, Aachen, West Germany, 1987, pp. 487-493.

60. Zang, C., Atreya, A., and Lee, K., "Sooting Structure of Methane Counter-Flow Diffusion Flames with Preheated Reactants and Dilution by Products of Combustion", *Twenty-Fourth Symposium (International) on Combustion*, the Combustion Institute, 1992 pp. 1049-1057.

61. Warnatz, J., "The Mechanism of High Temperature Combustion of Propane and Butane", *Combust. Sci. Tech.*, 34: 177-200 (1983).

62. McEnally, C.S. and Pfefferle, L.D., "Aromatic and Linear Hydrocarbon Concentration Measurements in Non-Premixed Flame", *Combust. Sci. Tech.*, 116-117: 183-209 (1996).

63. Kazakov, A. and M. Frenklach, "On the Relative Contribution of Acetylene and Aromatics to Soot particle Surface and Growth" *Combust. Flame*, 112: 270-274 (1998).

64. Vincitore, A.M. and Senkan, S.M., "Polycyclic Aromatic Hydrocarbon Formation in Opposed Flow Diffusion Flames of Ethane", *Combust. Flame*, 114: 259-266 (1998).

65. Gulder O, and D.R. Snelling, "Formation and Temperature of Soot Particles in Laminar Diffusion Flames with Elevated Temperature" *Twenty-Third Symposium (International) on Combustion*/The Combustion Institute, 1990 pp. 1509-1515.

66. Liu, G.E, Ye, Z.Y., and Sohrab, "On Radiative Cooling and Temperature Profiles of Counter-Flow premixed Flames", S.H., *Combust. Flame* 64: 193-201 (1986).

67. Sohorab, S.H., Z.Y. Ye and C.K. Law, "Theory of Interactive Combustion of Counter-flow", *Combustion and Flame*, 45: 27-45 (1986).

68. Senkan, S. and Castaldi, M., "Formation of Polycyclic Aromatic Hydrocarbons (PAH) in Methane Combustion: Comparative New results From Premixed Flames", *Combust. Flame* 107: 141-150 (1996).

69. Haynes B.S., and Wagner, H.Gg., "Soot Formation", Prog. Energy Combust. Sci. 7: 229-273 (1981).

70. Glassman I., "Combustion", 2 nd. ed., Academic Press Inc., 1987.

71. Glassman I., and Yaccarino P., "The Temperature Effect in Sooting Diffusion Flames", *Eighteenth Symposium (International) on Combustion/* the Combustion Institute, 1992 pp. 1049-1057.

72. Schug K.P., Y. Manheimer-Timmat, P. Yaccarino, and I. Glassman, "Sooting Behavior of Behavior of Gaseous Hydrocarbon Diffusion Flames and the Influence of Additives", *Combust. Sci. and Tech.*, 22: 235-250 (1980).

73. Wang, H., D.X. Du., C.J. Sung and C.K. Law, "Experiments and Numerical Simulation on Soot Formation in Opposed-Jet Ethylene Diffusion Flames", *XIV th Symp. (Int.) on Combust.*, The C. I., pp. 2359-2368 (1996).

74. Axelbaum R.L., Flower W.L. and Law C.K., "Dilution and Temperature Effects of Inert Addition on Soot Formation in Counter-Flow Diffusion Flames", Combust. Sci and Tech., 1988, 61: 51-73.

75. Frenklach, M., Yuan, T., Sixteenth International Symposium on Shock Tubes and Waves, Aachen West Germany, 1987, pp. 487-493.

76. Randolph, A.L. and Law, C.K., Twenty-Firth Symposium (International) on Combustion, The Combustion Institute, 1986, pp. 1125-1131.

77. Beatrice, C., C. Bertoli, and N.D. Giacomo, "The New Findings on Combustion Behavior of Oxygenated Synthetic Diesel Fuels", *Combust. Sci. and Tech.*, 1998, 137: 31-50.

78. Leung, K.M., and Lindstedt, R.P., "Detailed Kinetic Modeling of C_1-C_3 Alkane Diffusion Flames", *Combust. Flame* 102: 129-160 (1995).

79. Flagan R.C. and Seinfeld, J.H, "Fundamentals of Air Pollution Engineering", Prentice Hall, Englewood Cliffs, New Jersey, 1998.

APPENDIX A: Experimental set up

Experimental set up:

1. View of counter-flow diffusion flame burner, microprobe and micrometer A-2

2. Original draft (hand drawing) of counter-flow burner A-3

3. Vacuum Pump characteristics A-7

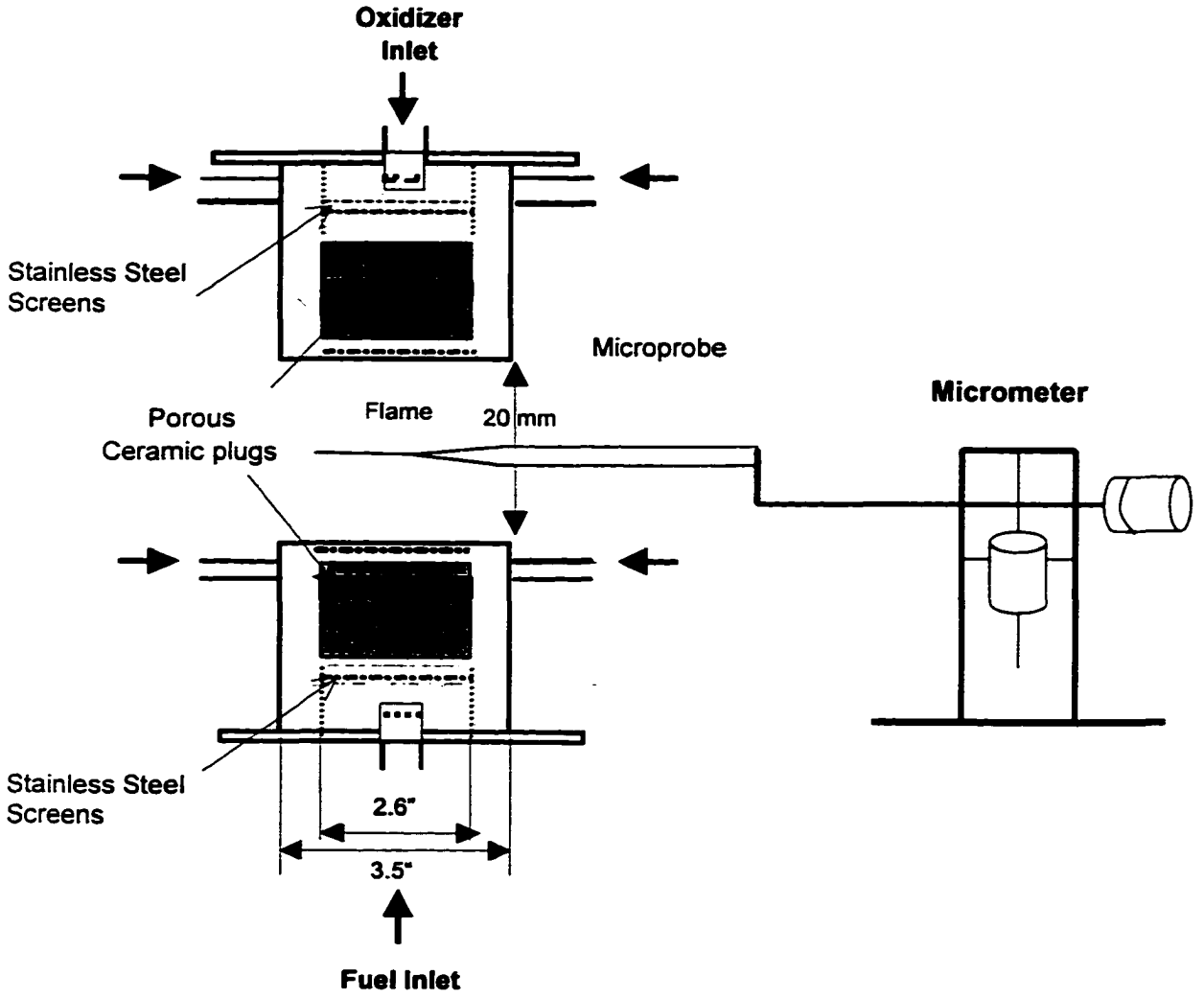

1. View of counter-flow diffusion flame burner, microprobe and micrometer.

Item 3

Cross section
Not to scale

BURNER DRAFT

(A) GROOVED
TO ASSIST WELD LOCATION

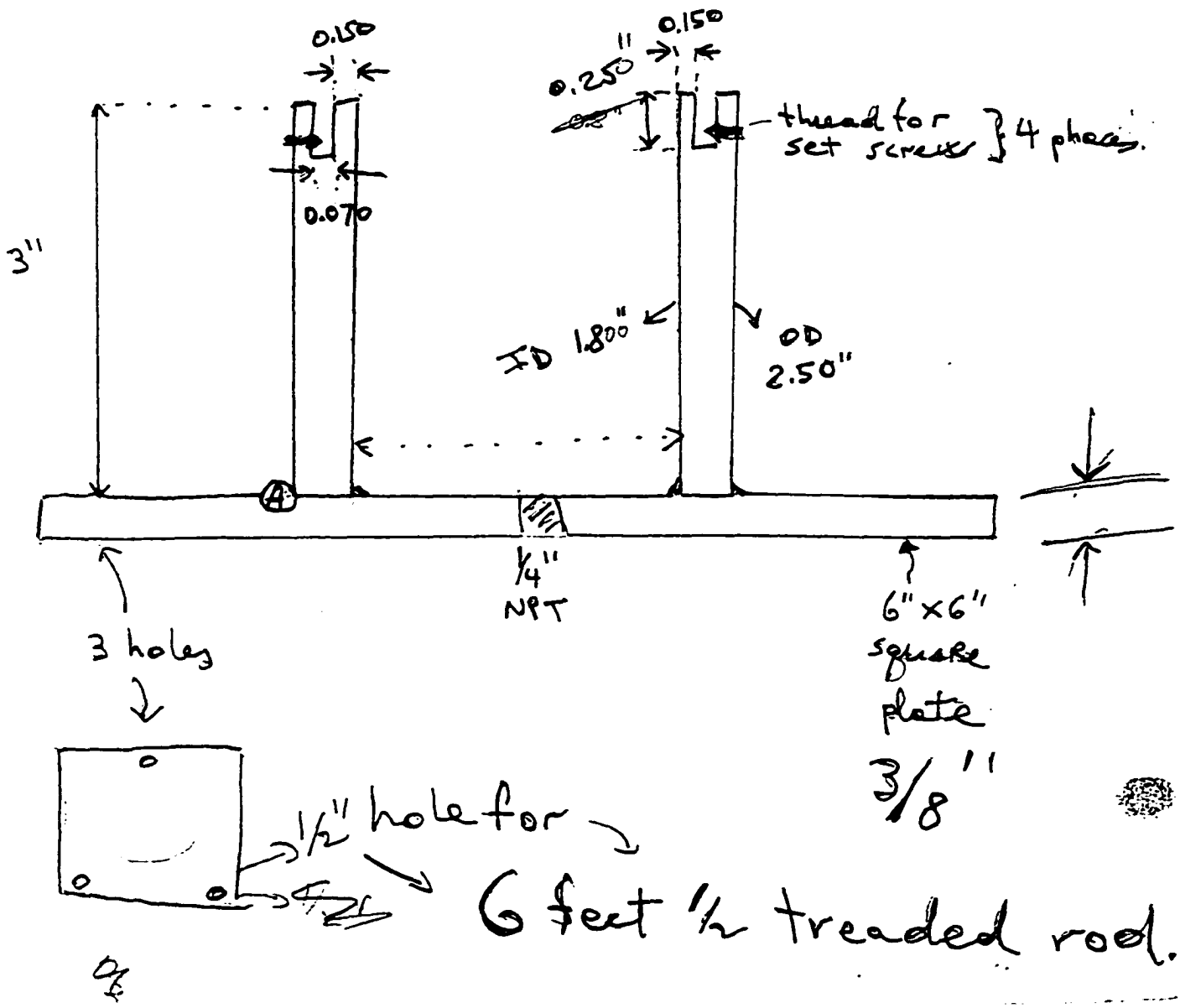

Item 2

CROSS SECTION

NOT To SCALE

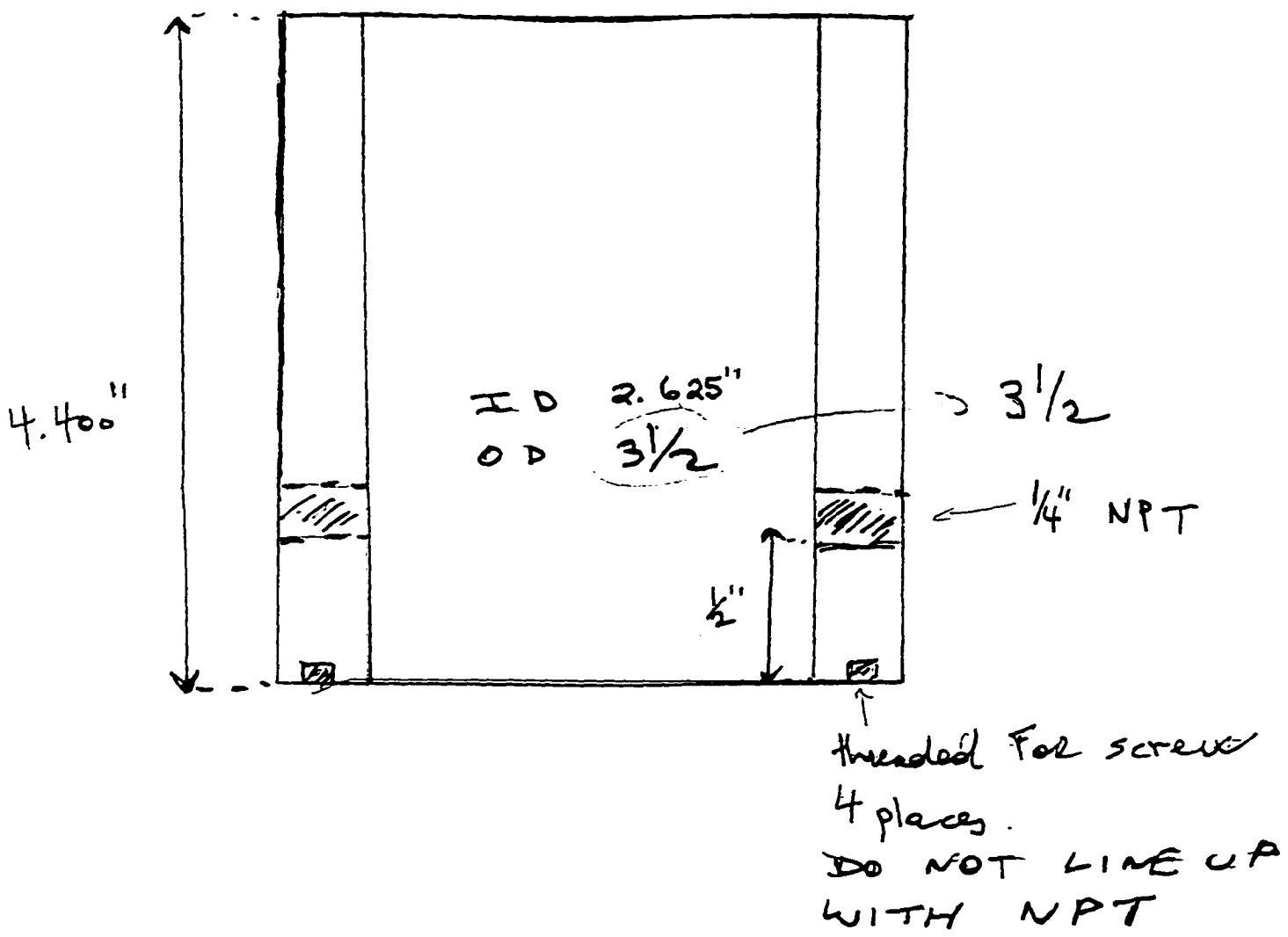

ASSEMBLY BURNER:

- Item 1
- Item 2
- Item 3

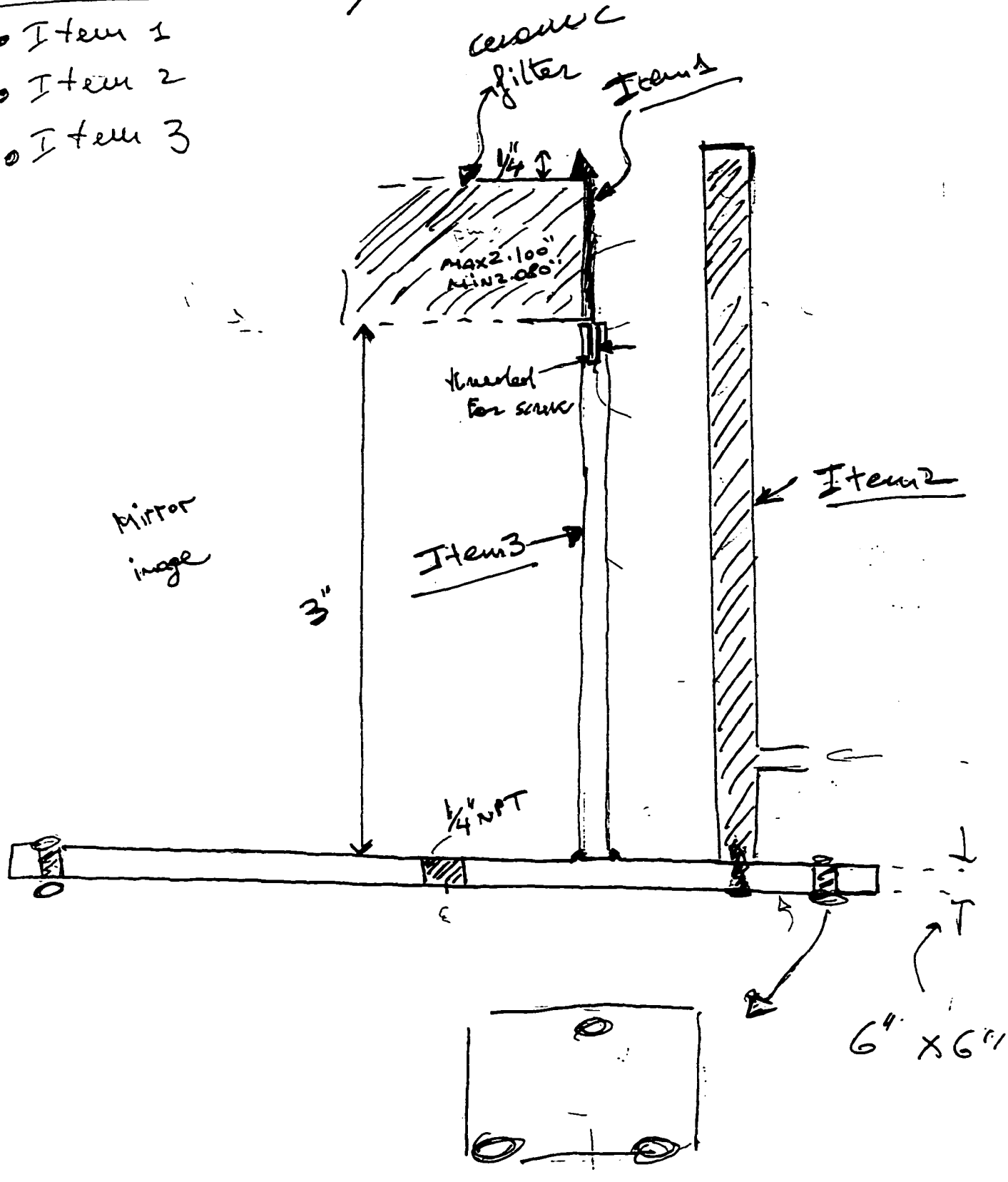

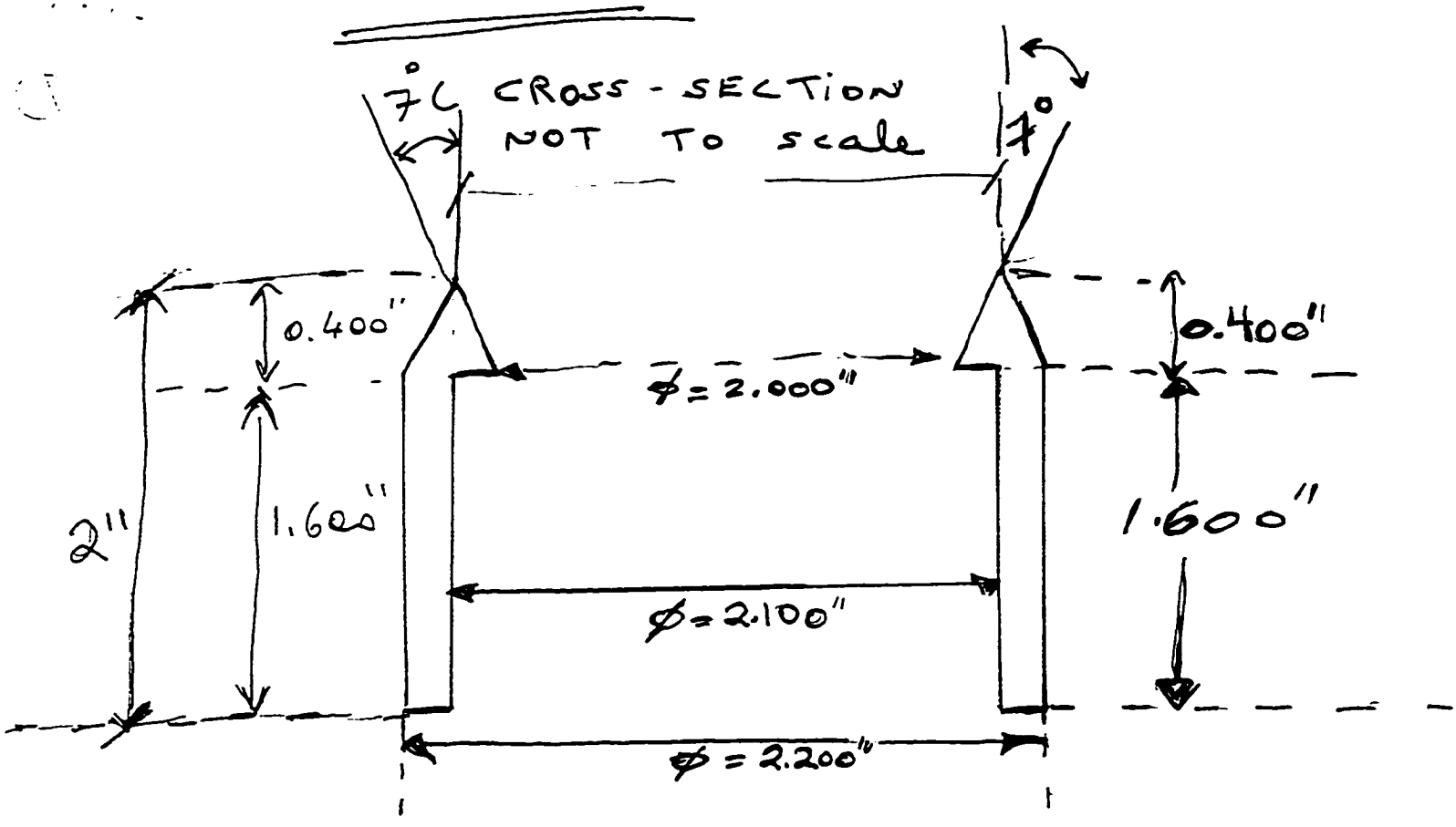

INNOVATIVE TECHNOLOGY WORLDWIDE

KNF NEUBERGER, INC.

KNF Neuberger, Inc., Two Black Forest Road, Trenton, NJ 08691-9428 · Phone: (609) 890-8600 · Fax: (609) 890-8323

Diaphragm Vacuum Pumps and Compressors

N 035.0 AT.11I
N 035.0 ST.11I
(Electrically Heated)

Dimensions: (in)

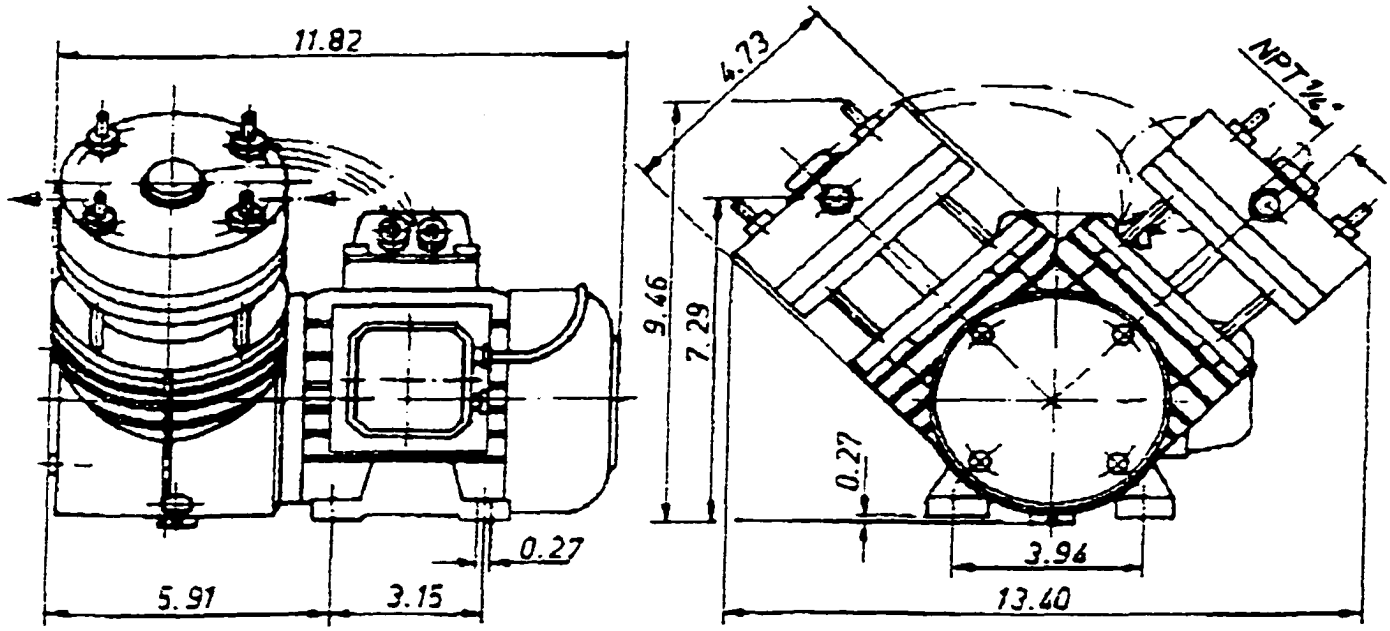

Technical Data: Measured @ atmospheric pressure @ +20°C (+68°F)
Separately for each head.

Performance Characteristics (Per Head)

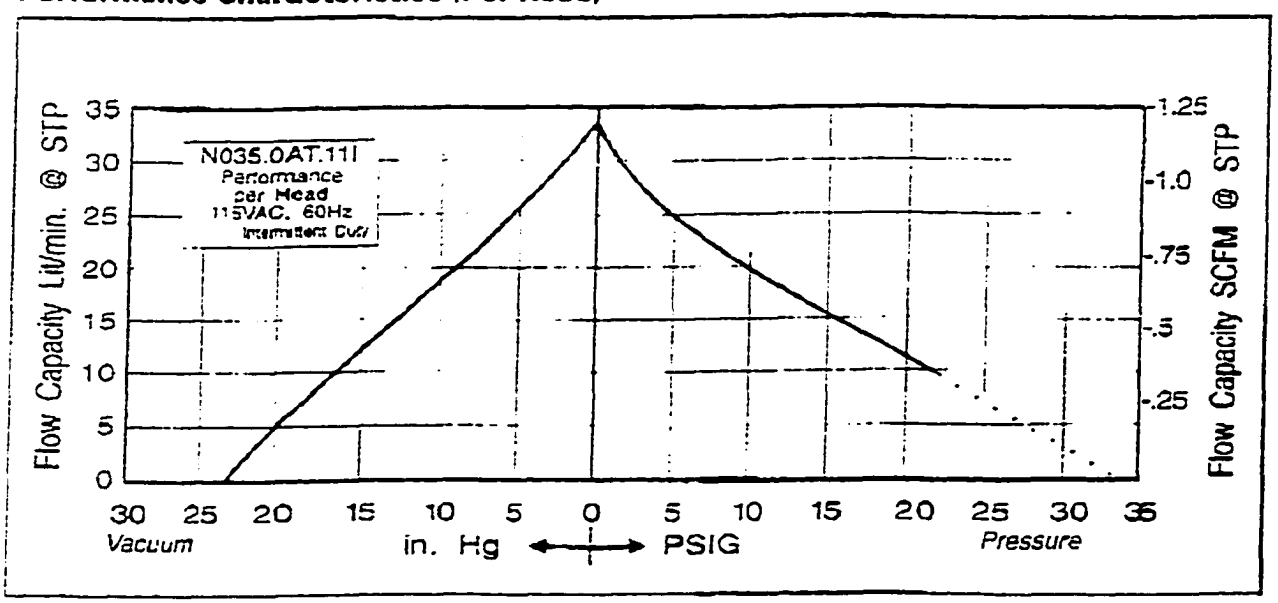

Flow Capacity: 34 Std. liters/min. (1.2 scfm) per head
Max. Vacuum: 24 in. Hg
Max. Pressure: 22 psig continuous

Voltage: 115 VAC, 60 Hz
Heating Time: Approx. 15 min. to +200°C (+400°F)
Weight: 32.8 lb (14.8 kg)

APPENDIX B: Flame Characteristics

Flame characteristics with and without additives:

1. Report on fuel and oxidizer composition, flow rates and gas flow-meter readings:

a) Additive	0%	(Pure Fuel) (C_3 H_8)	B-2
b) Ethanol	10%		B-3
c) Ethanol	15%		B-4
d) DMC	10%		B-5
e) DMC	15%		B-6

2. Raw data (in area count) of the flame species detected by Gas Chromatography:

a) Flame species profile without additives B-7

b) DMC addition data B-8

c) Ethanol addition data B-10

Data **DMC** **ADDITIVE ADDITION AS PERCENTAGE (%) of FUEL FLOW**

	Burner		
Propane	Diameter	0.05334	m
	Shroud		
C3H8	Diameter	0.066675	m

Equiv. Ratio **1.79**
(slightly fuel rich)

Dimethyl (C3H6O3)	1.069	densityliq (Kg/l)	
Carbonate	90.08	Mol.Weight	

		Vpump (ml/m	ngas(mol/mliq	(g/min)
(Additive FUEL %)	**0%**	0.000	0.000	0.000

	Propane	N_2	Air	O2	Air	N2	CH4
	603-G	**605-G**	**605-G**	**604-G**	**605-G**	**605-G**	**603-G**
B0	2.52	2.66	2.46	6.30	2.46	2.66	5.81
B1	15.84	7.28	8.12	16.48	8.12	7.28	26.68
B2	5.3348	-0.05	-0.089	-0.004	-0.089	-0.05	4.4235

Velocity	**Air-Total**	**C3H8 (16.33%**	**DMC (%)**	**C3H8**	**N2 (83.66%**	**Air (68.97%)**	**O2 (31.02 %)**	**Coflow Air**	**Coflow N2**
cm/sec	SLPM	SLPM	SLPM	SLPM	SLPM	SLPM	SLPM	SLPM	SLPM
10	**13.41**	**2.19**	-	**2.19**	**11.22**	**9.25**	**4.16**	**7.64**	**7.64**
11	14.75	3.15	-	3.15	11.59	5.60	9.14	8.30	8.30
12	16.09	4.02	-	4.02	12.07	6.11	9.98	9.05	9.05
13	17.43	4.36	-	4.36	13.07	6.62	10.81	9.80	9.80
14	18.77	4.69	-	4.69	14.08	7.13	11.64	10.56	10.56
15	20.11	5.03	-	5.03	15.08	7.64	12.47	11.31	11.31
16	21.45	5.36	-	5.36	16.09	8.15	13.30	12.07	12.07
17	22.79	5.70	-	5.70	17.09	8.66	14.13	12.82	12.82
18	24.13	6.03	-	6.03	18.10	9.17	14.96	13.58	13.58
19	25.47	6.37	-	6.37	19.11	9.68	15.79	14.33	14.33
20	26.81	6.70	-	6.70	20.11	10.19	16.63	15.08	15.08
21	28.16	7.04	-	7.04	21.12	10.70	17.46	15.84	15.84
22	29.50	7.37	-	7.37	22.12	11.21	18.29	16.59	16.59

Data **DMC** **ADDITIVE ADDITION AS PERCENTAGE (%) of FUEL FLOW**

	Burner		
Propane	Diameter	0.05334	m
	Shroud		
C3H8	Diameter	0.066675	m

Equiv. Ratio **1.68**
(slightly fuel rich)

Dimethyl (C3H6O3)	1.069	densityliq (Kg/l)	
Carbonate	90.08	Mol.Weight	

		Vpump (ml/m	ngas(mol/m	liq (g/min)
(Additive FUEL %)	**10%**	0.766	0.009	0.819

	Propane	N_2	Air	O2	Air	N2	CH4
	603-G	**605-G**	**605-G**	**604-G**	**605-G**	**605-G**	**603-G**
B0	2.52	2.66	2.46	6.30	2.46	2.66	5.81
B1	15.84	7.28	8.12	16.48	8.12	7.28	26.68
B2	5.3348	-0.05	-0.089	-0.004	-0.089	-0.05	4.4235

Velocity	**Air-Total**	**C3H8 (16.33%**	**DMC (%)**	**C3H8**	**N2 (83.66%**	**Air (68.97%)**	**O2 (31.02 %)**	**Coflow Air**	**Coflow N2**
cm/sec	SLPM	SLPM	SLPM	SLPM	SLPM	SLPM	SLPM	SLPM	SLPM
10	**13.41**	**2.19**	**0.22**	**1.97**	**11.22**	**9.25**	**4.16**	**7.54**	**7.54**
11	14.75	3.15	0.32	2.84	11.59	5.60	9.14	8.30	8.30
12	16.09	4.02	0.40	3.62	12.07	6.11	9.98	9.05	9.05
13	17.43	4.36	0.44	3.92	13.07	6.62	10.81	9.80	9.80
14	18.77	4.69	0.47	4.22	14.08	7.13	11.64	10.56	10.56
15	20.11	5.03	0.50	4.53	15.08	7.64	12.47	11.31	11.31
16	21.45	5.36	0.54	4.83	16.09	8.15	13.30	12.07	12.07
17	22.79	5.70	0.57	5.13	17.09	8.66	14.13	12.82	12.82
18	24.13	6.03	0.60	5.43	18.10	9.17	14.96	13.58	13.58
19	25.47	6.37	0.64	5.73	19.11	9.68	15.79	14.33	14.33
20	26.81	6.70	0.67	6.03	20.11	10.19	16.63	15.08	15.08
21	28.16	7.04	0.70	6.34	21.12	10.70	17.46	15.84	15.84
22	29.50	7.37	0.74	6.64	22.12	11.21	18.29	16.59	16.59

Data **DMC** **ADDITIVE ADDITION AS PERCENTAGE (%) of FUEL FLOW**

	Burner		
Propane	Diameter	0.05334	m
	Shroud		
C3H8	Diameter	0.066675	m

Equiv. Ratio **1.63**

(slightly fuel rich)

Dimethyl (C3H6O3)	1.069	densityliq (Kg/l)
Carbonate	90.08	Mol.Weight

		Vpump (ml/m	ngas(mol/m	liq (g/min)
(Additive FUEL %)	**15%**	1.149	0.014	1.228

	Propane	N_2	Air	O2	Air	N2	CH4
	603-G	**605-G**	**605-G**	**604-G**	**605-G**	**605-G**	**603-G**
B0	2.52	2.66	2.46	6.30	2.46	2.66	5.81
B1	15.84	7.28	8.12	16.48	8.12	7.28	26.68
B2	5.3348	-0.05	-0.089	-0.004	-0.089	-0.05	4.4235

Velocity	**Air-Total**	**C3H8 (16.33%**	**DMC (%)**	**C3H8**	**N2 (83.66%**	**Air (68.97%)**	**O2 (31.02 %)**	**Coflow Air**	**Coflow N2**
cm/sec	SLPM	SLPM	SLPM	SLPM	SLPM	SLPM	SLPM	SLPM	SLPM
10	**13.41**	**2.19**	**0.33**	**1.86**	**11.22**	**9.25**	**4.16**	**7.54**	**7.54**
11	14.75	3.15	0.47	2.68	11.59	5.60	9.14	8.30	8.30
12	16.09	4.02	0.60	3.42	12.07	6.11	9.98	9.05	9.05
13	17.43	4.36	0.65	3.70	13.07	6.62	10.81	9.80	9.80
14	18.77	4.69	0.70	3.99	14.08	7.13	11.64	10.56	10.56
15	20.11	5.03	0.75	4.27	15.08	7.64	12.47	11.31	11.31
16	21.45	5.36	0.80	4.56	16.09	8.15	13.30	12.07	12.07
17	22.79	5.70	0.85	4.84	17.09	8.66	14.13	12.82	12.82
18	24.13	6.03	0.91	5.13	18.10	9.17	14.96	13.58	13.58
19	25.47	6.37	0.96	5.41	19.11	9.68	15.79	14.33	14.33
20	26.81	6.70	1.01	5.70	20.11	10.19	16.63	15.08	15.08
21	28.16	7.04	1.06	5.98	21.12	10.70	17.46	15.84	15.84
22	29.50	7.37	1.11	6.27	22.12	11.21	18.29	16.59	16.59

Data **ETHANOL ADDITIVE ADDITION AS PERCENTAGE (%) of FUEL FLOW**

	Burner		
Propane	Diameter	0.05334	m
	Shroud		
C3H8	Diameter	0.066675	m

Equiv. Ratio **1.70**
(slightly fuel rich)

ETHANOL	**(C2H5OH)**	0.789	densityliq (Kg/l)		
		46.07	Mol.Weight		
			Vpump (ml/m	**ngas(mol/m**	**mliq (g/min)**
(Additive FUEL %)		**10%**	0.531	0.009	0.419

	Propane	N_2	Air	O2	Air	N2	CH4
	603-G	**605-G**	**605-G**	**604-G**	**605-G**	**605-G**	**603-G**
B0	2.52	2.66	2.46	6.30	2.46	2.66	5.81
B1	15.84	7.28	8.12	16.48	8.12	7.28	26.68
B2	5.3348	-0.05	-0.089	-0.004	-0.089	-0.05	4.4235

Velocity	**Air-Total**	**C3H8 (16.33%)**	**Ethanol (%)**	**C3H8**	**N2 (83.66%)**	**Air (68.97%)**	**O2 (31.02%)**	**Coflow Air**
cm/sec	SLPM	SLPM	SLPM	SLPM	SLPM	SLPM	SLPM	SLPM
10	**13.41**	**2.19**	**0.22**	**1.97**	**11.22**	**9.25**	**4.16**	**7.54**
11	14.75	3.15	0.32	2.84	11.59	5.60	9.14	8.30
12	16.09	4.02	0.40	3.62	12.07	6.11	9.98	9.05
13	17.43	4.36	0.44	3.92	13.07	6.62	10.81	9.80
14	18.77	4.69	0.47	4.22	14.08	7.13	11.64	10.56
15	20.11	5.03	0.50	4.53	15.08	7.64	12.47	11.31
16	21.45	5.36	0.54	4.83	16.09	8.15	13.30	12.07
17	22.79	5.70	0.57	5.13	17.09	8.66	14.13	12.82
18	24.13	6.03	0.60	5.43	18.10	9.17	14.96	13.58
19	25.47	6.37	0.64	5.73	19.11	9.68	15.79	14.33
20	26.81	6.70	0.67	6.03	20.11	10.19	16.63	15.08
21	28.16	7.04	0.70	6.34	21.12	10.70	17.46	15.84

Data **ETHANOL ADDITIVE ADDITION AS PERCENTAGE (%) of FUEL FLOW**

	Burner		
Propane	Diameter	0.05334	m
	Shroud		
C3H8	Diameter	0.066675	m

Equiv. Ratio **1.67**
(slightly fuel rich)

ETHANOL (C2H5OH)	0.789	densityliq (Kg/l)			
	46.07	Mol.Weight			
		Vpump (ml/m	**ngas(mol/m**	**mliq (g/min)**	
(Additive FUEL %)	**15%**	0.796	0.014	0.628	

	Propane	N_2	Air	O2	Air	N2	CH4
	603-G	**605-G**	**605-G**	**604-G**	**605-G**	**605-G**	**603-G**
B0	2.52	2.66	2.46	6.30	2.46	2.66	5.81
B1	15.84	7.28	8.12	16.48	8.12	7.28	26.68
B2	5.3348	-0.05	-0.089	-0.004	-0.089	-0.05	4.4235

Velocity	**Air-Total**	**C3H8 (16.33%)**	**Ethanol (%)**	**C3H8**	**N2 (83.66%)**	**Air (68.97%)**	**O2 (31.02%)**	**Coflow Air**
cm/sec	SLPM	SLPM	SLPM	SLPM	SLPM	SLPM	SLPM	SLPM
10	**13.41**	**2.19**	**0.33**	**1.86**	**11.22**	**9.25**	**4.16**	**7.64**
11	14.75	3.15	0.47	2.68	11.59	5.60	9.14	8.30
12	16.09	4.02	0.60	3.42	12.07	6.11	9.98	9.05
13	17.43	4.36	0.65	3.70	13.07	6.62	10.81	9.80
14	18.77	4.69	0.70	3.99	14.08	7.13	11.64	10.56
15	20.11	5.03	0.75	4.27	15.08	7.64	12.47	11.31
16	21.45	5.36	0.80	4.56	16.09	8.15	13.30	12.07
17	22.79	5.70	0.85	4.84	17.09	8.66	14.13	12.82
18	24.13	6.03	0.91	5.13	18.10	9.17	14.96	13.58
19	25.47	6.37	0.96	5.41	19.11	9.68	15.79	14.33
20	26.81	6.70	1.01	5.70	20.11	10.19	16.63	15.08
21	28.16	7.04	1.06	5.98	21.12	10.70	17.46	15.84

DATA : a) Flame Species profile without additives (Area count)

Date	Position	mm	Methane	Ethane	Ethylene	N-Hexane	Propane	Acetylene	N-Butane	Propylene	Propyne	Benzene
16-Mar			RT 7.197	RT 7.4	RT 7.6	RT 12.3	RT 8.1	RT 8.9	RT 9.4	RT 9.66	RT 11.19	RT 16.38
0	baseline	0	3.53E+01	8.39E+03	9.42E+04	0.00E+00	1.98E+07	2.68E+04	0.00E+00	6.14E+02	2.18E+03	0.00E+00
1	FP -2	7	7.46E+04	3.23E+04	2.46E+05	6.84E+03	1.05E+07	8.21E+04	1.50E+03	2.65E+05	6.46E+03	5.01E+03
3	FP-1	8	1.33E+05	1.47E+05	6.98E+05	8.61E+03	4.40E+06	3.76E+05	7.99E+03	3.56E+05	1.12E+04	4.38E+03
4	FP	9	1.54E+05	1.68E+05	9.03E+05	7.52E+03	1.17E+06	3.82E+05	4.05E+03	3.23E+05	1.55E+04	3.78E+03
5	FP	9	1.63E+05	1.77E+05	9.43E+05	8.17E+03	1.27E+06	4.02E+05	4.28E+03	3.43E+02	1.84E+04	4.12E+03
6	FP	9	1.58E+05	1.77E+05	9.11E+05	7.79E+03	1.53E+06	4.12E+05	5.00E+03	3.37E+02	1.71E+04	4.04E+03
7	FP	9	1.55E+05	1.72E+05	8.99E+05	7.61E+03	1.40E+06	3.99E+05	4.62E+03	3.33E+05	1.71E+04	4.13E+03
Aver.	FP	9	1.57E+05	1.73E+05	9.14E+05	7.77E+03	1.34E+06	3.99E+05	4.49E+03	1.64E+05	1.70E+04	4.02E+03
8	FP+ 2	11	1.70E+05	1.77E+05	9.53E+05	7.97E+03	1.26E+06	4.02E+05	4.17E+03	3.47E+05	1.68E+04	4.14E+03
9	FP+ 3	12	3.38E+03	1.60E+03	1.26E+04	0.00E+00	4.63E+04	5.01E+03	0.00E+00	9.08E+03	6.09E+02	0.00E+00
10	FP+ 4	13	8.01E+02	0.00E+00	0.00E+00	0.00E+00	1.31E+04	7.18E+02	0.00E+00	0.00E+00	0.00E+00	0.00E+00
11	FP+ 5	14	0.00E+00	0.00E+00	0.00E+00	0.00E+00	1.64E+04	0.00E+00	0.00E+00	0.00E+00	0.00E+00	0.00E+00
12		16	0.00E+00	0.00E+00	0.00E+00	0.00E+00	5.88E+03	7.95E+02	0.00E+00	0.00E+00	0.00E+00	0.00E+00
13		16	0.00E+00	0.00E+00	0.00E+00	0.00E+00	2.79E+03	0.00E+00	0.00E+00	0.00E+00	0.00E+00	0.00E+00

PPM Calculation — **Y= aX+b**

Equations from calibration curves — **X (PPM) = Y (Area)-b/a**

		a		b
Methane	Y=	23.72	X +	325.07
Ethane	Y=	34.629	X +	743.481
Ethylene	Y=	81.95	X	
propane	Y=	41.07	X +	986.64
Acetylene	Y=	105.18	X	

PPM Calculation

Equations from calibration curves

N-Butane	Y=	46.83	X + 1416.81
N-Hexane	Y=	58.17	X
N-Pentane	Y=	47.23	X
Propylene	Y=	148.85	X
Propyne	Y=	199.89	X

DATA: b) DMC addition

Date	DMC 10%		n-butane	propylene		propyne	n-hexane	benzene
17-Mar		mm	RT 9.4	RT 9.66	RT 10.33	RT 11.19	RT 12.3	RT 16.4
FP = 9	baseline	0						
(flame plane)	FP no add	9	2777	309303	25436	14780	4631	0
	FP+10%	9	3395	293618	25953	895	6034	2949
	FP+10%	9	3089	306568	25637	17516	6553	3158
	FP+10%	9	3152	304421	25540	17423	6783	3182
	FP+10%	9	3574	314648	27009	15958	6671	3330
	FP	9	4054	323273	28559	15516	8166	4119
	FP	9	4283	343085	38111	18400	7792	4040
	FP	9	5001	337403	36861	17122	7613	4127
	FP	9	4624	333073	38828	17083		
	Average	9	4490.5	334208.5	35589.75	17030.25	7857	4095.333
17-Mar	**DMC 15%**	mm	**RT 9.4**	**RT 9.66**	**RT 10.33**	**RT 11.19**	**RT 12.3**	**RT 16.4**
FP = 9	baseline	0						
(flame plane)	FP no add	9	4490.5	334208.5	35589.75	17030.25	7857	4095.333
	FP + 15%	9	4802	214592	16886	7866	4454	2031

DATA: b) DMC addition

Date	DMC 10%		methane	ethane	ethylene	propane	acetylene	
17-Mar		mm	RT 7.197	RT 7.4	RT 7.6	RT 8.1	RT 8.9	RT 9.2
FP = 9	baseline	0						
(flame plane)	**FP no add**	**9**	146640	148439	879941	740559	329190	5050
	FP+10%	9	162443	171761	835826	1002251	347310	6671
	FP+10%	9	170745	171266	864624	828929	334400	5739
	FP+10%	9	170171	172270	850684	872447	334611	5860
	FP+10%	9	173000	179802	876144	995671	356252	6690
	FP	9	154143	167509	902983	1171873	382372	7451
	FP	9	163111	176560	943115	1266790	402094	7967
	FP	9	157683	176668	910530	1527777	412284	9374
	FP	9	154660	171936	899159	1404477	398530	8707
	Average	9	157399.25	173168.25	913946.8	1342729.3	398820	8374.8
17-Mar	**DMC 15%**	mm	RT 7.197	RT 7.4	RT 7.6	RT 8.1	RT 8.9	RT 9.2
FP = 9	baseline							
(flame plane)	FP no add	9	157399.25	173168.25	913946.8	1342729.3	398820	8374.8
	FP + 15%	9	109798	130389	535571	1646856	274008	9699
Summary								
17-Mar	NO additive (aver	9	157399.25	173168.25	913946.8	1342729.3	398820	8374.8
Aver. FP	DMC 15%	9	109798	130389	535571	1646856	274008	9699
Aver. FP	DMC 10%	9	169089.75	173774.75	856819.5	924824.5	343143.3	6240

DATA: c) ETHANOL addition

Date	**Ethanol 15%**		**methane**	**ethane**	**ethylene**	**propane**	**acetylene**	
20-Mar	Position	mm	RT 7.197	RT 7.4	RT 7.6	RT 8.1	RT 8.9	RT 9.2
FP = 8	baseline							
(flame plane)	A position	0	33793	10137	95544	18821308	33307	0
	FP-2 + 15%	6	95044	52288	334863	7353086	118677	6314
	FP no add	8	147190	170453	798110	2764209	429084	13659
	FP + 15%	8	154381	157595	787793	2336187	389570	11361
	FP + 15%	8	155072	153600	790454	2128120	369871	10451
	FP + 15%	8	153571	146793	767643	1770901	349017	8370
	FP +1 +15%	9	193166	158580	968148	432255	281102	2412
	FP+2 +15%	10	0	0	572	23752	696	0
	FP + 4 + 15%	12	0	0	0	0	0	0
19-Mar	**Ethanol 10%**	mm	RT 7.197	RT 7.4	RT 7.6	RT 8.1	RT 8.9	RT 9.2
FP = 9	baseline							
(flame plane)	A position	0	19192	3017	343994	6720234	9455	0
	FP no add	9	173222	184532	981675	1024684	401102	6037
	FP + 10%	9	164973	168623	909097	983569	367402	5883
	FP + 10%	9	164896	168268	906930	1027047	370498	5990
	FP + 10%	9	168181	168619	913883	961476	366065	5746
Summary								
20-Mar	NO additive	8	147190	170453	798110	2764209	429084	13659
Aver. FP	Ethanol 15%	8	154341.333	152662.667	781963.333	2078402.667	369486	10060.67
19-Mar	NO additive	9	173222	184532	981675	1024684	401102	6037
Avar. FP	Ethanol 10%	9	166016.667	168503.333	909970	990697.3333	367988.333	5873
Diff. Aver. 10% - 15%		9	-7.0326272	-9.40080315	-14.06713	109.7918907	0.40698754	71.30371

DATA: c) ETHANOL addition

Date	**Ethanol 15%**		**n-butane**	**propylene**		**propyne**	**n-hexane**	**benzene**
20-Mar	Position	mm	RT 9.4	RT 9.66	RT 10.33	RT 11.19	RT 12.3	RT 16.4
FP = 8	baseline							
(flame plane)	A position	0	0	77531	2472	2731	0	0
	FP-2 + 15%	6	2655	325070	7681	8483	8175	4628
	FP no add	8	7530	343777	27212	15054	8882	4427
	FP + 15%	8	6405	330472	26216	10998	7903	3906
	FP + 15%	8	5566	340684	25400	12162	8139	3838
	FP + 15%	8	4615	328168	24742	11677	7442	3665
	FP +1 +15%	9	1492	385401	23482	19457	10042	3710
	FP+2 +15%	10	0	0	564	0	0	0
	FP + 4 + 15%	12	0	0	0	0	0	0
19-Mar	**Ethanol 10%**	mm	**RT 9.4**	**RT 9.66**	**RT 10.33**	**RT 11.19**	**RT 12.3**	**RT 16.4**
FP = 9	baseline							
(flame plane)	A position	0	0	29141	577	832	9807	4155
	FP no add	9	3575	368122	31172	20789	7968	3567
	FP + 10%	9	3450	331628	27876	17837	7933	3646
	FP + 10%	9	3570	333399	27802	16709	8214	3867
	FP + 10%	9	3399	339050	27757	15793	8214	3867

APPENDIX C: Gas chromatography

C.1 Overview

Gas chromatography is adopted to identify and quantify the components of complex flame sample, as it is a technique that has the potential to provide high separation efficiency and good sensitivity. An overview is presented to benefit those unfamiliar with this technique as the author was prior to this study.

Chromatography encompasses a diverse and important group of methods that separates closely related components of complex mixtures; many of these are impossible by other means. In all chromatographic separations, the sample is dissolved in a mobile phase, which may be a gas, a liquid, or a supercritical fluid. This mobile phase is then forced through an immiscible stationary phase, which is fixed in place in a column or on a solid surface. The two phases are chosen so that the components of the sample distribute themselves between the mobile and the stationary phase to varying degrees [50, 49, 48, 46]. In Table 3-5 is reported a classification of column chromatographic methods.

Table C-1: Classification of Column Chromatographic Methods [48]

General Classification	Specific Method	Stationary Phase	Type of Equilibrium
Liquid chromatography (LC) (mobile phase: liquid)	Liquid-liquid, or partition	Liquid adsorbed on a solid	Partition between immiscible liquids
	Liquid-bonded phase	Organic species bonded to a solid surface	Partition/adsorption
	Liquid-solid, or adsorption	*Solid*	*Adsorption*
	Ion-exchange	Ion-exchange resin	Ion-exchange
	Size-exclusion	Liquid in interstices of a polymeric solid	Partition/sieving
Gas chromatography (GC) (mobile phase: gas)	Gas-liquid	Liquid adsorbed on a solid	Partition between gas and liquid
	Gas-bonded phase	Organic species bonded to a solid surface	Partition/adsorption
	Gas-solid	Solid	Adsorption

Gas Chromatography is characterized by the fact that the sample is vaporized and injected onto the head of a chromatographic column. Two types of gas chromatography are encountered: gas-solid chromatography (GSC) and gas-liquid chromatography (GLC) degrees, which is commonly indicated as GC analysis [50, 49, 48, 46].

GC analysis is based upon the partition of the analyte between a gaseous mobile phase and a liquid phase immobilized on the surface of an inert solid. *Elution* involves transporting a species through a column by continuous addition of fresh mobile phase. As is shown in Figure 3-8, a single portion of the sample, contained in the mobile phase, is introduced at the head of the column (time T_0 in Fig. 3-8), where upon the components of the sample distribute themselves between the two phases. Introduction of additional mobile phase (the *eluent*) forces the mobile phase containing a part of the sample down the column, where further partition between the mobile phase and the fresh portions of the stationary phase occurs (time T_1). Simultaneously, partitioning between the fresh solvent and the stationary phase takes place at the site of the original sample. Continued addition of mobile phase carry analyte molecules down the column in a continuous series of transfers between the mobile and the stationary phase. The average rate at which a species migrates depends upon the fraction of time it spends in the mobile phase. This fraction is small for substances that are strongly retained by the stationary phase (see compound B in Fig. 3-8) and is large where retention in the mobile phase is more likely (component A in Fig. 3-8). It is the difference in rates that cause the components in a mixture to separate into bands or zones located along the length of the column. Isolation of the separated species is then accomplished by passing a sufficient quantity of mobile

phase through the column to cause the individual bands to pass out the end, where they can be detected by appropriate detectors.

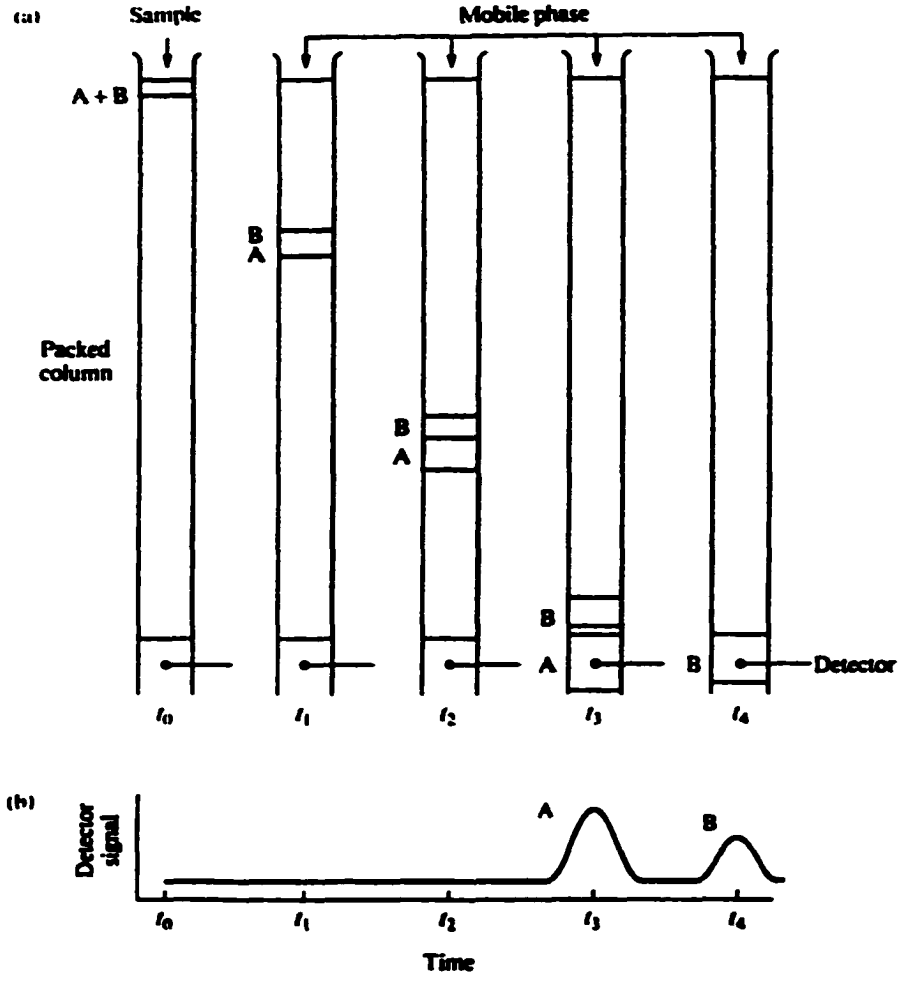

Figure C-1: Diagram showing the separation of a mixture of components A and B by column elution chromatography. The lower figure shows the output of the signal detector at the various stages of elution shown in the upper figure [48].

C.2 Chromatograms

If a detector that responds to the presence of analyte is placed at the end of the column and its signal is plotted as a function of time (as shown in Figure 3-10), a series of peaks is obtained. Such a plot is called *Chromatogram* and it is useful for both qualitative and quantitative analysis.

The position of the peak on the time axes serves to identify the components of the sample. The areas under the peaks provide a quantitative measure of the amount of each component. The time it takes after sample injection for the analyte peak to reach the detector is called *Retention time* [47].

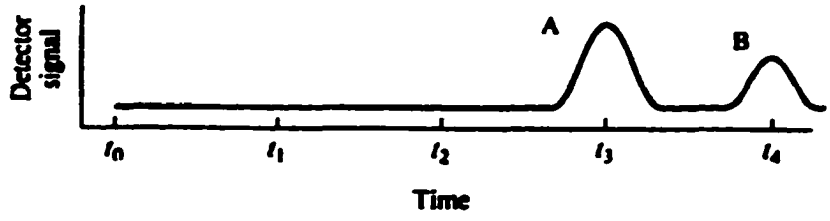

Figure C.2: General chromatogram shape [46].

C.3 Chromatographic Detectors

Detectors may be classified as "integrating" or "differentiating". An integrating detector gives a response proportional to the total mass of component in the eluted zone while a differentiating detector gives a response proportional to the concentration or mass flow rate of the eluted component. The most familiar example of a detector responding to concentration is the thermal conductivity detector (TCD). The flame ionization detector (FID) discussed before, is instead an example of a detector responding to mass flow rate. The chromatogram produced by a differentiating detector consists of a series of peaks, each of which correspond to a different component. The area under each peak is proportional to the total mass of that component. The ideal detector for gas chromatography has the following characteristics [46]:

- Adequate sensitivity
- Good stability and reproducibility
- A linear response to analytes that extends to several order of magnitude
- A temperature range from room temperature to at least 400 C.
- A short response time
- High reliability and easy to use
- Similarity in response toward all (or one class) analytes
- Nondestructive of sample.

C.4 Chromatographic Column Configurations

Because the actual separation of sample components is achieved in the column, the success or failure of a particular separation will depend to a large extend on the choice of column. Two general types of columns are encountered in gas chromatography:

- Packed column
- Open tubular (or capillary) column.

To date, the vast majority of gas chromatography has been carried out on packed columns. Currently, however, this situation is changing rapidly as capillary columns have present much more advantages. Capillary columns are open tubes of small diameter with a thin liquid film on the wall. Packed columns consist of an inert solid material supporting a thin film of non-volatile liquid. The tube may be glass, metal or plastic, coiled to fit the chromatographic oven. The solid support, type and amount of liquid phase, method of packing, length, and temperature of the column are important factors in obtaining the desired resolution (or peak separation) during the analysis.

The dimensions of the column govern the total amount of gas and liquid it will contain. Different types of capillary column are reported in Figure 3-11; WCOT columns result simply capillary tubes coated with a thin layer of the stationary phase. In SCOT columns, instead, the inner surface of the capillary is lined with a thin film (30-micron) of a support material such as diatomaceous earth. A PLOT column is, instead, characterized by etched porous layers [49]. Fused silica is generally used for manufacturing open tubular column (PLOT). The retention time for a solute on the column depends upon its partition ratio, which is related to the chemical nature of the stationary phase. Here, the

principle of "like dissolves like" applies, where "like" refers to the polarities of the solute and the immobilized liquid. Polarity is the electrical field effect in the immediate vicinity of a molecule and it is measured by the dipole moment of the species. Polar stationary phases contain functional groups such as –CN-, -CO, and –OH. Hydrocarbon type stationary phase is nonpolar. Polar analytes include alcohols, acid and amine; species medium polarity include ethers, ketones and aldehydes. Saturated hydrocarbons are nonpolar. When the polarity of the stationary phase matches that of the sample component, the order of elution is determinated by the boiling point of the eluents.

As shown in Table 3-7, the major advantage of capillary columns is their high number of total plates obtainable (or efficiency); capillary columns have higher permeability (i.e. they are open tubes) with small resistance and bigger length [46].

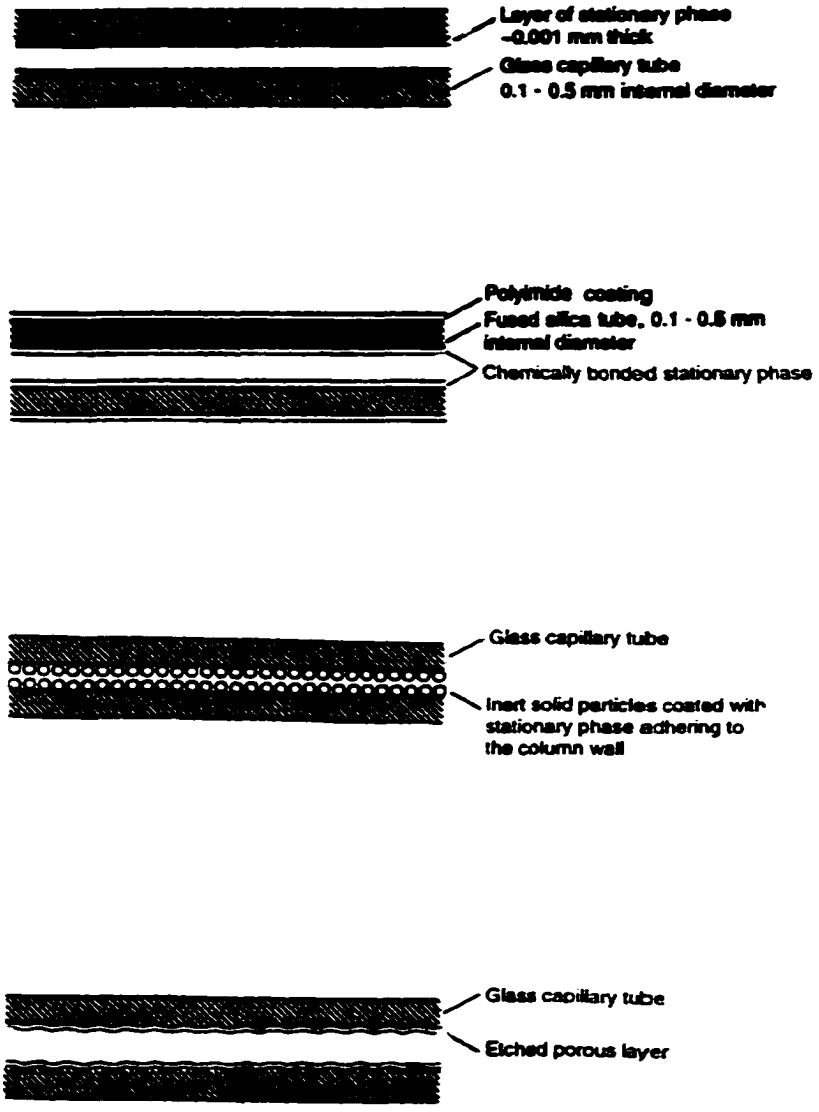

Figure C-3: Different Capillary Columns; in order: glass capillary column, fused silicabonded phase column, supported coated open tubular column (SCOT), Porous layer open tubular column (PLOT).

Table: C-2: Capillary columns versus packed columns [46].

	Capillary	Packed			
		1/16-in. O.D.	1/8-in. O.D.	1/4-in. O.D.	3/8-in. O.D.
Inside diam., inches	0.01-0.02	0.047	0.065	0.155	0.315
Maximum plates/ft	1000	1000	800	500	300
Practical length	300	60	60	60	100
Max. total plates	300,000	60,000	48,000	30,000	15,000
Amt. liquid phase, %	--	3	5	10	20
Liq. film thickness, μ	1	5	5	10	20
Mesh range	--	100/120	80/100	60/80	20/40
Permeability, $x10^7$ cm^2	200-800	1.5	2	3.5	4.0
Avg. linear vel, cm/sec.	25	10	10	7	7
Avg. flow rate, ml/min	1-3	10	20	70	120
Max. sample size, μl	0.010	1.0	2.0	20	1000

C.5 Temperature programming

Temperature programming is the controlled change of column temperature during an analysis. It is used to improve, simplify or accelerate the separation, identification and determination of sample components. Isothermal operation limits GC analysis to samples with similar volatility. At constant temperature (isothermal method), the early peaks, representing low boiling components, emerge so rapidly that sharp overlapping peaks result while higher boiling materials emerge as flat, immeasurable peaks. In some cases, high boiling components are not eluted and may appear in a later analysis as baseline noise or "ghost" peaks, which cannot be explained. With temperature programming, a

lower initial temperature is used and the early peaks are well resolved. Figure 3-12 shows the difference in the chromatogram between an isothermal method and a temperature programming method.

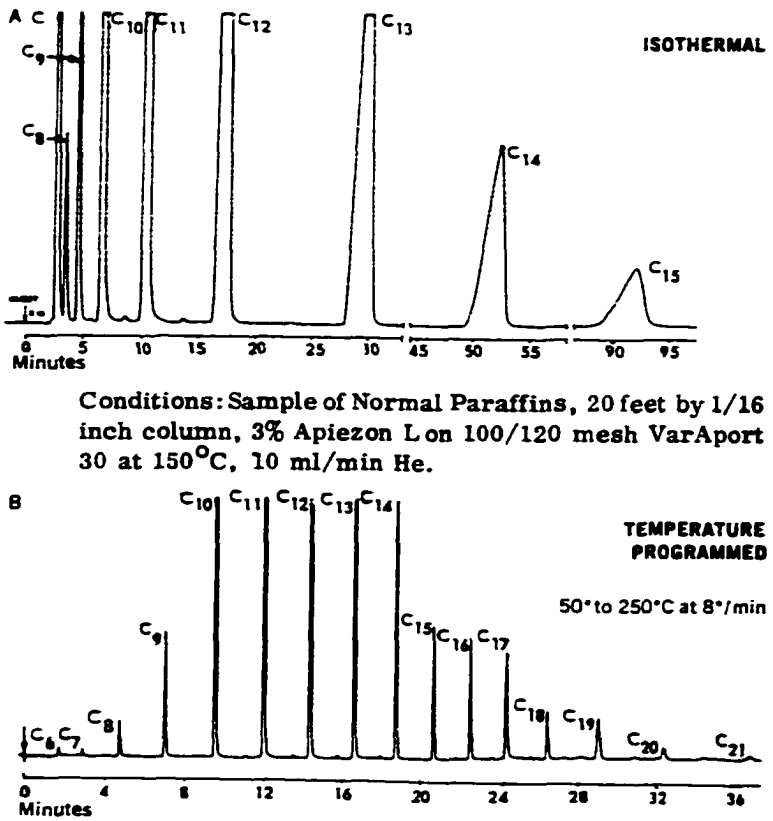

Figure C-4: Comparison of Isothermal and Temperature Programmed Chromatograms [46].

As the temperature increases, each higher boiling component is "pushed" out by the rising temperature. High boiling components are eluted earlier and as sharp peaks, similar in shape to the early peaks. Thus, temperature programming allows the proper selection of temperature, which will result in a well-resolved peak and a total analysis time shorter than isothermal operation. Programmed temperature gas chromatography (PTGC) is simply a means for obtaining the ideal temperature range for the separation of

each narrow boiling point fraction or component. PTGC has been used in this study for the previous reasons (see Figure 3-6).

The FID is quiet stable with temperature programmed operation since it is not sensitive to small temperature changes. A limit in PTGC is the maximum temperature of the capillary column in use [46].

C.6 The Van Deemter equation

To better understand the way a chromatographic column works during separation it is necessary to introduce same fundamental chromatographic definition and parameters by which column performance and gas chromatography can be improved.

The true separation of two consecutive peaks is measured by the *Resolution*, indicated as R_S. *Resolution* is a measure of both the column and the solvent efficiency. Its expression is as follows:

Solvent Efficiency results from the solute-solvent interaction and determines the

$$R_S = \frac{2[(t_R)_B - (t_R)A]}{W_A + W_B}$$

relative position of solute bands on a chromatograph. It is expressed as ratio of peak maxima. As regards chromatographic Column Efficiency, two related terms are widely used as quantitative measures:

- *Plate height* (H)
- *Number of theoretical plates* (N)

The two are related by the equation N= L/H, where L is the length of the column. The efficiency of a column increases as *the Number of Plates* becomes greater and as the

Plate Height becomes smaller. The genesis of the previous terms (Plate height, Number of theoretical plates.) is a pioneering theoretical study of Martin and Synge in which they treated a chromatographic column as if it were made up of numerous discrete but contiguous narrow layers called "theoretical plates". At each plate, equilibration of the species between the mobile and stationary phase was assumed to take place. Movement of the analyte down the column was then treated as a stepwise transfer of equilibrated mobile phase from one plate to the next. The plate theory successfully accounts for the Gaussian shape of chromatographic peaks and their rate of movement. Because chromatographic bands are generally assumed to be Gaussian in shape, it is convenient to define the efficiency of a column in terms of variance per unit length of column. Thus, the plate height H is defined as

$$H=\sigma^{*}\sigma/L \qquad (1)$$

The relationship between plate height and column variables can be expressed also as:

$$H= A+ B/u+ Cu \qquad (2)$$

This is known as the van Deemter equation. Here the constants A, B and C are coefficients of eddy diffusion, longitudinal diffusion, and mass transfer, respectively [46]. In the particular case of Capillary columns, the Van Deemter equation (2) reduces to the Golay equation (3):

$$H= B/ u + C *u \qquad (3)$$

Since capillary columns are not filled with particles, the phenomenon known as *Band Broadening*, due to the multi-path effect or eddy diffusion (A term), does not exist while it comes from the other two terms. *Band Broadening* lowers the efficiency of the column as a separating device.

Longitudinal diffusion (B/u) is a *Band Broadening* process in which analytes diffuse from the concentrated center of a band to the more dilute regions ahead of and behind the band center, that is, toward and opposed to the direction of flow of the mobile phase. The longitudinal diffusion is inversely proportional to the mobile phase velocity.

Band Broadening from mass transfer effects, arises because the many flowing streams of a mobile phase within a column and the layer of immobilized liquid making up the stationary phase both have finite widths. Consequently time is required by for analyte molecules to diffuse from the interior of these phases to their interface where transfer occurs. Both longitudinal broadening and mass-transfer broadening depend upon the rate of diffusion of analyte molecules but the direction of diffusion is different in the two cases; In the first case broadening arises from the tendency of molecules to move in directions that tend to parallel the flow, whereas mass-transfer broadening occurs from diffusion that tends to be right angles to the flow.

In seeking optimum conditions for achieving a desired separation, it is important to act on the column performance in terms of reducing zone broadening or altering relative migration rates of the components. Optimizing column performance means improving *Resolution*. This is possible acting on many fundamental parameters such as the selectivity factor (α), the capacity factor (K), the number of plates (N) or the plate height (H) as addressed elsewhere [46, 48, 49, 50].

*

APPENDIX D: Gas Chromatography

1. PLOT Column Characteristics D-2
2. PLOT Column Temperature Programming D-3
3. Chromatograms of gas sample at the flame plane position D-5

    a) Additive 0% (data March 16) D-5
    b) DMC 10% (by volume) (data March 17) D-6
    c) DMC 15% (by volume) (data March 17) D-7
    d) Ethanol 10% (by volume) (data March 19) D-8
    e) Ethanol 15% (by volume) (data March 20) D-9

4. Calibration Gas Standards

    a) SCOTTY IV-CAT NO. 2-3470-U D-10
    b) SCOTTY IV-CAT NO. 501832 D-11

5. Calibration curves D-12

HP-PLOT/Al203

Installation and Conditioning

Columns and Supplies

November 1993

Before using your new HP-PLOT column, please review the following installation and conditioning information.

Column Installation

Before you install your PLOT column, please do the following:

1. **Make sure the gas line in your system is moisture-free.** The use of a moisture trap and an in-line filter is recommended.

2. **Use helium or nitrogen as your carrier gas.** Many types of hydrogen contain moisture and, therefore, are not suitable for use with your PLOT column.

Column Conditioning

1. **After installing the PLOT column, condition it using the following oven temperature program (table 1):**

Table 1. Column Conditions

Initial temperature:	60°C
Rate:	5 to 10°C/min
Final temperature:	180°C
Final time:	180 min
Gas flow:	40 to 60 cm/sec

2. **Repeat the program run until the signal level comes down to 20 pA or lower for the FID.**

   Note: Due to strong adsorption property of alumina, repeat conditioning may result in a variation (slight shifting) of the retention time in comparison to that in the test chromatogram. This will not affect column performance.

3. **If the signal level is still high after three separate conditioning runs, bake the column at 150°C for 24 hours.** Increasing gas flow will shorten the conditioning time.

4. **Whenever you suspect column contamination during a GC run** (i.e., if water, polar compounds, or hydrocarbons larger than C_{10} get into the column), **recondition the column by running the above temperature program three to five times.**

5. **To maintain the installed column between use, bake it at 100 to 150°C with continuous gas purging.**

   Note: Slight opacity in the coating of PLOT column is due to the manufacturing process and does not affect column performance.

Printed in USA 11/93
Part No. 19091-91010
Revision A

PART# 19095P-S25 COLUMN ID: 0.53 MM FILM THICKNESS: 15.0 um
SERIAL# 57149217 COLUMN LENGTH: 50.0 METER PHASE RATIO: 10

SETPOINTS: INJ TEMP = 250 C OVEN TEMP = 100 C CHART SPEED = 0.70 CM/MIN
DET TEMP = 250 C AREA REJECT = 1000 ATTENUATION = 2^3

START PENDING
RUN # 9 JUN 13, 1997 07:33:45
START

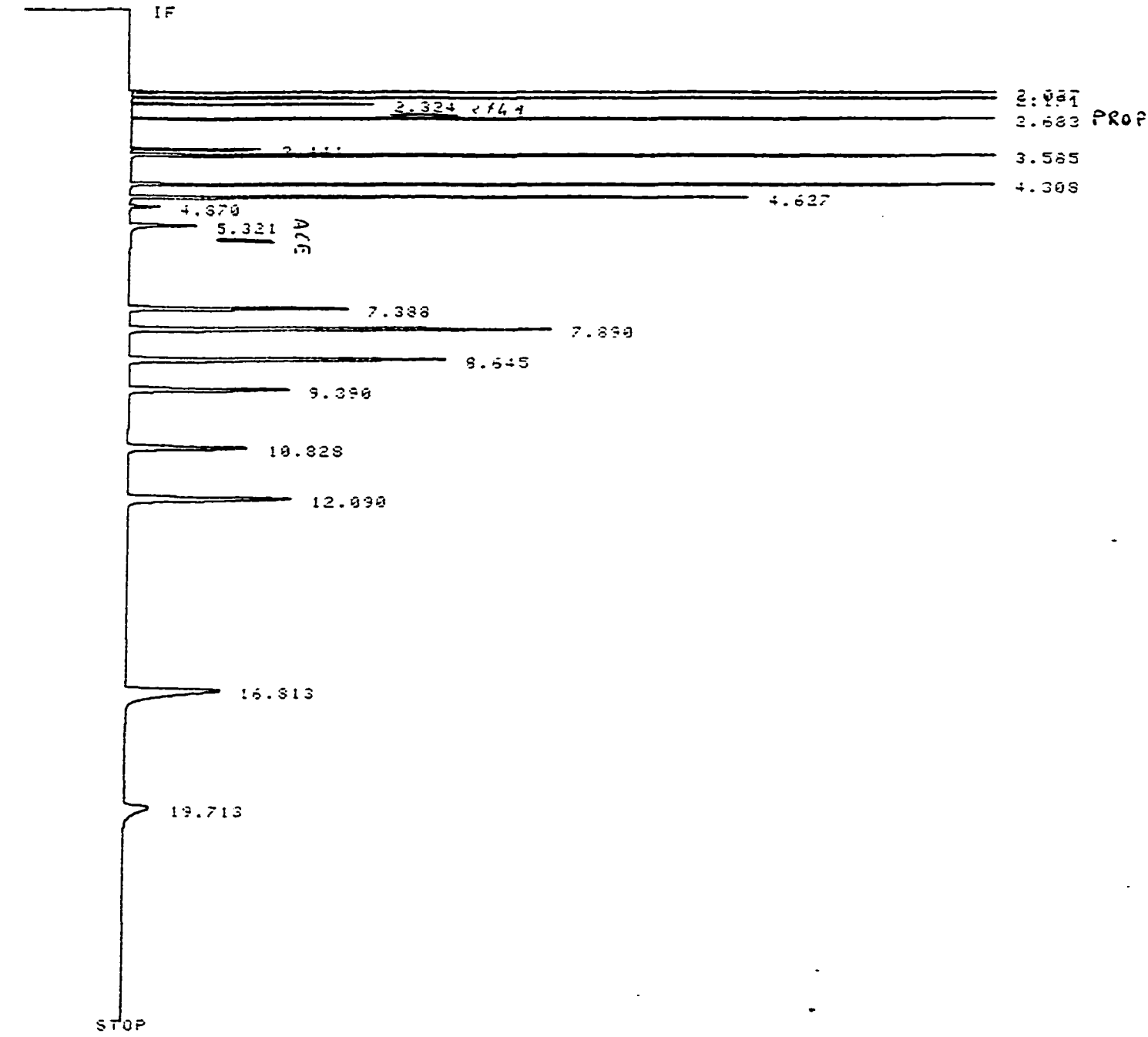

Closing signal file M:SIGNAL .BNC

RT	AREA	WIDTH(50%)	HEIGHT	COMPOUND
2.027	66535	0.0154	67695	METHANE
2.171	71387	0.0147	76007	ETHANE

3.585	171677	0.0247	108745	PROPYLENE
4.398	128087	0.0297	67661	ISO-BUTANE
4.627	89553	0.0323	43410	N-BUTANE
4.870	4895	0.0358	2140	PROPADIENE
5.321	17181	0.0568	4741	ACETYLENE
7.383	54925	0.0552	15589	TRANS-2-BUTENE
7.890	116014	0.0609	29824	1-BUTENE
8.645	97066	0.0674	22568	ISOBUTYLENE
9.390	53197	0.0725	11499	CIS-2-BUTENE
10.826	46715	0.0849	8624	ISO-PENTANE
12.090	73503	0.0967	11662	PENTANE
16.613	76253	0.1749	6831	1,3-BUTADIENE
19.713	22332	0.2014	1737	PROPYNE

****
* TEST CALCULATIONS *
* SERIAL# 5714931? *
****

PLATES/METER	PENTANE	1650 THEORETICAL
		1330 EFFECTIVE
CAPACITY FACTOR, K	PENTANE	5.0
RETENTION INDEX	PROPYLENE	362.8
	ACETYLENE	417.5

REORDER HEWLETT-PACKARD PART NUMBER 19095P-925

TESTED BY: _____

DATE: 06-13-97

Method File : C:\STAR\SOOT.MTH
Sample ID : Manual Sample

Injection Date: 16-MAR-99 6:21 PM Calculation Date: 16-MAR-99 6:43 PM

Operator : rub
Workstation:
Instrument : Varian Star #1
Channel : Front = FID

Detector Type: 3800 (1000 Volts)
Bus Address : 44
Sample Rate : 10.00 Hz
Run Time : 21.978 min

********** Star Chromatography Workstation ******* Version 4.51 **********

Chart Speed = 0.87 cm/min Attenuation = 32 Zero Offset = 5%
Start Time = 0.000 min End Time = 21.978 min Min / Tick = 1.00

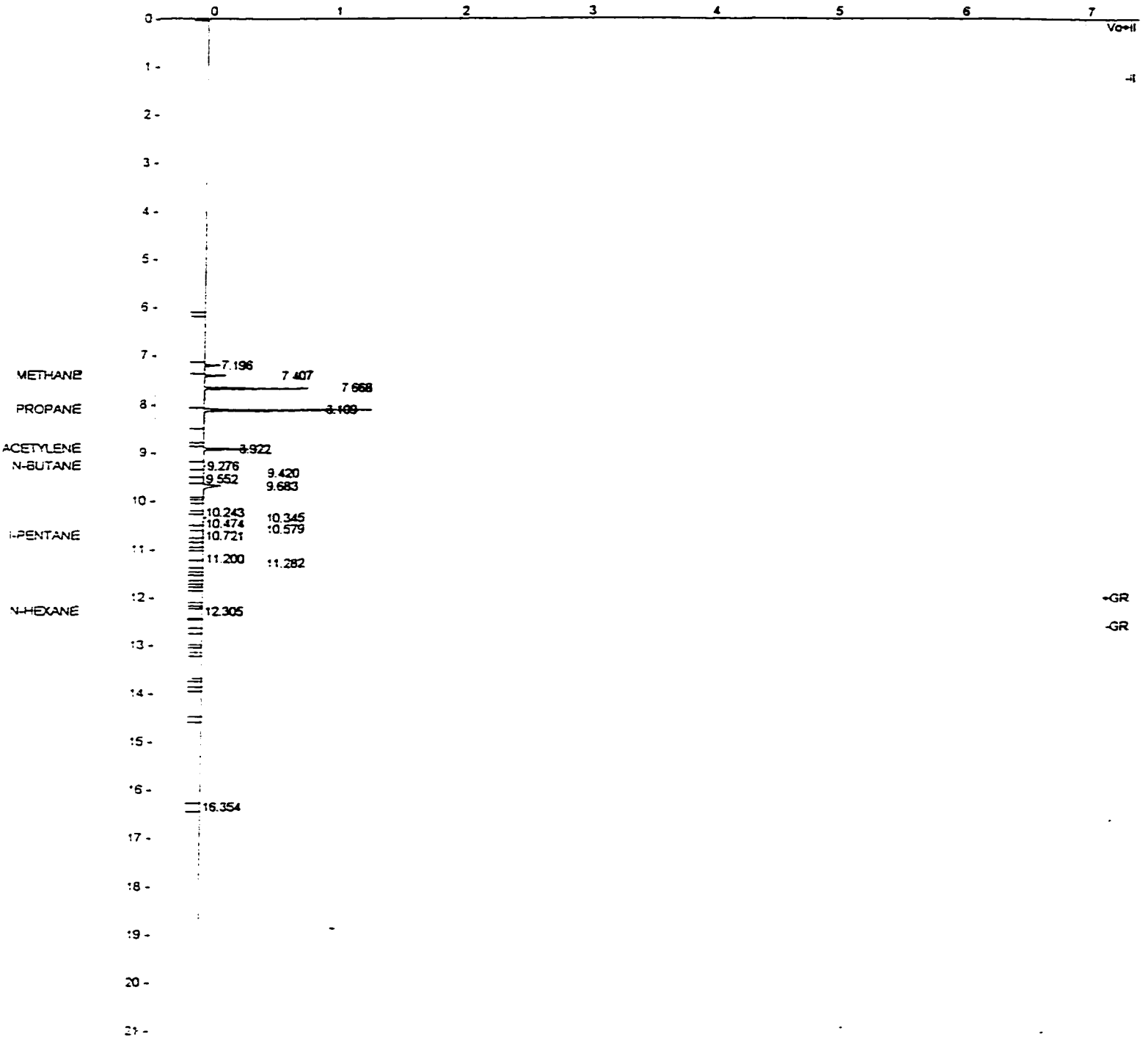

Method File : C:\STAR\3001.MTH
Sample ID : Manual Sample

Injection Date: 17-MAR-99 4:09 PM Calculation Date: 11-JUN-99 8:18 PM

Operator : rub
Workstation:
Instrument : Varian Star #1
Channel : Front = FID

Detector Type: 3800 (1000 Volts)
Bus Address : 44
Sample Rate : 10.00 Hz
Run Time : 21.978 min

********** Star Chromatography Workstation ******* Version 4.51 **********

Chart Speed = 0.87 cm/min Attenuation = 32 Zero Offset = 5%
Start Time = 0.000 min End Time = 21.978 min Min / Tick = 1.00

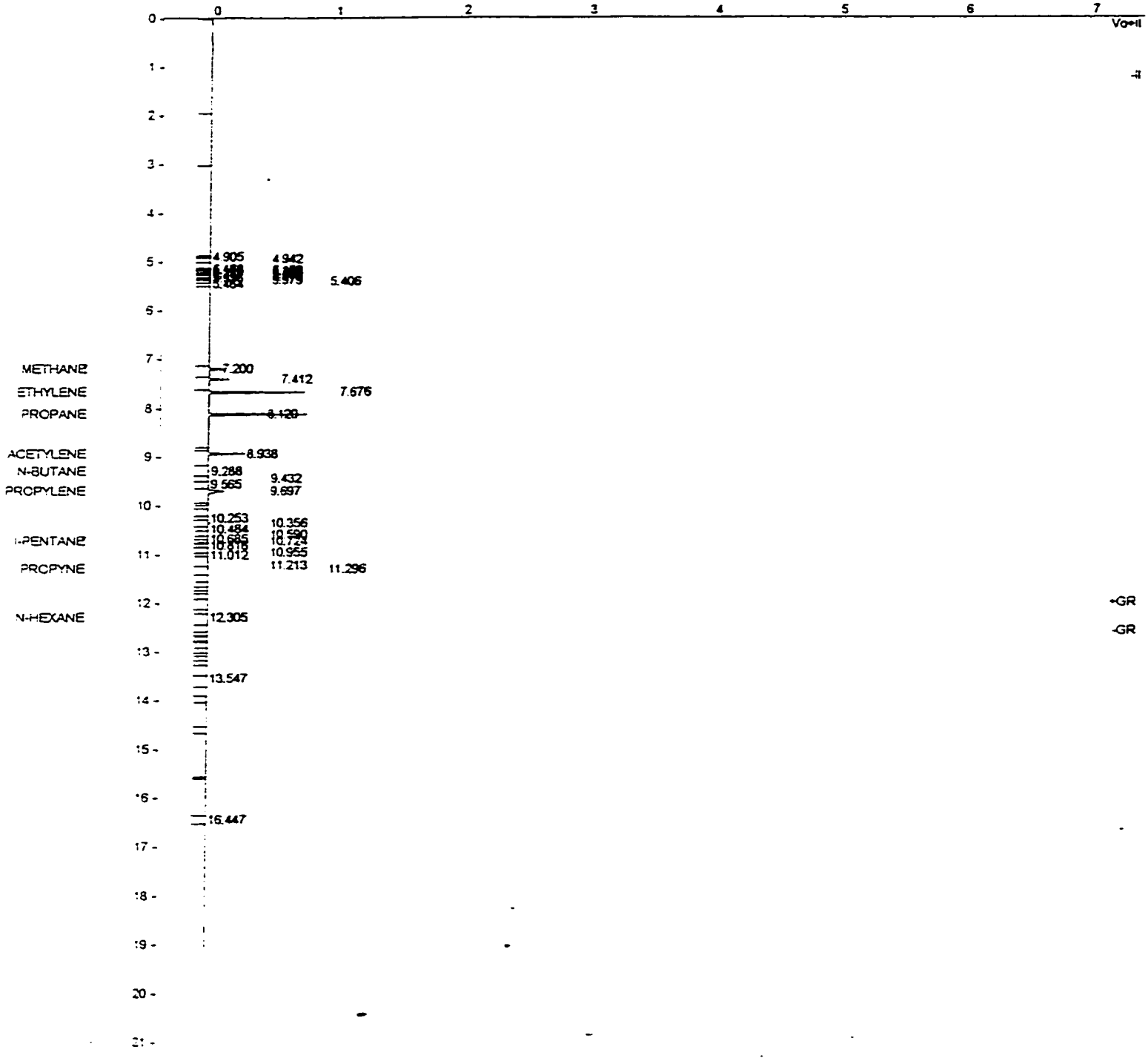

Method File : C:\STAR\SOOT.MTH
Sample ID : Manual Sample

Injection Date: 17-MAR-99 6:23 PM Calculation Date: 17-MAR-99 6:45 PM

Operator : rub
Workstation:
Instrument : Varian Star #1
Channel : Front = FID

Detector Type: 3800 (1000 Volts)
Bus Address : 44
Sample Rate : 10.00 Hz
Run Time : 21.978 min

********** Star Chromatography Workstation ******* Version 4.51 **********

Chart Speed = 0.87 cm/min Attenuation = 32 Zero Offset = 5%
Start Time = 0.000 min End Time = 21.978 min Min / Tick = 1.00

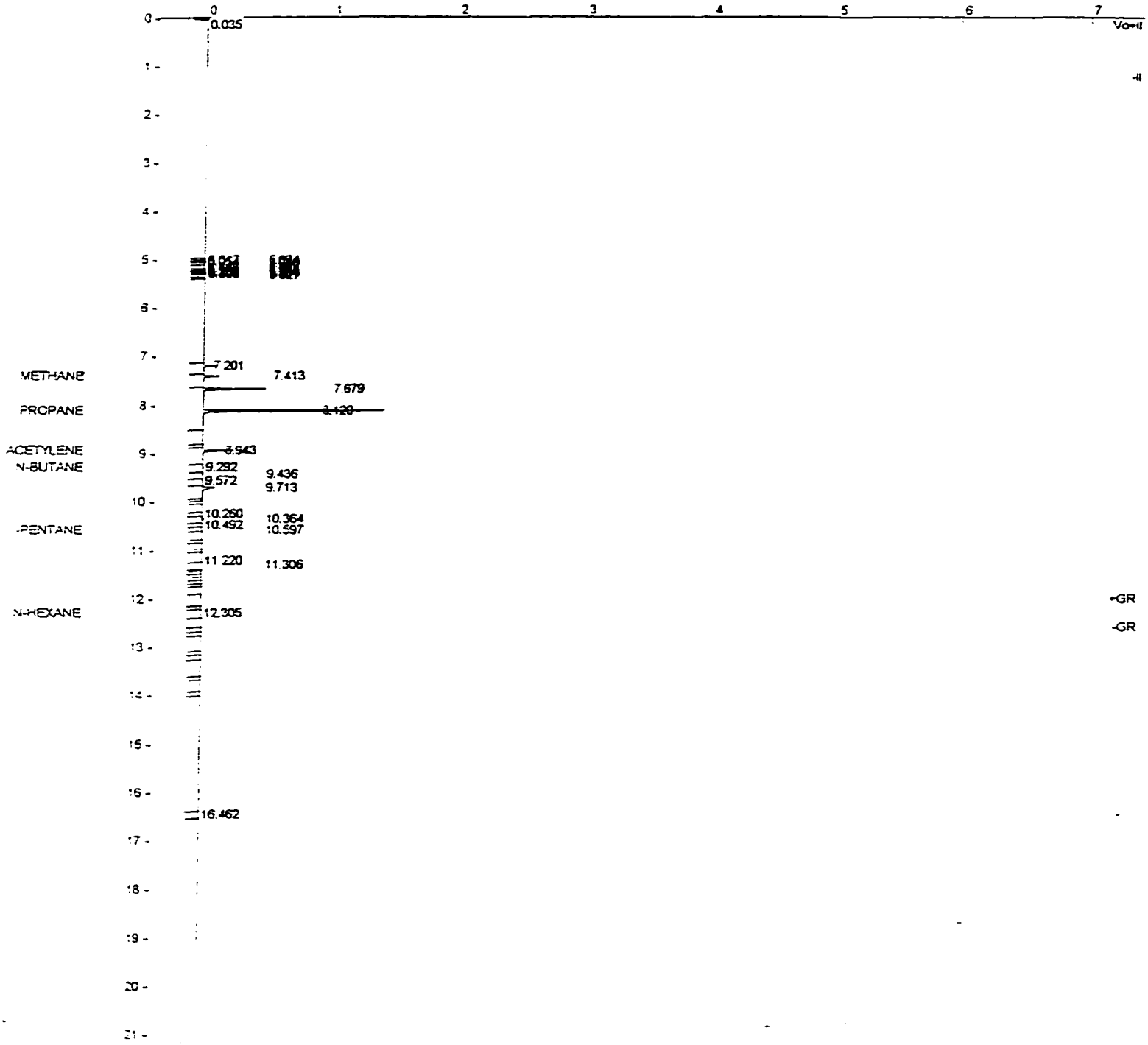

Method File : C:\STAR\SOOT.MTH
Sample ID : Manual Sample

Injection Date: 19-MAR-99 5:29 PM Calculation Date: 19-MAR-99 5:51 PM

Operator : rub
Workstation:
Instrument : Varian Star #1
Channel : Front = FID

Detector Type: 3800 (1000 Volts)
Bus Address : 44
Sample Rate : 10.00 Hz
Run Time : 21.978 min

********** Star Chromatography Workstation ******* Version 4.51 **********

Chart Speed = 0.87 cm/min Attenuation = 32 Zero Offset = 5%
Start Time = 0.000 min End Time = 21.978 min Min / Tick = 1.00

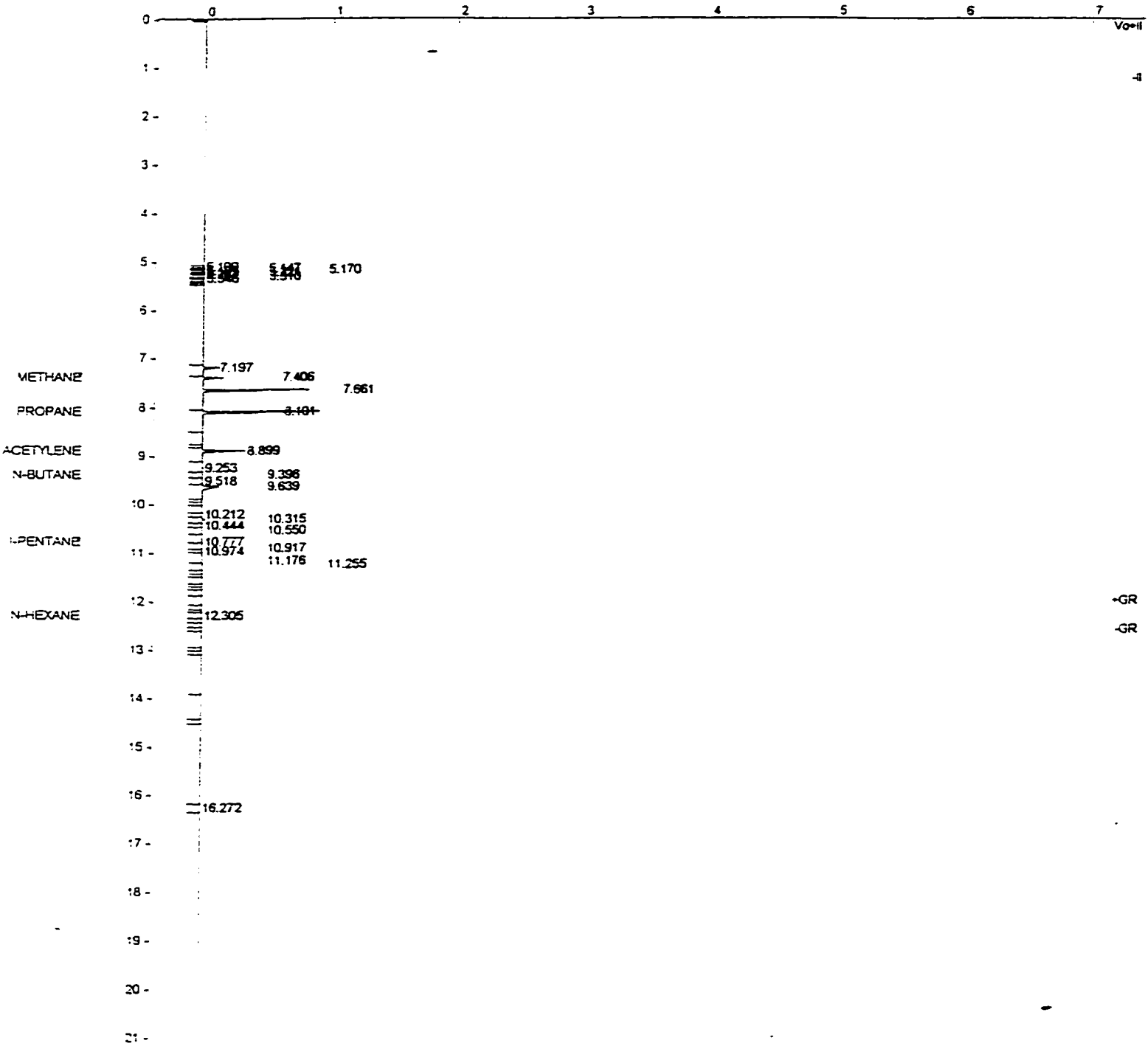

Method File : C:\STAR\SOOT.MTH
Sample ID : Manual Sample

Injection Date: 20-MAR-99 3:10 PM Calculation Date: 20-MAR-99 3:32 PM

Operator : rub
Workstation:
Instrument : Varian Star #1
Channel : Front = FID

Detector Type: 3800 (1000 Volts)
Bus Address : 44
Sample Rate : 10.00 Hz
Run Time : 21.978 min

********** Star Chromatography Workstation ******* Version 4.51 **********

Chart Speed = 0.87 cm/min Attenuation = 32 Zero Offset = 5%
Start Time = 0.000 min End Time = 21.978 min Min / Tick = 1.00

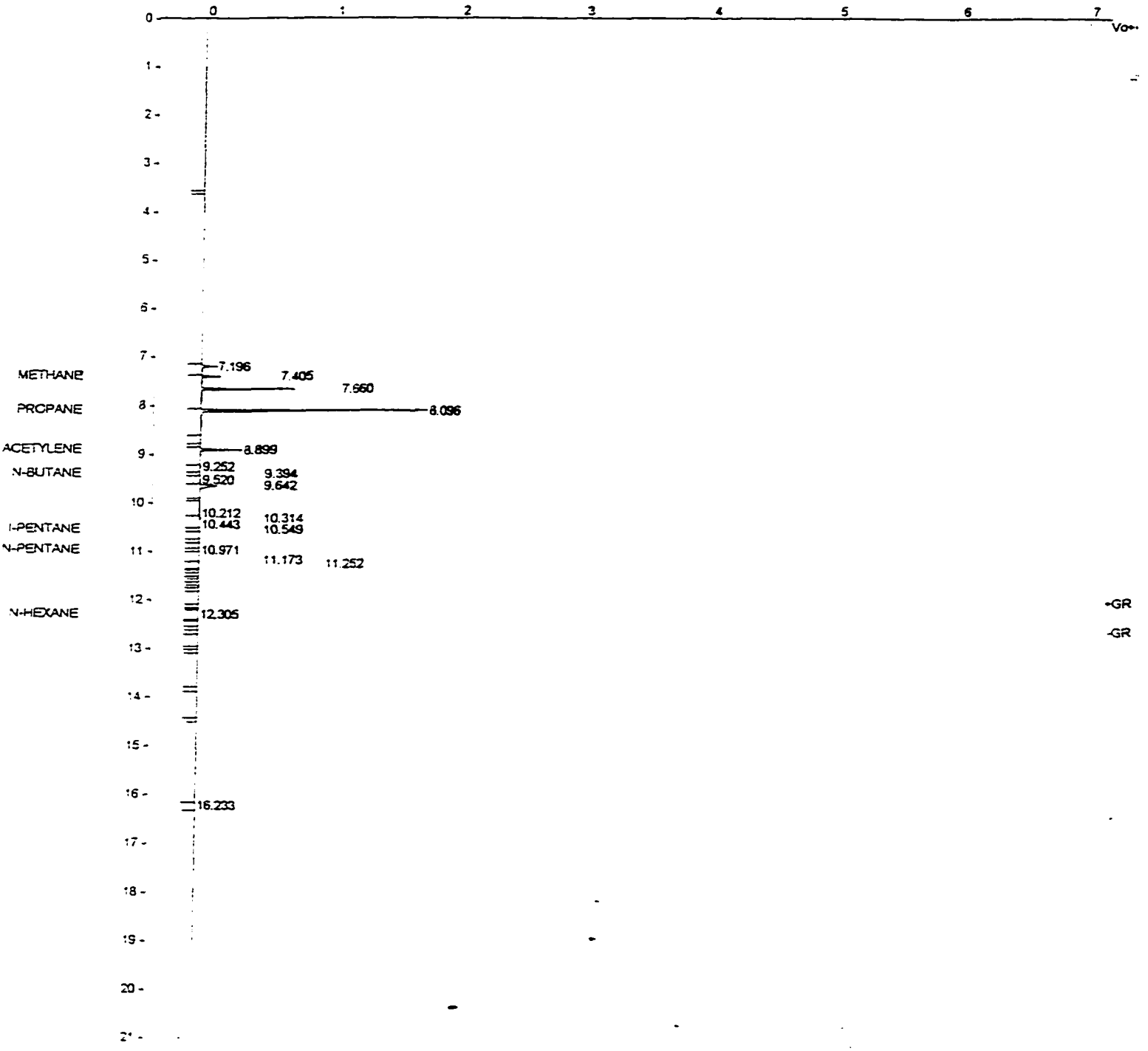

Title : Calibration Gas Mix: SCOTTY IV-CAT NO. 2-3470-U (15 PPM)
Run File : C:\STAR\TESTRUN\SLITSOOT\SLITSOOT\MARCH 23\CALIB001.RUN
Method File : c:\star\soot.mth
Sample ID : Default Sample

Injection Date: 23-MAR-99 3:20 PM Calculation Date: 16-JUN-99 6:36 PM

Operator : rub
Workstation:
Instrument : Varian Star #1
Channel : Front = FID

Detector Type: 3800 (1000 Volts)
Bus Address : 44
Sample Rate : 10.00 Hz
Run Time : 21.978 min

********** Star Chromatography Workstation ******* Version 4.51 **********

Run Mode : Calibration
Peak Measurement: Peak Area
Calculation Type: External Standard
Level : 1

Peak No.	Peak Name	Ret. Time (min)	Time Offset (min)	Area (counts)	Sep. Code	Width 1/2 (sec)	Status Codes
1	METHANE	7.196	0.001	677	BB	1.1	
2	ETHANE	7.405	0.003	1252	BB	1.0	
3	ETHYLENE	7.662	0.001	1259	BB	1.0	
4	PROPANE	8.103	0.007	1645	BB	1.0	
5	ACETYLENE	8.906	0.001	1682	BB	1.0	
6	N-BUTANE	9.395	0.157	2163	BB	1.1	
7	PROPYLENE	9.678	0.056	1136	BB	1.4	
8	N-PENTANE	10.871					M
9	PROPYNE	11.222	0.011	2492	PB	2.1	
10	N-HEXANE	12.305					M
11	N- HEPTANE	14.340					M
12	BENZENE	15.961					M
13	N-OCTANE	18.337					M
	Totals:		0.237	12306			

Status Codes:
M - Missing peak

Total Unidentified Counts : 0 counts

Detected Peaks: 9 Rejected Peaks: 1 Identified Peaks: 13

Multiplier: 1 Divisor: 1

Baseline Offset: -1 microVolts

Noise (used): 29 microVolts - monitored before this run

Manual injection

Title : Calibration Gas Mix. SCOTTY IV CAT NO. 501832 (1000 PPM)
Run File : C:\STAR\TESTRUN\SLITSOOT\SLITSOOT\MARCH 24\CALIB001.RUN
Method File : c:\star\soot.mth
Sample ID : Default Sample

Injection Date: 24-MAR-99 10:11 AM Calculation Date: 14-JUN-99 8:16 PM

Operator : rub
Workstation:
Instrument : Varian Star #1
Channel : Front = FID

Detector Type: 3800 (1000 Volts)
Bus Address : 44
Sample Rate : 10.00 Hz
Run Time : 21.978 min

********** Star Chromatography Workstation ******* Version 4.51 **********

Run Mode : Calibration
Peak Measurement: Peak Area
Calculation Type: External Standard
Level : 2

Peak No.	Peak Name	Ret. Time (min)	Time Offset (min)	Area (counts)	Sep. Code	Width 1/2 (sec)	Status Codes
1	METHANE	7.196	-0.000	23861	BV	1.0	
2	ETHANE	7.403	-0.001	35650	VB	1.0	
3	ETHYLENE	7.661					M
4	PROPANE	8.097	-0.005	42063	BB	1.0	
5	ACETYLENE	8.905					M
6	N-BUTANE	9.238	0.022	591	BB	1.0	
7		9.378	0.000	48207	BB	1.0	
8	PROPYLENE	9.622					M
9	N-PENTANE	10.871	-0.029	51412	PB	1.3	
10	PROPYNE	11.211					M
11	N-HEXANE	12.305	0.000	55132	GR	0.0	
12	N- HEPTANE	14.340					M
13	BENZENE	15.961					M
14	N-OCTANE	18.337					M
	Totals:		-0.013	256916			

Status Codes:
M - Missing peak

Total Unidentified Counts : 48207 counts

Detected Peaks: 12 Rejected Peaks: 4 Identified Peaks: 13

Multiplier: 1 Divisor: 1

Baseline Offset: -2 microVolts

Noise (used): 35 microVolts - monitored before this run

Manual injection

Calibration Curve Report
File: c:\star\soot.mth
Detector: 3800 GC, Address: 44, Channel ID: Front

METHANE

External Standard Analysis
Curve Type: Linear
Origin: Ignore (Edited)
y = +2.372546e+001x +3.250769e+002

Resp. Fact. RSD: 33.26%
Corr. Coef.(R^2): 1.000000

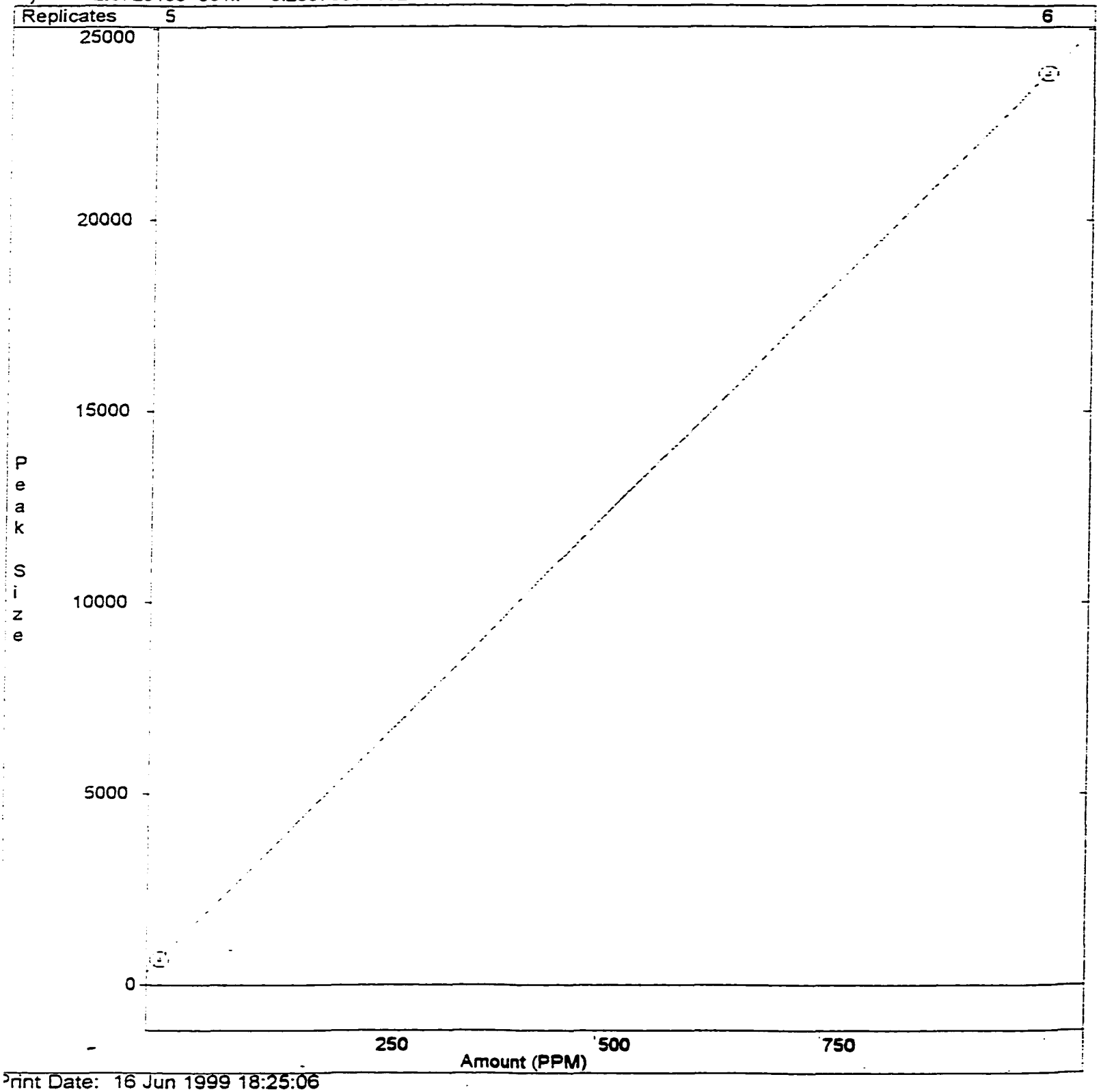

Print Date: 16 Jun 1999 18:25:06

Calibration Curve Report
File: c:\star\soot.mth
Detector: 3800 GC, Address: 44, Channel ID: Front

ETHANE

External Standard Analysis
Curve Type: Linear
Origin: Ignore
y = +3.462978e+001x +7.434810e+002

Resp. Fact. RSD: 44.92%
Corr. Coef.(R^2): 1.000000

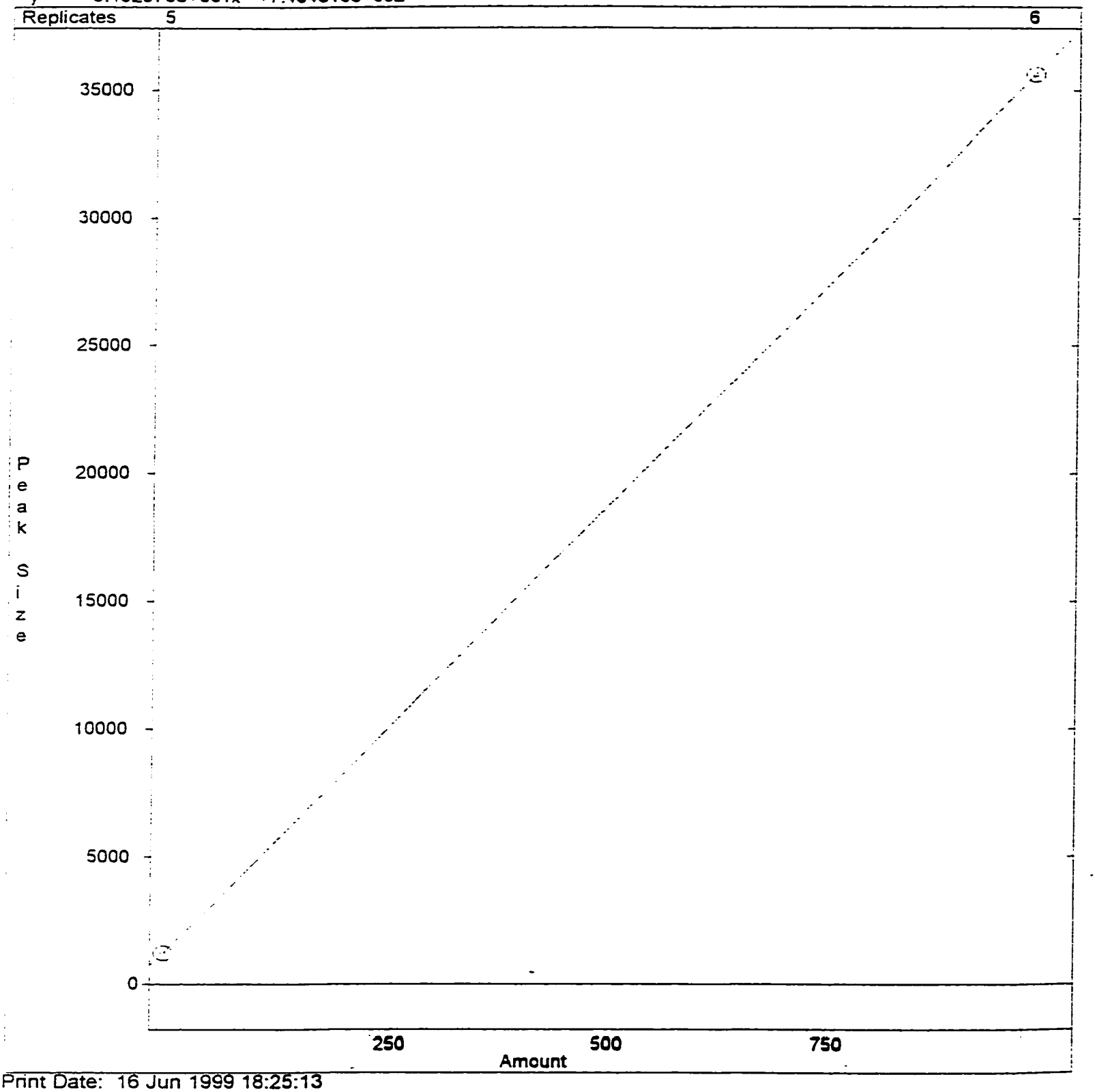

Print Date: 16 Jun 1999 18:25:13

Calibration Curve Report
File: c:\star\soot.mth
Detector: 3800 GC, Address: 44, Channel ID: Front

ETHYLENE

External Standard Analysis
Curve Type: Linear
Origin: Include
y = +8.195964e+001x -3.113065e-013

Resp. Fact. RSD: 0.0000%
Corr. Coef.(R^2): 1.000000

Replicates 5

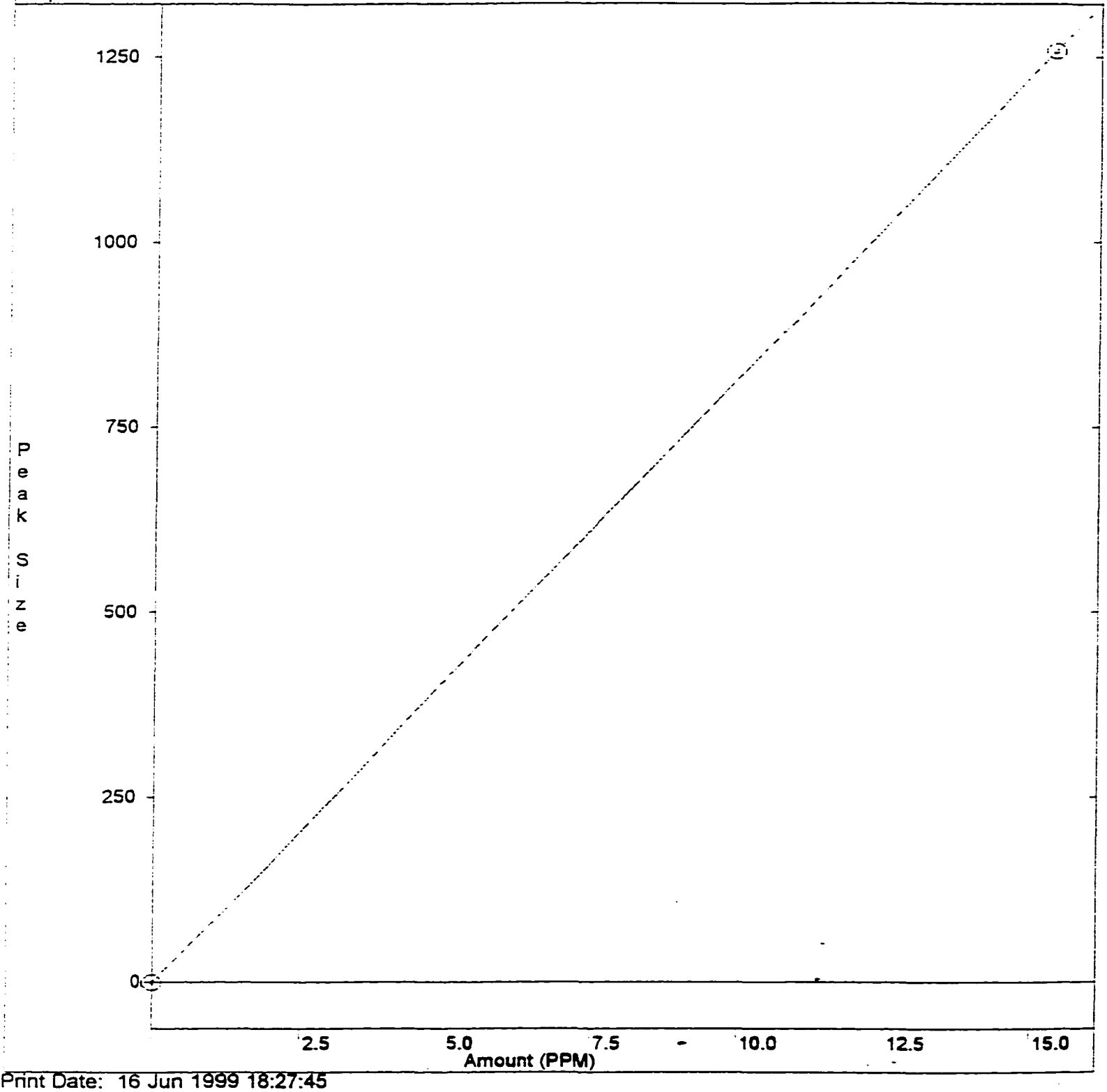

Print Date: 16 Jun 1999 18:27:45

Calibration Curve Report
File: c:\star\soot.mth
Detector: 3800 GC, Address: 44, Channel ID: Front

PROPANE

External Standard Analysis
Curve Type: Linear
Origin: Ignore
y = +4.107656e+001x +9.866428e+002

Resp. Fact. RSD: 45.45%
Corr. Coef.(R^2): 1.000000

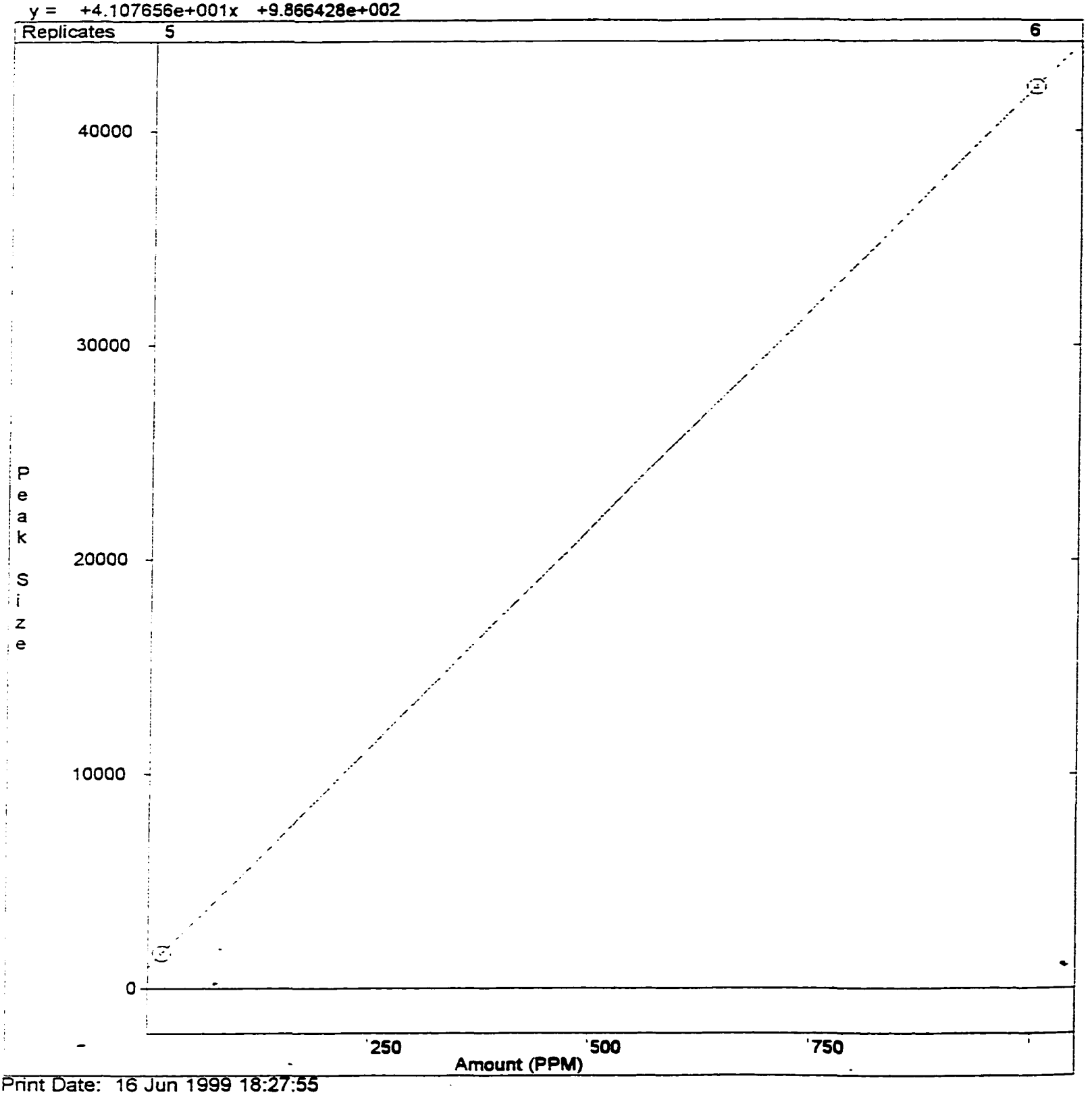

Print Date: 16 Jun 1999 18:27:55

Calibration Curve Report
File: c:\star\soot.mth
Detector: 3800 GC, Address: 44, Channel ID: Front

N-BUTANE

External Standard Analysis
Curve Type: Linear
Origin: Ignore
y = +4.683714e+001x +1.416816e+003

Resp. Fact. RSD: 65.23%
Corr. Coef.(R^2): 1.000000

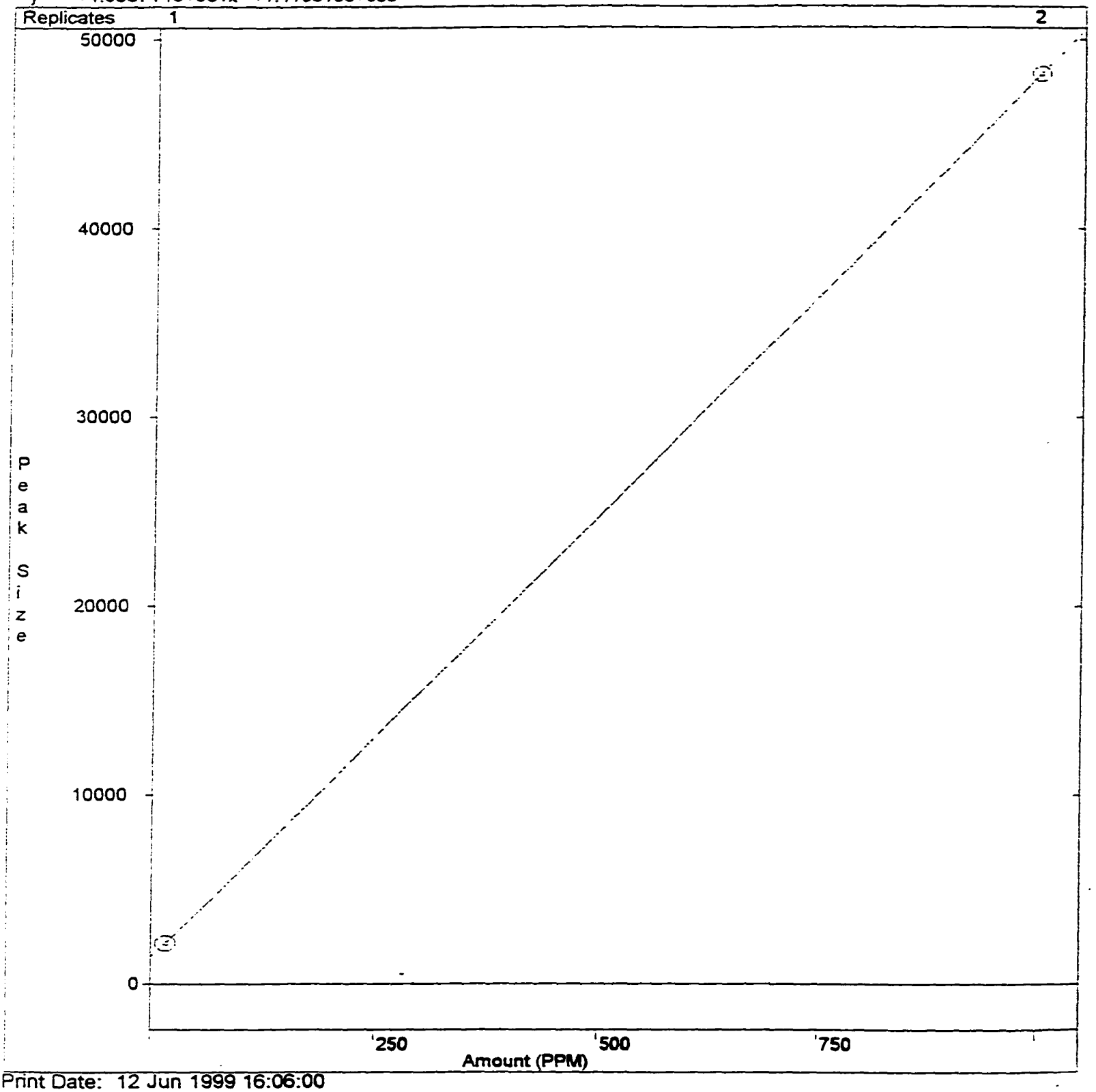

Print Date: 12 Jun 1999 16:06:00

Calibration Curve Report
File: c:\star\soot.mth
Detector: 3800 GC, Address: 44, Channel ID: Front

ACETYLENE

External Standard Analysis
Curve Type: Linear
Origin: Include
y = +1.051845e+002x +4.920508e-013

Resp. Fact. RSD: 0.0000%
Corr. Coef.(R^2): 1.000000

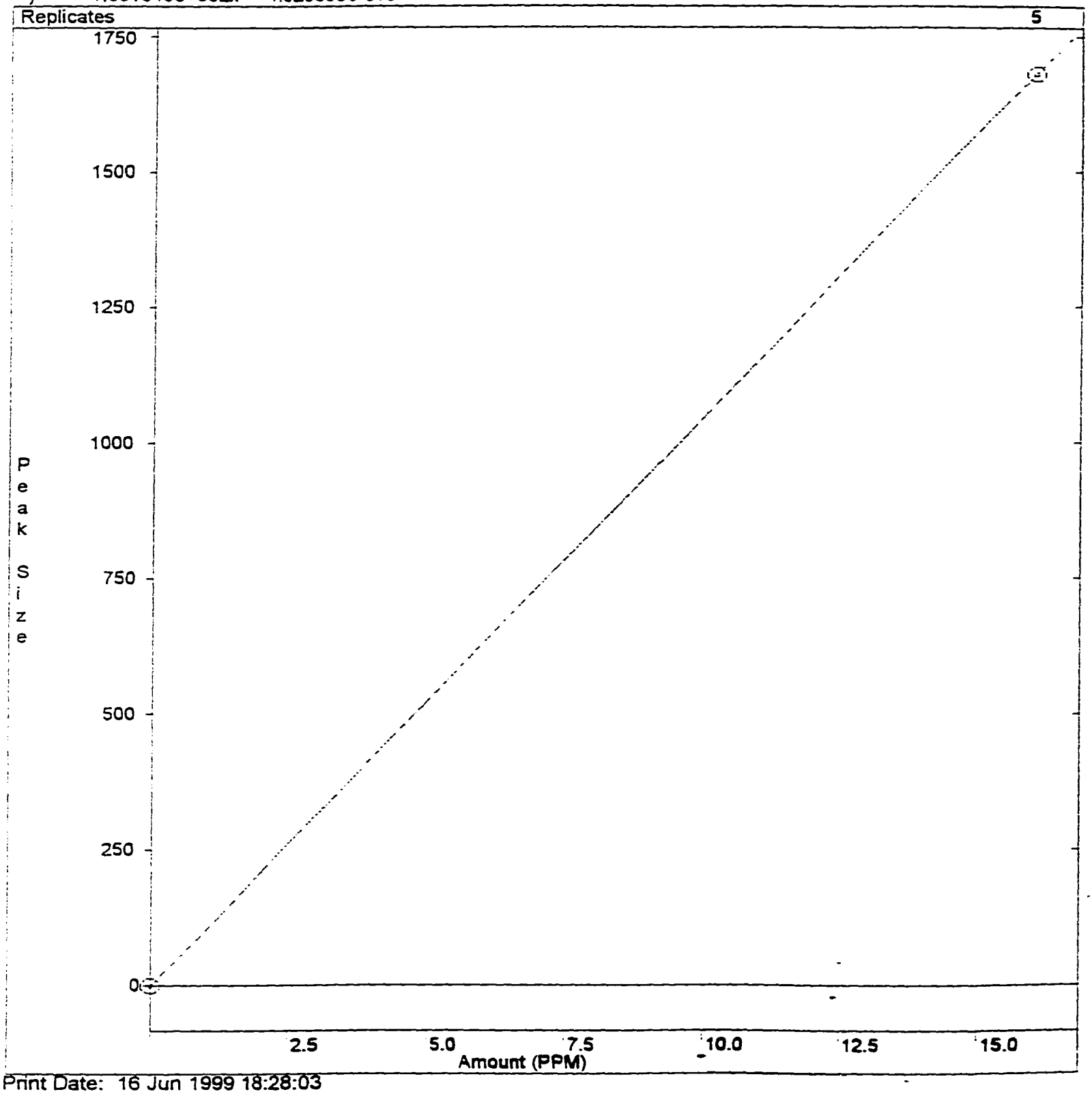

Print Date: 16 Jun 1999 18:28:03

Calibration Curve Report
File: c:\star\soot.mth
Detector: 3800 GC, Address: 44, Channel ID: Front

PROPYLENE

External Standard Analysis
Curve Type: Linear
Origin: Force (Edited)
y = +1.488544e+002x

Resp. Fact. RSD: 68.73%
Corr. Coef.(R^2): 0.667625

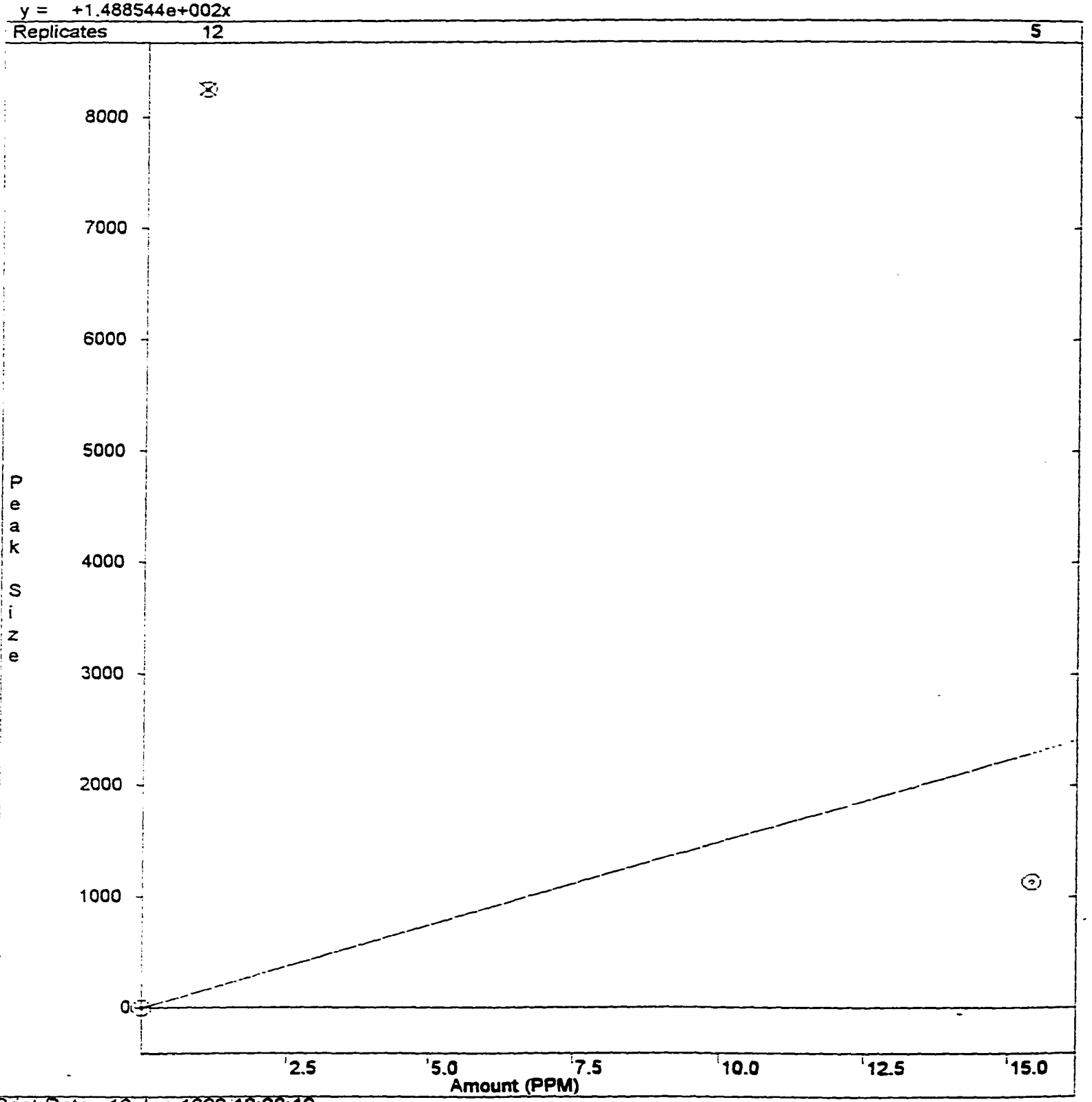

Print Date: 16 Jun 1999 16:28:19

Calibration Curve Report
File: c:\star\soot.mth
Detector: 3800 GC, Address: 44, Channel ID: Front

N-HEXANE

External Standard Analysis
Curve Type: Linear
Origin: Force (Edited)
y = +5.770010e+001x

Resp. Fact. RSD: 90.96%
Corr. Coef.(R^2): 0.060372

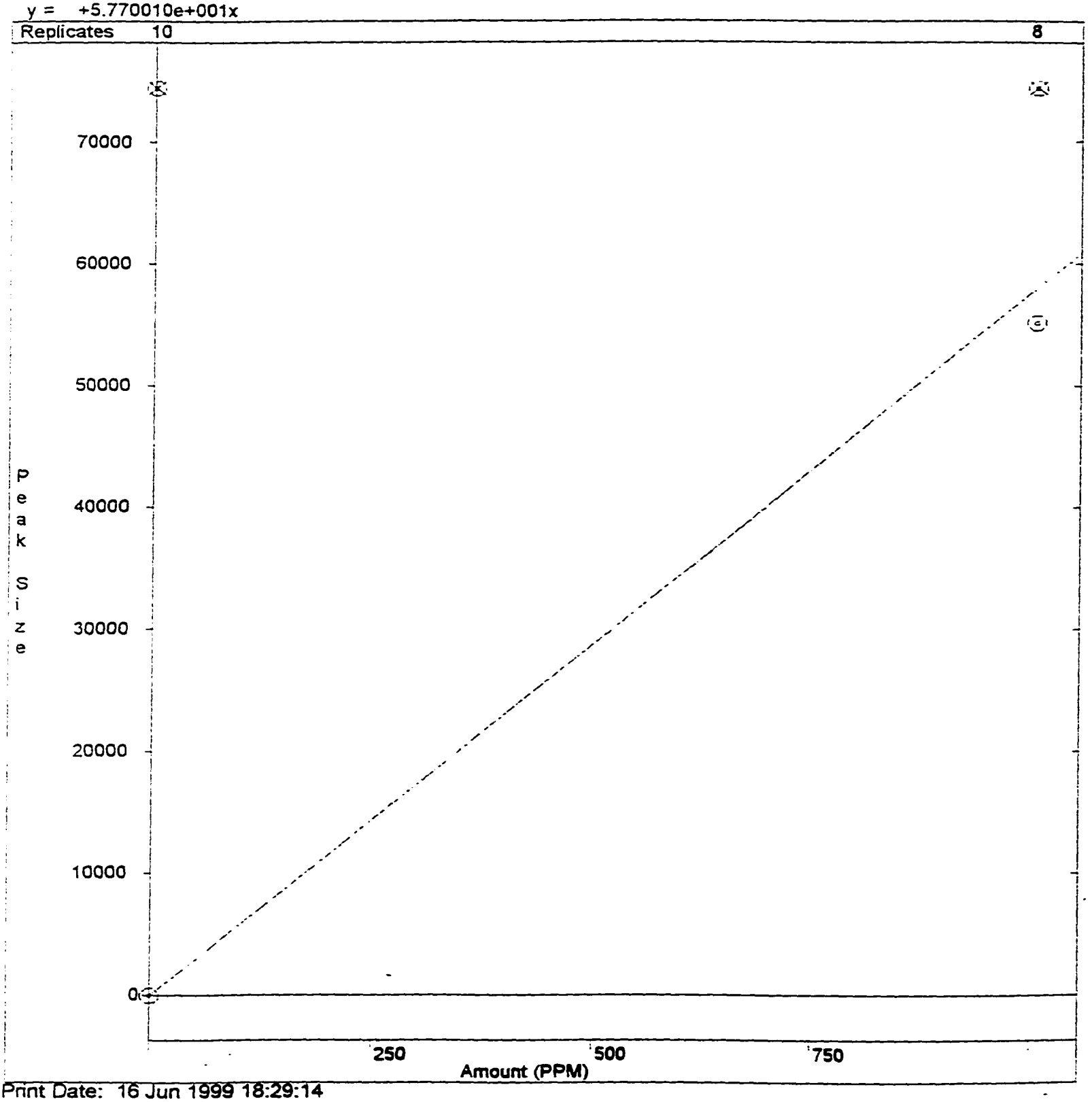

Print Date: 16 Jun 1999 18:29:14

Calibration Curve Report
File: c:\star\soot.mth
Detector: 3800 GC, Address: 44, Channel ID: Front

D - 20

N-PENTANE

External Standard Analysis
Curve Type: Linear
Origin: Force (Edited)
y = +4.786489e+001x

Resp. Fact. RSD: 118.12%
Corr. Coef.(R^2): 0.689332

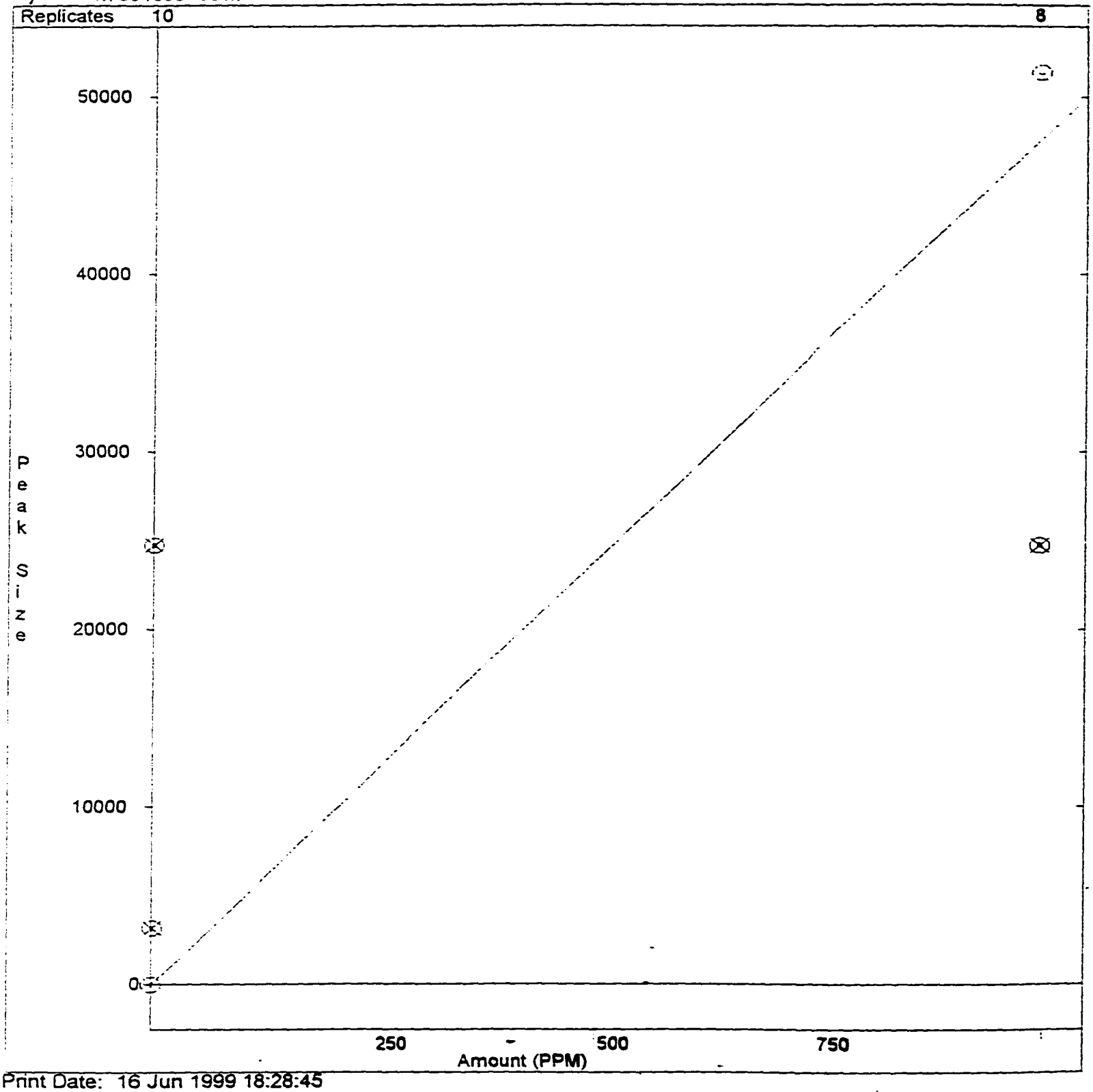

Print Date: 16 Jun 1999 18:28:45

Calibration Curve Report
File: c:\star\soot.mth
Detector: 3800 GC, Address: 44, Channel ID: Front

PROPYLENE

External Standard Analysis
Curve Type: Linear
Origin: Force (Edited)
y = +1.488544e+002x

Resp. Fact. RSD: 68.73%
Corr. Coef.(R^2): 0.667625

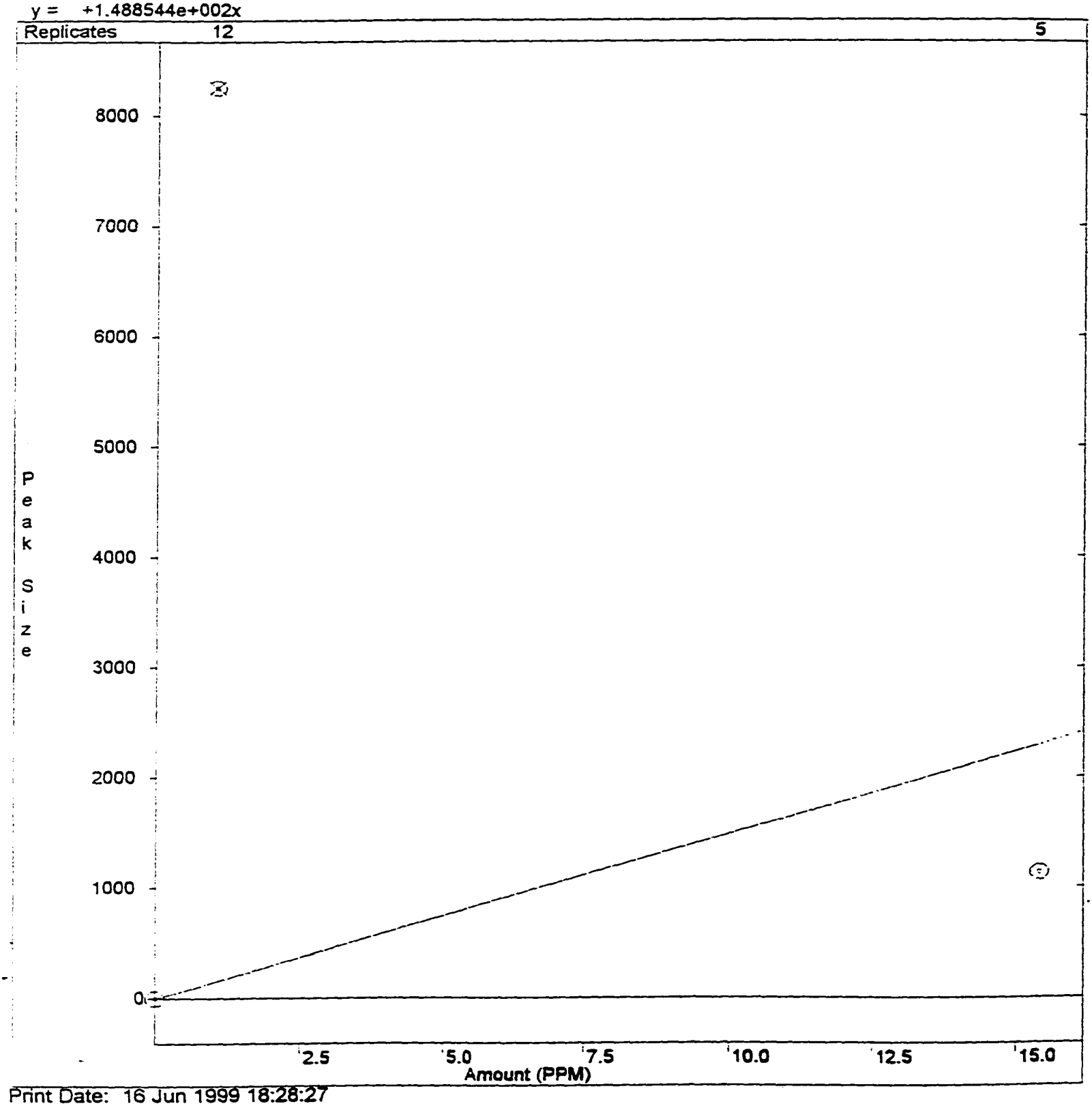

Print Date: 16 Jun 1999 18:28:27

Calibration Curve Report
File: c:\star\soot.mth
Detector: 3800 GC, Address: 44, Channel ID: Front

PROPYNE

External Standard Analysis
Curve Type: Linear
Origin: Force (Edited)
y = +1.998930e+002x

Resp. Fact. RSD: 66.64%
Corr. Coef.(R^2): 0.393656

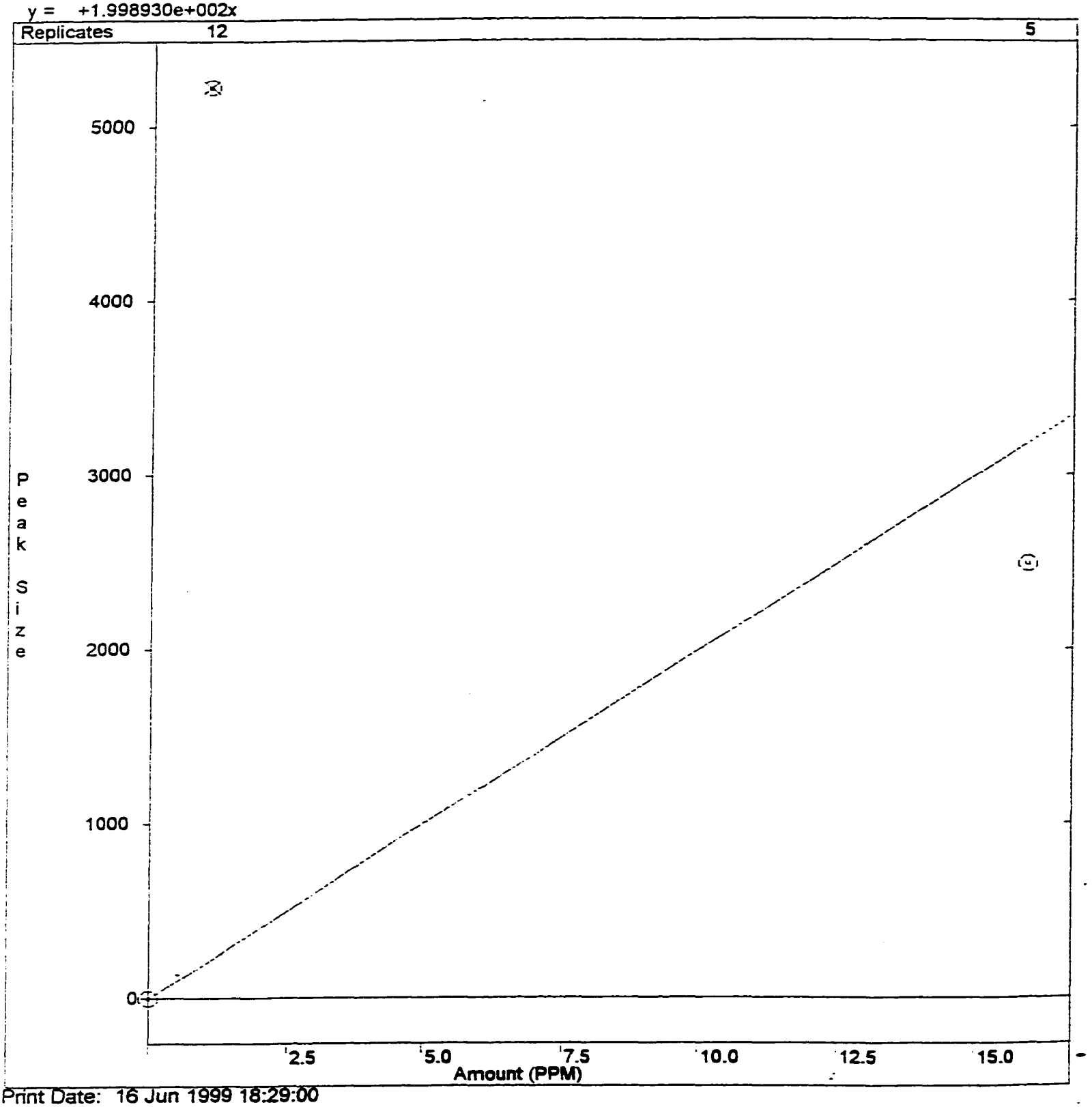

Print Date: 16 Jun 1999 18:29:00